Universidade de Lisboa

Faculdade de Ciências

Departamento de Física

HARDI Methods – Tractography Reconstructions and Automatic Parcellation of Brain Connectivity

Luís Lacerda

Dissertação

Mestrado Integrado em Engenharia Biomédica e Biofísica

Perfil em Radiações em Diagnóstico e Terapia

2012

Universidade de Lisboa

Faculdade de Ciências

Departamento de Física

HARDI Methods – Tractography Reconstructions and Automatic Parcellation of Brain Connectivity

Luís Lacerda

Dissertação orientada por Professor Doutor Flavio Dell' Acqua e Professor Doutor Hugo Alexandre Ferreira

Mestrado Integrado em Engenharia Biomédica e Biofísica

Perfil em Radiações em Diagnóstico e Terapia

2012

Table of Contents

Resumo

A neuroanatomia humana tem sido objecto de estudo científico desde que surgiu o interesse na organização do corpo humano e nas suas funções, quer como um todo quer através das partes que o constituem. Para atingir este fim, as autópsias foram a primeira forma de revelar algum conhecimento, o qual tem vindo a ser catalogado e sistematizado à medida que a medicina evolui. Passando por novas técnicas de conservação e tratamento de tecido humano, de que são exemplo as dissecções de Klinger, nas quais se fazem secções de material conservado criogenicamente, bem como por estudos histológicos através da utilização de corantes, conseguiu-se uma forma complementar de realizar estes estudos. Permanecia, no entanto, a impossibilidade de analisar *in vivo* a estrutura e função dos diferentes sistemas que constitutem o Homem.

Com o surgimento das técnicas imagiológicas o diagnóstico e monitorização do corpo humano, bem como das patologias a ele associadas, melhoraram consideravelmente. Mais recentemente, com o aparecimento da ressonância magnética (MRI: do Inglês "Magnetic Resonance Imaging"), tornou-se possível estudar as propriedades magnéticas do tecido, reflectindo as suas características intrínsecas com base na aplicação de impulsos de radiofrequência. Através de ressonância magnética é possível estudar essas propriedades em vários núcleos atómicos, sendo mais comum o estudo do hidrogénio, pois somos maioritariamente consistituídos por água e gordura.

Uma vez que só é possível medir variações do campo magnético, aplicam-se impulsos de radiofrequência para perturbar o equilíbrio dos spins e medir os seus mecanismos de relaxação, os quais, indirectamente, reflectem a estrutura do tecido. Contudo, o sinal medido é desprovido de qualquer informação espacial. De facto, para podermos proceder a essa quantificação, é necessária a utilização de gradientes de campo magnético, que permitem modificar localmente a frequência de precessão dos protões, através da alteração local do campo magnético, permitindo assim, adquirir o sinal de forma sequencial. A informação obtida constitui uma função variável no espaço e através da transformação de Fourier pode ser quantificada em frequências espaciais, sendo estes dados armazenados no espaço k. O preenchimento deste espaço, caracterizado por frequências espaciais, bem como os gradientes de campo magnético que são aplicados, permitem determinar a resolução da imagem que podemos obter, aplicando uma transformação de Fourier inversa.

O estudo da ressonância magnética não se restringe à análise da estrutura mas também ao estudo da função e difusão das moléculas de água. A difusão é um processo aleatório, que se

traduz pelo movimento térmico das moléculas de água, e o seu estudo permite inferir sobre o estado do tecido e microestrutura associada, de uma forma não invasiva e *in vivo*. A técnica de imagiologia de ressonância magnética ponderada por difusão (DWI: do Inglês "Diffusion Weighted Imaging") permite o estudo da direccionalidade das moléculas de água e extracção de índices que reflectem directamente a integridade dos tecidos biológicos. De modo a sensibilizar as moléculas de água à difusão, é necessário aplicar sequências de ressonância magnética modificadas, nas quais se aplicam gradientes de campo magnético de difusão para quantificar o deslocamento das moléculas e a sua relação com o coeficiente de difusão das mesmas.

Num ambiente livre e sem barreiras a difusão das moléculas de água é isotrópica, uma vez que se apresenta igual em todas as direcções. Todavia, tal não se verifica no corpo humano. A presença destas barreiras leva a que, na verdade, apenas possa ser medido um coeficiente de difusão aparente. Este, por sua vez, traduz a interacção entre as moléculas de água com a microestrutura e, como tal, uma anisotropia na sua difusão. Como caso particular de difusão anisotrópica a nível cerebral, tem-se a difusão das moléculas de água na matéria branca, uma vez que esta apresenta uma direccionalidade preferencial de acordo com a orientação dos axónios, visto estarem presentes menos restrições à sua propagação, ao contrário do que acontece com a direcção perpendicular (devido à membrana celular e às bainhas de mielina). Por oposição, a matéria cinzenta, constituída pelo aglomerado dos corpos celulares dos neurónios, e o líquido cefalorraquidiano apresentam uma difusão sem direcção preferencial (i.e. aproximadamente isotrópica).

A informação obtida através da difusão das moléculas de água encontra-se limitada pelo número de direcções segundo o qual aplicamos os gradientes de difusão. Deste modo, surgiu a imagiologia por tensor de difusão (DTI: do Inglês "Diffusion Tensor Imaging"). Esta técnica permite extrair informação acerca da tridimensionalidade da distribuição da difusão de moléculas de água através da aplicação de seis gradientes de difusão não colineares entre si. A distribuição destas moléculas pode, então, ser vista como um elipsóide, no qual o principal vector próprio do tensor representa a contribuição da difusão das moléculas segundo a direcção do axónio (ou paralela), sendo os dois restantes componentes responsáveis pela contribuição transversal.

Além da difusividade média (MD: do Inglês "Mean Diffusivity") e das contribuições da difusão paralela ($MD_{//}$) e perpendicular ($MD\perp$) às fibras, é também possível extrair outros índices, como a anisotropia fraccional (FA: do Inglês "Fractional Anisotropy"), que fornece

informação acerca da percentagem de difusão anisotrópica num determinado *voxel*. Para a matéria branca, tal como já foi referido, existe difusão preferencial e, portanto, a anisotropia fraccional será elevada. Por outro lado, para a matéria cinzenta e para o líquido cefalorraquidiano, verificar-se-á uma FA reduzida, devido à ausência de anisotropia.

Todavia, regiões com reduzida anisotropia fraccional podem camuflar regiões de conformação de cruzamento de fibras, ou fibras muito anguladas, que a imagiologia por tensor de difusão não consegue resolver. A razão para esta limitação reside no número reduzido de diferentes direcções de difusão que são exploradas, assim como o pressuposto de que a distribuição das moléculas de água é Gaussiana em todo o cérebro, o que não é necessariamente verdade.

A fim de se ultrapassar estas limitações, novas técnicas surgiram, nomeadamente as de elevada resolução angular (HARDI: do Inglês "High Angular Resolution Diffusion Imaging"). Estas fazem uso de uma aquisição em função de múltiplas direcções de gradiente e de uma diferente modelação dos dados obtidos, dividindo-se em dois tipos. As técnicas livres de modelos permitem extrair uma função de distribuição da orientação das fibras num determinado *voxel* directamente do sinal e/ou transformações da função densidade de probabilidade do deslocamento das moléculas de água. Contrariamente, as técnicas baseadas em modelos admitem existir determinados constrangimentos anatómicos e que o sinal proveniente de um determinado *voxel* é originado por um conjunto de sinais individuais de fibras, caracterizados por uma distribuição preferencial das direcções das fibras.

Todos estes métodos têm como objectivo principal recuperar a direcção preferencial da difusão das moléculas de água e reconstruir um trajecto tridimensional que represente a organização das fibras neuronais, pelo que se designam métodos de tractografia. Esta representa a única ferramenta não invasiva de visualização *in vivo* da matéria branca cerebral e o seu estudo tem revelado uma grande expansão associada ao estabelecimento de marcador biológico para diversas patologias. Adicionalmente, esta técnica tem vindo a tornar-se uma modalidade clínica de rotina e de diversos protocolos de investigação, sendo inclusivamente utilizada para complementar o planeamento em cirurgia, devido à natureza dos dados que gera. Particularmente no caso de dissecções manuais, nas quais os dados de tractografia são manuseados por pessoal especializado, com vista a realizar a parcelização de diferentes tractos de interesse, o processo é moroso e dependente do utilizador, revelando-se necessária a automatização do mesmo. Na realidade, já existem técnicas automáticas que fazem uso de

algoritmos de agregação[1], nos quais fibras são analisadas e agrupadas segundo características semelhantes, assim como técnicas baseadas em regiões de interesse, em que se extraem apenas os tractos seleccionados entre as regiões escolhidas.

O objectivo principal desta dissertação prende-se com a análise automática de dados de tractografia, bem como a parcelização personalizada de tractos de interesse, também esta automática. Em primeiro lugar, foi desenvolvido um algoritmo capaz de lidar automaticamente com funções básicas de carregamento dos ficheiros de tractografia, o seu armazenamento em variáveis fáceis de manusear e a sua filtragem básica de acordo com regiões de interesse de teste. Neste processo de filtragem é feita a avaliação das fibras que atravessam a região de interesse considerada. Assim, após a localização das fibras entre as regiões de interesse os tractos resultantes podem ser guardados de duas formas, as quais têm, necessariamente, que ser especificadas antes de utilizar o software: um ficheiro que contém todas as fibras resultantes da parcelização e outro que contém o mapa de densidade associado, isto é, o número de fibras que se encontra em cada *voxel*. Após esta fase inicial, a flexibilidade e complexidade do software foi aumentando, uma vez que foram implementados novos filtros e a possibilidade de utilizar regiões de interesse de diferentes espaços anatómicos padrão. Fazendo uma análise a esta última melhoria, pode referir-se que, através de um procedimento de registo não linear da imagem anatómica do espaço padrão ao espaço individual de cada sujeito, foi possível, de forma automática, guardar o campo de deformações que caracteriza a transformação e, assim, gerar regiões de interesse personalizadas ao espaço do sujeito. Estas regiões de interesse serviram depois para a parcelização básica e para seleccionar tractos, mas também para filtragens adicionais, como a exclusão de fibras artefactuosas[2] e um filtro especial, no qual apenas os pontos que ligam directamente as diferentes regiões são mantidos. Além do que já foi referido, recorreu-se também à aplicação de planos de interesse que actuam como constrangimentos neuroanatómicos, o que não permite, por exemplo, no caso da radiação óptica, que as fibras se propaguem para o lobo frontal.

Esta ferramenta foi utilizada com sucesso para a parcelização automática do Fascículo Arcuado, Corpo Caloso e Radiação Óptica, tendo sido feita a comparação com a dissecção manual, em todos os casos. O estudo do Fasciculo Arcuado demonstrou ser o teste ideal para a ferramenta desenvolvida na medida que permitiu identificar o segmento longo, assim como descrito na literatura. O método automático de duas regiões de interesse deu a origem aos

---

[1] do inglês, *clustering.*
[2] do inglês *spurious.*

mesmos resultados obtidos manualmente e permitiu confirmar a necessidade de estudos mais aprofundados. Aumentando a complexidade do estudo, realizou-se a parcelização do Corpo Caloso de acordo com conectividade estrutural, isto é, com diferentes regiões envolvidas em funções distintas. Procedeu-se deste modo, e não com base em informação acerca de divisões geométricas, uma vez que estas já demonstraram incongruências quando correlacionadas com subdivisões funcionais. O uso adicional de regiões de interesse para a exclusão de fibras demonstrou-se benéfico na obtenção dos mapas finais. Finalmente, incluiu-se a utilização de um novo filtro para realizar a parcelização da Radiação Óptica, comparando os resultados para DTI e SD(do Inglês "Spherical Deconvolution"). Foi possível determinar limitações na primeira técnica que foram, no entanto, ultrapassadas pela utilização de SD. O atlas final gerado apresenta-se como uma mais-valia para o planeamento cirúrgico num ambiente clínico.

O desenvolvimento desta ferramenta resultou em duas apresentações orais em conferências internacionais e encontra-se, de momento, a ser melhorada, a fim de se submeter um artigo de investigação original. Embora se tenha chegado a um resultado final positivo, tendo em conta a meta previamente estabelecida, está aberto o caminho para o seu aperfeiçoamento. Como exemplo disso, poder-se-á recorrer ao uso combinado das duas abordagens de parcelização automática e à utilização de índices específicos dos tractos, o que poderá trazer uma nova força à delineação dos tractos de interesse. Adicionalmente, é também possível melhorar os algoritmos de registo de imagem, tendo em conta a elevada variabilidade anatómica que alguns sujeitos apresentam.

Como nota final, gostaria apenas de salientar que a imagiologia por difusão e, em particular, a tractografia, têm ainda muito espaço para progredir. A veracidade desta afirmação traduz-se pela existência de uma grande variedade de modelos e algoritmos implementados, sem que, no entanto, exista consenso na comunidade científica acerca da melhor abordagem a seguir.

ABSTRACT

Diffusion weighted imaging (DWI) has provided us a non-invasive technique to determine physiological information and infer about tissue microstructure. The human body is filled with barriers affecting the mobility of molecules and preventing it from being constant in different directions (anisotropic diffusion). In the brain, the sources for this anisotropy arise from dense packing axons and from the myelin sheath that surrounds them.

Only with Diffusion Tensor Imaging (DTI) it was possible to fully characterize anisotropy by offering estimations for average diffusivities in each voxel. However, these methods were limited, not being able to reflect the index of anisotropic diffusion in regions with complex fibre conformations. It was possible to reduce those problems through the acquisition of many gradient directions with High Angular Resolution Diffusion Imaging (HARDI).

There are model-free approaches such as Diffusion Spectrum Imaging (DSI) and Q-ball Imaging (QBI) which retrieve an orientation distribution function (ODF) directly from the water molecular displacement. Another method is Spherical Deconvolution, which is a model-based approach based on the computation of a fibre orientation distribution (FOD) from the deconvolution of the diffusion signal and a chosen fibre response function.

Reconstructing the fibre orientations from the diffusion profile, generates a three-dimensional reconstruction of neuronal fibres (Tractography) whether in a deterministic, probabilistic or global way. Tractography has two main purposes: non-invasive and *in vivo* mapping of human white matter and neurosurgical planning. In order to achieve those purposes it is common to apply parcellation techniques which can be subdivided into ROI-based or Clustering base.

The aim of this project is to develop an automated method of tract-based parcellation of different brain regions. This tool is essential to retrieve information about the architecture and connectivity of the brain, overcoming time consuming and expertise related issues derived from manual dissections. Firstly we investigated basic functions to handle diffusion and tractography data. In particular, we focused on how to load track files, filter them according to regions of interest and save the output in different formats. Results were always compared with manual dissection. The developed tool increased complexity by introduction a new filtering and the use of regions of interest from different standard spaces, created trough non-linear registrations. Three major tracts of interest were analysed: Arcuate Fasciculus, Corpus Callosum and Optic Radiation.

KEY-WORDS

Magnetic Resonance Imaging (MRI); Diffusion Weighted Imaging (DWI); High Angular Resolution Diffusion Imaging (HARDI) methods; Orientation Distribution Function (ODF); Tractography; Parcellation, Clustering.

Acknowledgments

I would like to thank everyone that made this thesis possible.

First of all, I would like to thank my supervisor Dr. Flavio Dell' Acqua for all the patience, hard working afternoons and weekends, useful suggestions and corrections, and for being always there when I needed. His involvement in this project made it possible to achieve a great work and more important, for me to have fun, whilst doing something I like. Moreover, despite supervising me from Portugal, Dr Hugo Ferreira, my internal supervisor, managed to keep me supported and helped me whenever I needed. I would also like to thank both for their corrections of the manuscript.

For my officemate, Richard Joules, and for our endless discussions ranging from music to physics, I say to him a very thoughtful thank you for making my stay in London one of the best experiences of my life. To the rest of the group that I have encountered, namely Vincent Giampetro, Mick Brammer, Cédric Ginest, Gareth Barker, Steve Williams, David Slater, Marco Catani, Michel Thiebaut de Schoten, Stephanie Forkel, Leslie Annoushka and Heather Hipwell, my sincere thank you for making me feel at home and for helping me grow in every aspect.

I want to thank my friends and flatmates Débora and Filipa, for sharing with me the experience of living and studying in a foreign country.

I would also like to thank, Professor Eduardo Ducla Soares, for so warmly welcoming me five years ago, when I enrolled the course of Biomedical Engineering and Biophysics. Besides that, he has always encouraged me to give my best and look for opportunities where they arise. Dr Rita Nunes has also made it possible for me to get this opportunity by putting me in contact with London and to what expected me.

I would also like to thank to the Erasmus funding programme and Dr Guiomar Evans who helped me in every burocratic issue that I required.

There are not enough words to say how much I am grateful for all the help and support I got from my parents, Paula and Luís. For always making me believe in myself and cheering me when I was down, I thank them.

Last but definitely not least, I write a few words for my girlfriend, Maria João. If there was someone who encouraged me to endeavour such an adventure was her, even though we would be apart for several months. Not only she helped me whenever I needed but also kept the distance shorter by staying in touch with my almost every day. One of the reasons that made me find opportunities abroad was also to be able to build a life with her. I treasure her the most and I am sure that we will continue together.

Finally, I would like to dedicate this thesis to Philip Batchelor, with whom I was supposed to work. He sadly left us last year, but we will hold is memory..

List of Figures

List of abbreviations

2D	Two Dimensional
3D	Three Dimensional
6D	Sixth Dimensional
ADC	Apparent Diffusion Coefficient
BW	Bandwith
CHARMED	Composite Hindered And Restricted Model Of Diffusion
CSF	Cerebrospinal Fluid
DKI	Diffusional Kurtosis Imaging
DSI	Diffusion Spectrum Imaging
DTI	Diffusion Tensor Imaging
DWI	Diffusion Weighted Imaging
EPI	Echo Planar Imaging
ECG	Electrocardiogram
FA	Fractional Anisotropy
FID	Free Induction Decay
FOD	Fiber Orientation Distribution
FOF	Fibre Orientation Function
FOV	Field Of View
FRT	Funk–Radon Transform
GE	Gradient Echo
GF	Frequency-Encoding Gradient
GM	Grey Matter
GP	Phase-Encoding Gradient
GS	Slice-Selection Gradient
HARDI	High Angular Resolution Diffusion Imaging
HMOA	Hindrance Modulated Orientational Anisotropy
IFOF	Inferior Fronto Occipital Fasciculus
IT	Inversion Time
LGN	Lateral Geniculate Nucleus
MCMC	Markov Chain Monte Carlo
MESD	Maximum Entropy Spherical Deconvolution
MIP	Maximum Projection Intensity

MRI	Magnetic Resonance Imaging
NEX	Number of Excitations
OD	Orientation Dispersion
ODF	Orientation Density Function
PAS-MRI	Persistant Angular Structure - Mri
PDF	Probability Density Function
PGSE	Pulsed Gradient Spine Echo
PSD	Pulse Sequence Diagram
QBI	Q-Ball Imaging
QSI	Q-Space Imaging
RA	Relative Anisotropy
RF	Radio Frequency
RL-SD	Richardson-Lucy Spherical Deconvolution
ROI	Region Of Interest
RMSE	Root Mean Square Error
SAR	Specific Absorption Rate
SD	Spherical Deconvolution
SE	Spin Echo
SNR	Signal To Noise Ratio
TE	Echo Time
TR	Repetition Time
TRSE	Twice Refocused Spin Echo
WM	White matter

Motivation

The title of this thesis is "HARDI Methods – Tractography Reconstructions and Automatic Parcellation of Brain Connectivity" and has the main purpose of developing an automated method to parcellate different brain regions. This will generate a rather important tool for the study of structural connectivity on the brain and to further matching of functional data, with the final purpose of providing a different and more accurate way to perform neurosurgical planning.

1 – Introduction

The study of anatomy has long been seen as a quest for the understanding of human body, something that is well established nowadays. However, neuroanatomy is still one of the most open topics in science since there are several cognition functions and relations between anatomical structures that are still not known. The latest decades brought new ways to study the human brain, marking a side by side evolution with the traditional techniques of autopsying and dissections.

The main aim of this thesis is to study diffusion of water molecules by magnetic resonance imaging and make use of the retrieved information to infer three dimensional pathways of human white matter (WM). This representations is still far from perfect, however, it allows us to infer about structural connectivity in a macroscopical scale and therefore is very useful for generating maps of human white matter and to help in neurosurgical planning, for example. Furthermore, as these procedures are very time consuming and user dependent, it is essential to automate the process. An automatic tool for the automatic parcellation of different brain regions is then developed, and applied to three major tracts: Arcuate Fasciculus, Corpus Callosum and Optic Radiation.

This thesis is divided into eight main chapters: this introduction, four chapters related to basic principles, about Magnetic Resonance Imaging (MRI) (chapter 2), Diffusion and HARDI methods (chapter 3), Tractography (chapter 4) and Parcellation Techniques (chapter 5) important to this work; Methods (chapter 6), Results (chapter 7), Discussion (chapter 8); Conclusion / future prospects (Chapter 9).

2 – Magnetic Resonance Imaging

Magnetic Resonance Imaging (MRI) is a non-invasive diagnosis technique whose principal objective is to generate morphological images of the human body, particularly with great resolution and contrast at tissue level. However, it can also be used as a technique that gives physiological information. In MRI we are interested in the magnetic properties of atomic nuclei, in particular for the hydrogen nucleus, which consists of a proton, and for its properties like the quantum number of spin. Other nuclei may be used in MRI but there is a preference for hydrogen due to its abundance in fat and in water. MRI allows for a great variety of sequences to be obtained when different acquisition parameters are changed, depending on the specific objective of the study.

2.1 – Physical Principles

When placed in a static magnetic field, protons are oriented according to its direction and a difference can be observed regarding two different energy levels: a predominance of protons in the direction parallel to the magnetic field when compared to the antiparallel direction. Protons have a higher probability of being oriented according to the static magnetic field direction, because it corresponds to the least energy state (more probable).
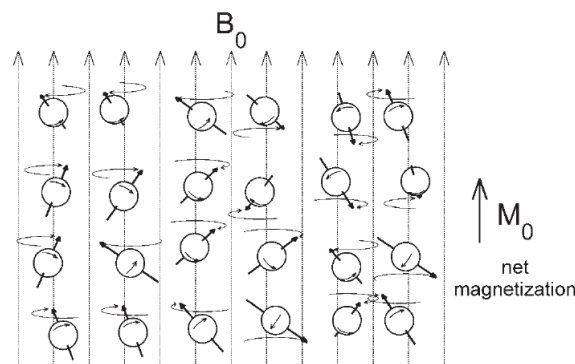
Figure 1 - Precessional movement, resulting from the action of an external magnetic field. In this case, it can be seen that there is a relative higher number of protons oriented according the magnetic field, giving rise to a net longitudinal magnetization M0 (Pottumarthi 2006)**.**

Because protons do not instantly get oriented with the external magnetic field with respect to their energy, having constant switches of position between states, nuclei aren't immediately aligned with the field but instead develop a precessional movement towards it. We can determine the Larmor frequency (ω) at which the proton spins around the magnetic field direction using the formula 1:

$$\omega = \gamma * B_0 \text{ where } \gamma (gyromagnetic\ ratio) = \frac{2\pi * \nu}{B_0} \qquad\qquad 1$$

Protons do not precess in phase and due to a predominance of magnetic moments oriented with the magnetic field a M_0 component arises resulting of the vectorial sum of the magnetic moments oriented with the field (**Figure 1**). This component is called longitudinal magnetization.

Since we can only measure magnetic field disturbances, we have to oscillate longitudinal magnetization over the xy plane, originating a new component, called transverse magnetization,

M_{xy}. To interfere with the spins equilibrium one need to emit a Radio Frequency (RF) pulse in the x direction, exactly with the Larmor frequency, so that protons can now precess in a new direction and coherently (in phase) (R. Hashemi, W.G Bradley 2010). The extent and intensity of the RF pulse allows one to control the flip angle of the longitudinal magnetization to the xy plane.
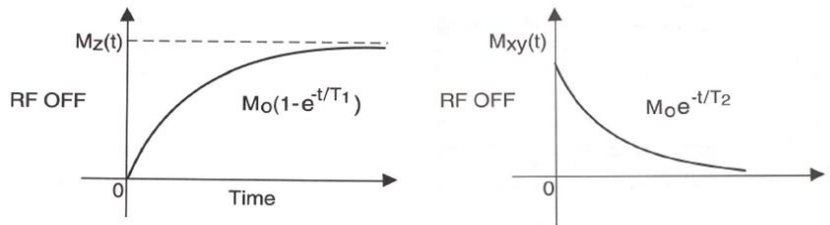
Figure 2 - Longitudinal magnetization recovery mechanism (left) and Transverse magnetization relaxation mechanism (right) (R. Hashemi, W.G Bradley 2010)**.**

Two different time periods can be defined in relation to the above mechanisms (**Figure 2**), after the suspension of the RF pulse:

- T1, or spin-lattice relaxation, is the time that takes for 63% of longitudinal magnetization to recover along z axis, after pulse application, leading to the passage of the spins from the antiparallel level to parallel level, with energy devolution to the lattice. This change in spins state happens mainly due to an interaction with magnetic fluctuations of the lattice, and the time it takes depends on the mobility of protons in different molecules.

- T2, or spin-spin relaxation, consists in the relaxation of transverse magnetization, from a certain value, which is determined from the RF pulse duration/intensity. The interactions between spins will lead to a faster dephasing as the small magnetic field originated by each spin influences the other. Basically, if the dephasing velocity of the spins is higher, T2 is short and if, on the other hand, spins take longer to dephase, T2 is long. If we also take in account the inherent field inhomogeneities, we will get T2* which is shorter than T2 because it leads to faster dephasing.

The variation of the transverse magnetization is detected by a coil, and using Faraday's law of induction, ($\varepsilon = \frac{d\phi_B}{dt}$), an electric current is induced and decays exponentially as relaxation undergoes. This signal is called Free Induction Decay (FID) since the nucleus precesses "freely" without the application of a RF pulse.

2.2 – Imaging Sequences

As stated before there is a great variety of sequences in MRI and here only two will be shown, which are important to understand further concepts along this thesis.

2.2.1 - Spin Echo

The first sequence is one of the most widely used sequences in MRI: Spin Echo (SE) sequence. This technique consists of the application of a 90º RF pulse, followed by a time span, t, after which we apply another pulse, of 180º instead of 90º, resulting in the retrieval of information after a total time 2t. Like we have seen before, at the moment the RF pulse is suspended, protons lose they coherence and start dephasing, with different frequencies. After a

certain period t, by applying a 180º pulse, we change the orientation of spin precession, and the ones which were precessing faster (**Figure 3** A) are now behind those that precessed at a lower frequency (**Figure 3** B). This will lead to a regain of coherence after the same amount of time, t, and to the emission of a spin echo, since phase differences will cancel out. The amount of time that goes from the application of the first 90º RF pulse and the maximum of the echo is called echo time (TE).

MRI entails gathering a large amount of spatial information and the spatial resolution is determined by the number of times the sequence is repeated in each excitation. Therefore it requires several excitation pulses to acquire different signals. Following this, we can establish another important parameter, repetition time (TR) that is the time span between the application of two consecutive 90º RF pulses.
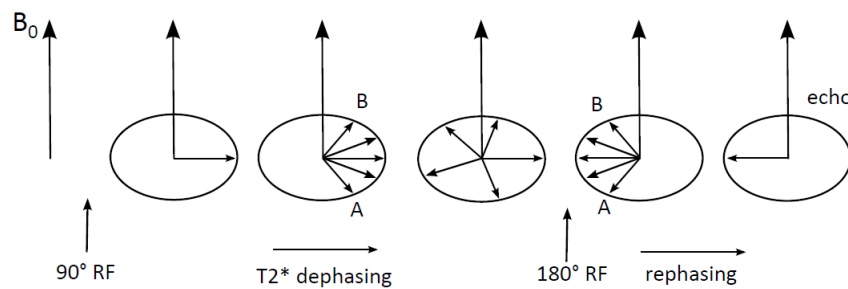
Figure 3 - Phase changes during Spin Echo procedure.

Nowadays, the sequence that is used the most is Fast Spin Echo, a modified sequence of the one represented above. In this sequence, instead of acquiring one echo as a separate phase encoded step, each echo is recorded as an individual line into one single k-space. One of the great advantages of this technique is the fact that allows considerable savings regarding scan time. Those savings are proportional to the length of echoes that are generated, i.e, number of 180º RF pulses that are applied after the first 90º RF pulse (Carroll et al. 2010).

The process of spatially decode the FID and how it is stored in k-space will be explained under the section Image acquisition.

2.2.2 - Gradient Echo

These techniques are very similar to Spin Echo techniques and rely on reduced acquisition times. To accomplish fast acquisitions, the nutation angle (α) is frequently chosen below 90º, in order to allow a more rapid longitudinal magnetization recover. The optimal angle for a particular value of TR and a specific tissue is given by $\cos(\alpha_e) = e^{\frac{-TR}{T1}}$ and is called the Ernst angle. Unlike spin echo related techniques in gradient echo (GE), the measured echo is not originated by a 180º RF pulse but from polarity inversion of field gradients, thus the name for this technique. After the initial 90º RF pulse the first gradient pulse is applied and the spin population that gradually starts to precess with different frequencies, will regain coherence by the application of a gradient with inverse polarity and same intensity (Hendrix 2004). One great advantage over spin echo technique is that the extra burden given by the emission of a 180º RF pulse is avoided, yielding less heating by the patients.
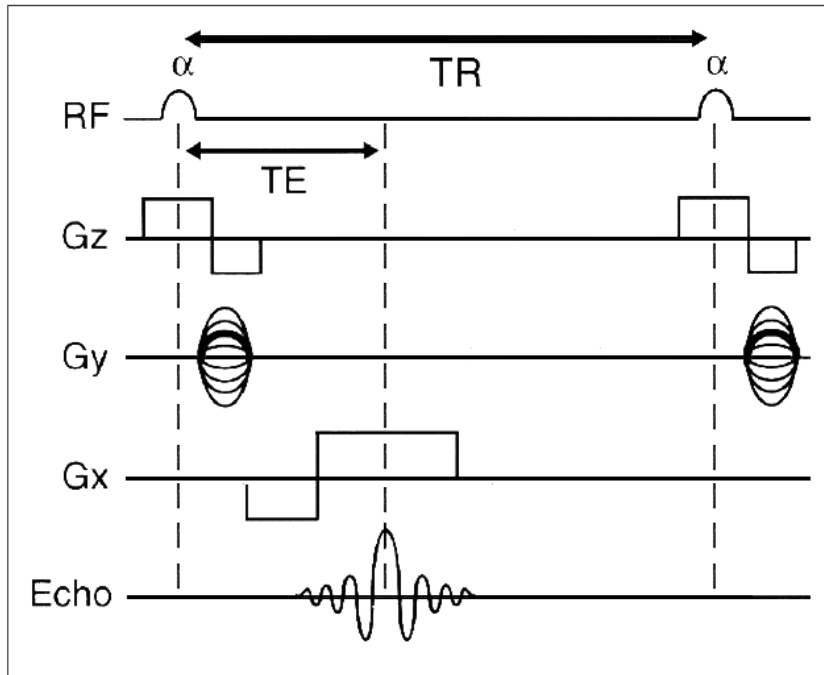
Figure 4 - Gradient Echo sequence Pulse Sequence Diagram (PSD) (R. Hashemi, W.G Bradley 2010)**.**

2.2.3 - Echo Planar Imaging

Echo Planar Imaging (EPI) is one the fastest sequence mode in MRI by generating images in the order of tens of milliseconds. It can be very useful to study physiological phenomena such as diffusion (David S Tuch 2002; Le Bihan et al. 2001) and perfusion. This sequence allows us to get a full image after the application of a single 90º RF pulse. The generated echoes are seen as individual phase-encoding steps and are obtained by just applying gradients with different polarities (like in gradient echo imaging) or an *echo train* (series of 180º RF pulses in SE type sequences). In order to achieve this, there are heavy requirements in terms of how fast gradients can change and the maximum intensity they can achieve. It is also very important to have RF receiver and transmitter coils that do not induce eddy-currents distortion (Turner et al. 1990).

2.3 – Image Acquisition

FID is received from all protons with no spatial discrimination and in order to get it, we need to specify the x,y,z coordinates of the signal, by the use of gradients. A gradient is a particular spatial change of magnetic field, which consists in an increase or decrease of intensity. Thus, protons present themselves with a slightly different precessional frequency at different positions, reflecting the anatomical structure of tissue. A magnetic field is then created by flowing an electric current through a coil. When we change the electric currents orientation, we also change the magnetic field orientation. In MRI, pairs of coils are used in directions x,y and z with same intensity but different polarity, so that one can lead to an increase in the magnetic field and on the other hand a decrease, establishing the magnetic field gradients.

Spin-echo pulse sequence
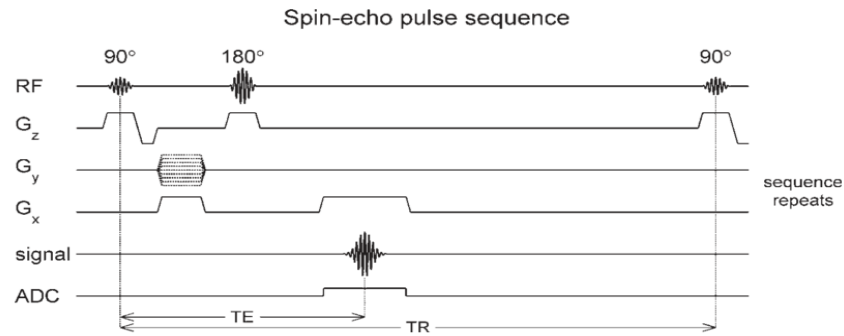
Figure 5 - Spin echo PSD (Pottumarthi 2006)**.**

The usual procedure followed to acquire an image is now presented (accordingly to **Figure 5**) for standard SE sequence. We first activate a gradient in z direction (same direction as static magnetic field) in order to select our region of interest (ROI), simultaneously to the emission of a 90º RF pulse. This is called the Slice-Selection Gradient (GS). The pulse is emitted with a certain bandwidth (centred in a ω_0 frequency) in order to stimulate a determined region Δz, instead of just an infinitesimal thin 2D slice. Only in this region, resonance is observed. The slice can be interpreted as a 3D matrix, whose basic element is a voxel.

After the slice has been selected, we still need to know how to get individual information from each voxel. We consider for example a 256 x 256 matrix in which each column and row must be differentiated. After this procedure, between the first 90º RF pulse emission and the TE another gradient is applied. As a result, protons will precess with slightly different speeds along y axis, showing phase differences proportional to its localization. Therefore this gradient is called Phase-Encoding Gradient (GP) due to phase coding. During the echo reading we apply the last gradient in the x direction and the spins start to act differently along this axis. This is known as Frequency-Encoding Gradient (GF), since it is related to a frequency coding.

By applying these gradients we linearly vary the frequency with spatial position (Larkman & Rita G Nunes 2007). Therefore, at this point we start to fill a new matrix, called k-space, with unprocessed information through the application of Fourier transform in which each line corresponds to a phase encoding step, letting us now know the spatial encoding. As a single phase encode step is responsible for filling one line in k-space, the number of phase encoding steps will determine image resolution, which entails repeating the sequence. Namely, the shift considered when sampling k-space is inversely proportional to the Field of View (FOV) and the highest spatial frequency inversely proportional to the voxel size (R. Hashemi, W.G Bradley 2010).

Data in k-space are spatial frequencies of the image, where the central ones contribute with image contrast and most part of the signal of tissues, while peripheral frequencies provide high detail about the image itself, but little information about contrast. Performing the inverse Fourier transform will allow one to arrive at image space from the spatial frequency space (k-space).

2.4 – Image Parameters

For any type of sequence there are several parameters that can be defined by the user, accordingly to the study he is undergoing and which will influence image acquisition:

➔ Time parameters such as TE, TR, the flip angle and for inversion techniques (not scoped in this text) the inversion time (IT);

➔ Spatial parameters like the FOV which is defined as the size of the spatial encoding area, slice thickness and the matrix size specify image resolution both in plane (number of pixels) and in depth.

Ultimately we can get information about the signal to noise ratio (SNR) based on the following formula:

$$SNR = \left(\frac{FOVx}{Nx}\right)(FOVy)\Delta z \sqrt{\frac{NEX}{(Ny)(BW)}} \hspace{2cm} 2$$

where $FOVx$ e $FOVy$ represent the field of view in directions x e y, respectively (in mm), Nx and Ny the matrix dimensions, NEX the number of excitations, Δz the slice thickness and BW the pulse bandwidth.

The acquisition time is calculated by the multiplication of the matrix size, TR and the number of excitations.

2.5 – Safety

Even though the study of magnetic resonance imaging hasn't been proven unsafe, there are three main safety-related issues that can be identified: static magnetic fields, field gradients and RF pulses (Crook & Robinson 2009). The ongoing evolution in research has lead to the use of static magnetic fields of higher intensities. Both blood flow and the alignment of external segments of rod cells in retina are influenced by these magnetic fields. High fields can also cause nauseas since they disturb the vestibular system in the inner ear, when the subject moves close to the magnet. Regarding field gradients, we can identify excitation of cardiac tissue (even if only above 3% of the excitation plateau); peripheral nerve stimulation and inner ear stimulation as previously described. RF pulses may lead to the increasing Specific Absorption Rate (SAR) which translates the rate of absorbed energy by the body when exposed to a radio frequency electromagnetic field, measured in W/Kg. In this manner, termic deposition is increased on body surface.

Despite being a non-invasive and involving non-ionizing radiation, this technique is not risk free, being one of the greatest security issues the presence of metallic objects closer to the MRI scanner.

Figure 6 - MR related accident by bringing metallic objects to the scanner room (NessAiver 2008)**.**

Efforts need to be done so that patients that have metallic objects like *pacemakers* and cochlear implants may be safely scanned, without any risk of damaging the patient and/or destroying such devices.

One other recommendation often given to subjects is to avoid keeping their arms in a closed loop to avoid the generation of electric currents and the subsequent burn. Claustrophobia is another topic that is recurring in MRI, but new strategies have been devised whether to make it more appealing in the case of infant imaging or in the increasing of bore size by hardware modifications.

Most of the scanner used nowadays make use of superconducting magnet which relies on helium to cool down the magnet to a critical temperature in which the resistance to electric current is null. *Quenching* is a type of instrumental accidents that derives from the overheating of helium that may begin to boil, gradually replacing the air in the scanner room, leading to suffocation (Andrew Simmons & Hakansson 2011).

3 – Diffusion Weighted Imaging

Diffusion has long been observed as the random displacement of particles in a fluid by Robert Brown (1828). It was first described mathematically when Adolf Fick stated that the diffusion of matter is proportional to the gradient of its concentration with a proportionality factor k, which is "dependent according to the nature of substances", yielding a net displacement from high to low concentrated regions (Philibert 2005). It was not until the work by Einstein that the Brownian motion (in honour of its discoverer) and the diffusion coefficient (D) could be quantified and calculated by evaluating the average mean displacement of particles (R) over time (t) (formula 3).

$$D = \frac{<R^2>}{6t} \qquad\qquad 3$$

It should be stated that diffusion depends on temperature (there is a different diffusion coefficient for different temperatures), molecular weight and viscosity of the medium (Le Bihan 1995). Applying the concepts underlying diffusion and MRI has provided us a non-invasive technique to determine physiological information as well as quantify the random thermal movement of water molecules, making it possible to infer about tissue microstructure, through the use of Diffusion Weighted Imaging (DWI) (Le Bihan et al. 1986).

3.1- Basic Principles

In a medium with no considerable barriers, water molecules displacement is constant in every direction, i.e., we are in the presence of an isotropic diffusion. However, the human body is filled with barriers such as cell membranes, axon fibres, amongst others, leading the mobility of molecules to be affected and yielding an anisotropic diffusion which is not constant for different directions (Beaulieu & Allen 1994). In the particular case of parallel axon fibres, diffusion is much more pronounced in the direction of fibres and not in the transverse direction (S Mori & P. B. Barker 1999; D Alexander 2006). It has been studied that the sources for this anisotropy arise from dense packing axons (and their axonal membranes) and from the myelin sheath that surrounds them, hindering diffusion in the transverse direction(Beaulieu 2002).

3.1.1 - Sequence Pulsed Gradient Spin Echo (PGSE)

In such environment where diffusion is restricted we can only infer a mean displacement of water molecules since their diffusion is hindered to some extent by underlying interaction with tissue. Therefore we measure an Apparent Diffusion Coefficient (ADC), which is to some level a percentage of isotropic diffusion and not really the intrinsic diffusion value, and take conclusions about tissue microstructure. In order to calculate the ADC parameter there is the need to sensitize water molecules to diffusion. Depending on the direction of the applied diffusion-encoding gradient we are able to detect several different values according to different directions (Stejskal & Tanner 1965). The sequence originally elaborated by Stejskal and Tanner can be visualized in **Figure 7**.
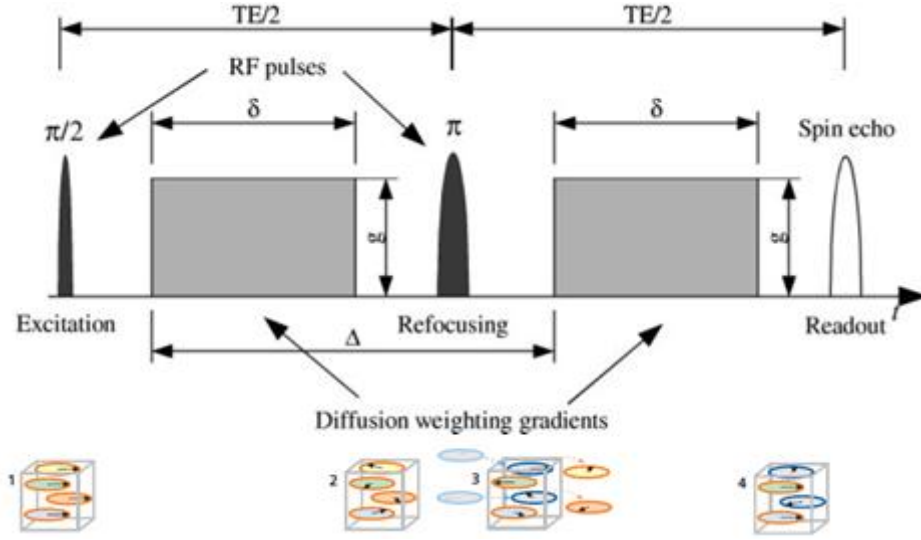
Figure 7 - Pulsed Gradient Spine Echo (PGSE) Adapted from (Minati & We 2007) (S Mori & P. B. Barker 1999) **.**

The general excitation pulse used in DWI is an extension of the general Spin Echo procedure and it is called Pulsed-Gradient Spin Echo. Having into account that measurements in this technique are influenced by spin motion we apply an initial gradient pulse of determined intensity (G) and duration (δ) that offsets the phase of all the spins in a voxel (**Figure 7** (2)); time TE/2 corresponds to the application of a 180º RF pulse that inverts the phase of the population of spins; after a certain time lapse (Δ) from the first gradient, another one of inverse polarity is applied causing the spins to rephase; however, spins move from original position retaining a residual phase offset that allows diffusion quantification (**Figure 7** (4)).

It is also important to know that when we refer to sensitizing gradients and their effect on molecules, we will measure a phase offset of a whole population of spins. Therefore we can talk about finding a phase-distribution function. Besides the natural signal attenuation due to relaxation mechanisms (via T2 relaxation), at the time of measuring the signal, diffusion weighting and the application of the gradients will yield additional attenuation. The expression for the measured signal will then be:

$$S = S_0 e^{(-bD)} \qquad\qquad 4$$

where S_0 is the signal intensity in the absence of diffusion weighting, D is the diffusion coefficient (or ADC) and b is the diffusion weighting factor, a combination of the parameters stated in formula 5 (Stejskal & Tanner 1965) (Price 1997)

$$b = \gamma^2 \delta^2 G^2 (\Delta - \frac{\delta}{3}) \qquad\qquad 5$$

Knowing the signal intensity of the non-weighted diffusion image and the weighted one, while bearing in mind the value of b, allows the determination of the diffusion coefficient (D) that translates water molecules movement. The direction in which the gradient pulse is applied changes the signal intensity in that direction, if diffusion is not isotropic.

The larger the diffusion the smaller will be the signal intensity in diffusion weighted images, since there was more time for spins to dephase, hence the brightest areas will

12

correspond to less diffusion (qualitative maps). In the other hand if we choose to present ADC maps, the brightest areas will be characterized by higher diffusion as we are measuring directly the extent of diffusion rather than signal intensity itself (quantitative maps).

3.1.2 - Artefacts & Corrections

There is a wide range of artefacts that one may encounter in magnetic resonance imaging. They range from magnetic field heterogeneities due to poor shimming (responsible for keeping a homogeneous magnetic field), image distortion as a result of patient's motion and many others. As it is not in the scope of this thesis to thoroughly detail all kinds of artefacts, the choice was made to talk about two major ones that affect MR images, in particular diffusion imaging: cardiac gating and eddy currents distortion.

3.1.2.1 - Eddy Currents/Twice Refocused Spin Echo

An important source of heterogeneities in the magnetic field comes from eddy currents that are generated by the rapid switching of the gradients. This switching produces an electric field at any close conducting surface. The field generated by the eddy currents combines with the intended gradient field to create waveforms distortions, which can result in images artefacts and signal loss. Particularly, it changes the nominal diffusion weighting by biasing the expected gradient intensity and may also leave a geometrical distortion in the image, if it is still decaying at the time of measuring the signal (P J Basser & D. K. Jones 2002).

In the PGSE sequence developed by Stejskal and Tanner, a single refocusing pulse was used to regain phase coherence and lead to the production of the echo to be measured. However, many diffusion sequences can be created using multiple refocusing pulses. The use of more than one refocusing pulse, permits more intervals between the application of pulses and only requires that the amount of spin defocusing and refocusing is the same in the end, when compared to the expected SE sequence. This conclusion lead to the development of a new sequence, namely Twice Refocused Spin Echo (TRSE), that allows to mitigate the eddy current generated by the rapidly switching on and off of the field gradients (T G Reese et al. 2003).
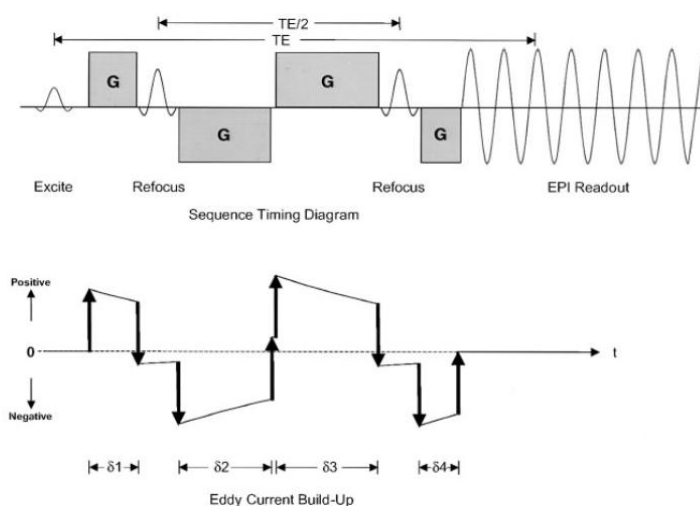
Figure 8 - Twice Refocused Spin echo PSD (T G Reese et al. 2003)**.**

As it relies on shorter intervals between pulses, eddy current build up is lower due to the shorter decay of residual fields during the gradient pulses. Furthermore, by changing the geometry of the pulses into different lengths, the residual fields can be entirely cancelled.

3.1.2.1 - Pulsatile effects/ Cardiac gating

In order to detect the microscopical movement of water molecules, diffusion imaging makes use of sensitizing gradients. However, by doing so we will also generate a great sensitivity to bulk motion such as pulsatile motion of the brain, making the signal dependent on the velocity flows within the object as well as its displacement. This will take the object to displace even by a small amount during acquisition cycles which will cause a discontinuity in k-space and a ghost like artifact, as seen in **Figure 9**, when we generate the image (Turner et al. 1990).
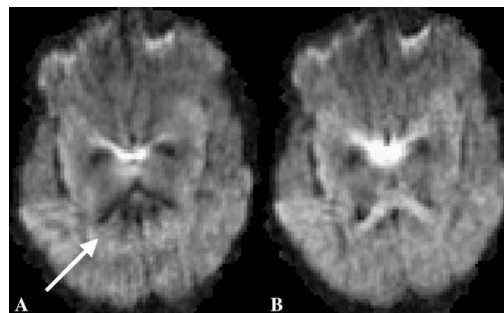
Figure 9 - Image acquired without (A) and with Cardiac gating (Rita G Nunes et al. 2005)**.**

In order to overcome this limitation, the idea arose of acquiring data during periods of low cardiac pulsation motion, technique that was denominated cardiac gating (Habib et al. 2010).

Cardiac gating may be achieved by synchronizing MRI acquisition with the recording of an Electrocardiogram (ECG) and triggering data acquisition based on the position of the cardiac cycle R-wave. It is then possible to apply delay times on the acquisition so that it can be made during diastole without contamination of pulsatile effects (Carroll et al. 2010). However, rapidly switching gradients may cause significant artefacts on the ECG and therefore ruin the gating. For this purpose, peripheral cardiac gating arose which consisted in acquiring a representative signal of the cardiac cycle through the use of a pulse oximeter. Systolic peaks were then detected in order to trigger the acquisition.

Nonetheless, triggering the acquisition is more time consuming and it is documented that brain regions mostly affected reside below the Corpus Callosum. For this purpose, strategies that included acquiring slices of the upper part of the brain during the critical portion of the cardiac cycle improved time acquisition by adapting the number of slices to the maximum estimated heart rate (Rita G Nunes et al. 2005).

3.2- Diffusion Tensor Imaging

Simple diffusion may be explained using a scalar parameter D. However, a tensor it is required to characterize anisotropy, in particular to describe molecular mobility along different directions. Diffusion Tensor Imaging (DTI) was able to overcome this limitation, by providing estimation for the average diffusion or the degree of anisotropy in each voxel as well as the main direction of diffusivities in each voxel and the diffusion values associated with these directions. (P J Basser et al. 1994) The expression for the obtained signal is now:

$$\ln\frac{S}{S_0} = -\sum_i^3 \sum_j^3 b_{ij} \mathbf{D}_{ij} \qquad\qquad 6$$

where b_{ij} is now the b-matrix and $\mathbf{D}_{ij}$ is the diffusion tensor. The b-matrix is calculated from the magnetic field gradient pulse sequences and requires only 6 non-colinear different gradient directions to compute the diffusion tensor, along with the non-diffusion (S_0) image (Mattiello et al. 1994). To improve the estimative of our tensor it is usual to acquire more than the 6 required directions, however other approaches rather than linear regression in the above case are required (T E J Behrens & Johansen-berg 2009).

The diffusion tensor can be represented by an ellipsoid (**Figure 10**) whose: main axis give the main direction of diffusion for that voxel; eccentricity translates the degree of anisotropy and its symmetry (isotropic diffusion would generate a sphere); length is calculated by the amount of displacement of water molecules.
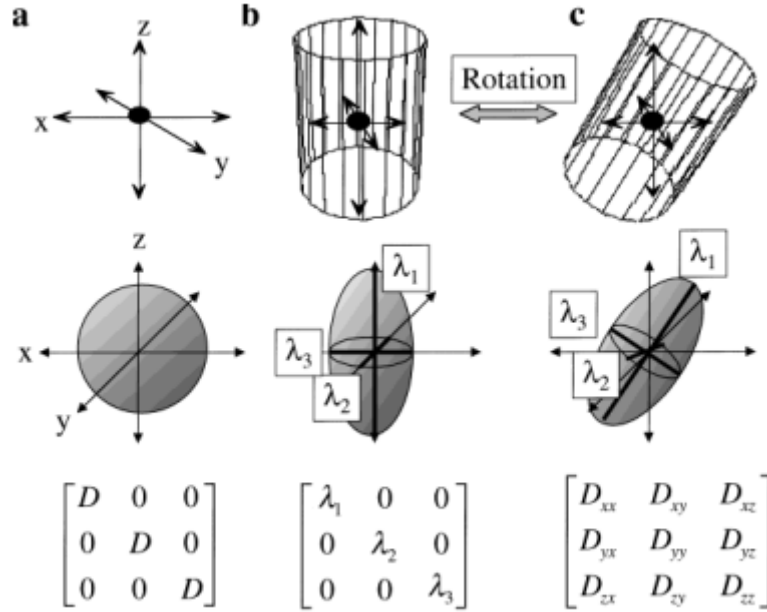
Figure 10 - Diffusion given by an ellipsoid. adapted from (S Mori & P. B. Barker 1999)**.**

The diagonal elements of the tensor correspond to diffusivities along three orthogonal axes, while the off diagonal elements correspond to the correlation between displacements along those orthogonal axes. By convention the first eigenvalue λ_1 translates the direction with higher extent of diffusion, that is axial or parallel diffusivity whilst both λ_2 and λ_3, quantify radial diffusivity (perpendicular to the main direction of diffusion).

The eigenvector/eigenvalue system provides a framework that rotates with the diffusion tensor, and thus any index of anisotropy that is defined within this framework, will be independent of the orientation of the tensor with respect to the laboratory frame of reference (D. K. Jones 2008). However, the principal axis coordinate is unknown and the applied gradient directions (v) generally do not coincide with principal axis system. Therefore it is necessary to apply a rotation matrix (A) that describes the orientation of the principal axis of diffusion tensor regarding the system frame of reference (Dell'Acqua et al. 2007).

$$D(v,A)_{app} = v^T A^T \begin{bmatrix} \lambda_1 & 0 & 0 \\ 0 & \lambda_2 & 0 \\ 0 & 0 & \lambda_3 \end{bmatrix} Av \qquad\qquad 7$$

In order to better characterize diffusion there are several quantities that can be calculated from the tensor such as the trace of the tensor, relative anisotropy (RA) and fractional anisotropy (FA) (P J Basser 1995). The first measure is the sum of the three eigenvalues and it provides a rotationally invariant (yields the same value despite rotation). It is equivalent to 3 times the average diffusivity, so the mean diffusivity (MD - $\bar{\lambda}$) is trace divided by 3.

$$RA = \sqrt{\frac{1}{2}} \frac{\sqrt{(\lambda_1-\bar{\lambda})^2 + (\lambda_2-\bar{\lambda})^2 + (\lambda_3-\bar{\lambda})^2}}{\bar{\lambda}} \qquad\qquad FA = \sqrt{\frac{3}{2}} \frac{\sqrt{(\lambda_1-\bar{\lambda})^2 + (\lambda_2-\bar{\lambda})^2 + (\lambda_3-\bar{\lambda})^2}}{\sqrt{\lambda_1^2 + \lambda_2^2 + \lambda_3^2}} \qquad 8$$

For both RA and FA indexes the numerator is related to the variance of the three eigenvalues. FA measures the fraction of the tensor that relates to anisotropic diffusion. The FA index is normalized between zero (when diffusion is isotropic) and one (when diffusion is constrained along one axis only – maximum of anisotropy). The denominator of RA is simply the mean diffusivity, making this index identical to a coefficient of variation, i.e. standard deviation divided by the mean. It is possible to design a colour map of fractional anisotropy which can give us a more direct visualization of the direction of diffusion, blue corresponding to superior-inferior, green to anterior-posterior and red to media-lateral direction (**Figure 11**).
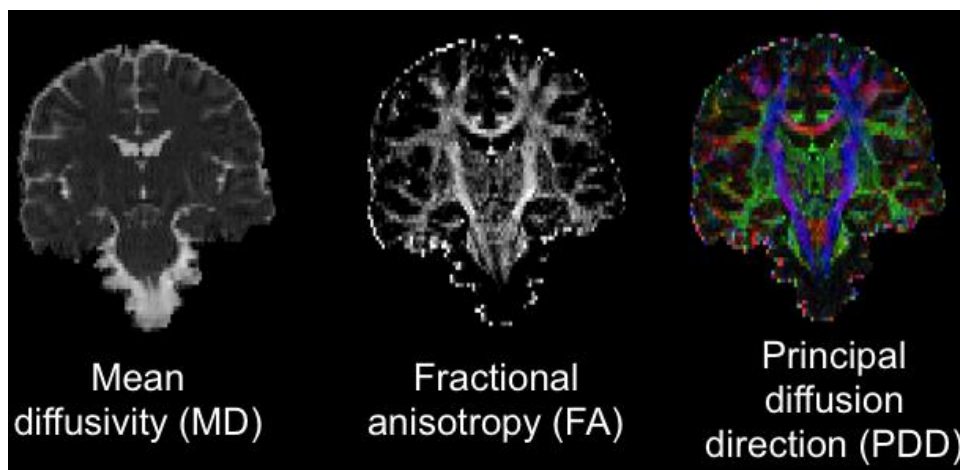
Figure 11 - Indexes that can be extracted with diffusion imaging (Berman 2005)**.**

A major drawback of DTI is the fact that the Gaussian model used may be a poor fit to experimental data, and in regions where fibre crosses, DTI is no longer capable of reflecting the index of anisotropic diffusion and fibre orientation, since there is no longer one single fibre orientation. New models have came along the years to overcome those problems.
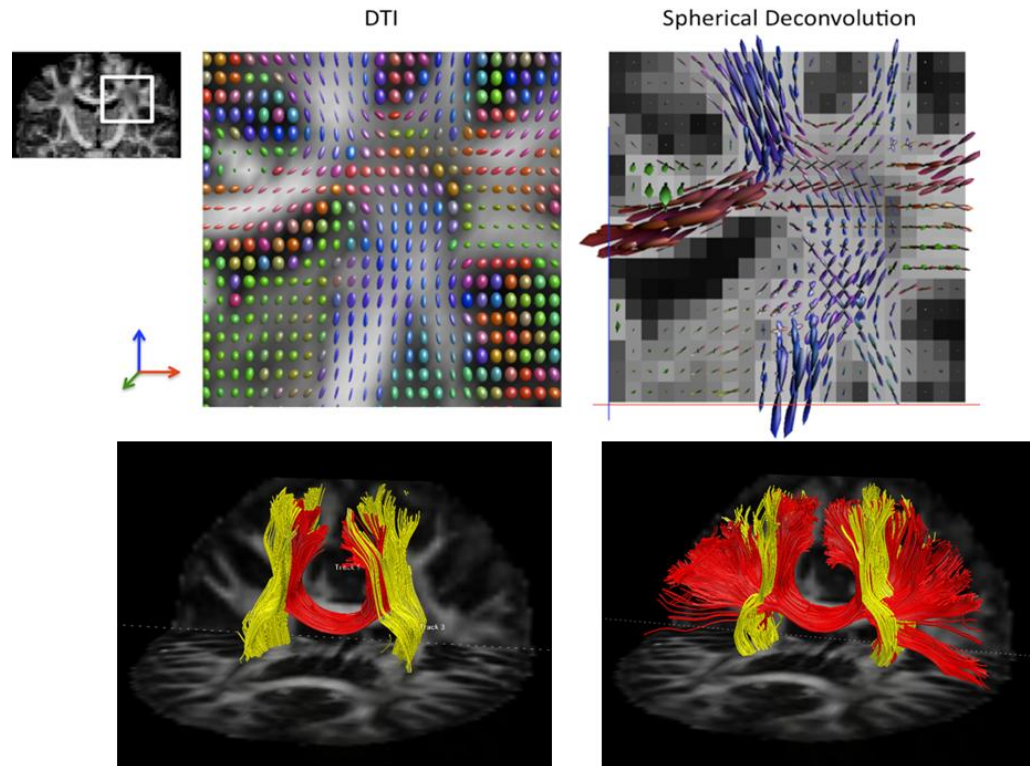
Figure 12 - Tractography results for the Corpus Callosum with DTI and Spherical Deconvolution (Dell'acqua et al. 2010)**.**

3.3 – Diffusional Kurtosis Imaging

Recent investigation has proven that the study of Diffusional Kurtosis Imaging (DKI) provides additional information about biologic tissues and present itself as technique that may bring new features into the identification and characterization of pathologies (Jensen & Helpern 2010). DKI makes the assumption that water molecules not always behave accordingly to a Gaussian distribution, but sometimes present some deviations. Therefore, the deviation regarding that distribution, kurtosis, can be measured in order to help gather information where DTI cannot, for example in isotropic structures such as grey matter (Jensen et al. 2005). A study of 6 healthy subjects has shown that mean kurtosis values are significantly higher in white matter than grey matter (GM), reflecting structural differences between these two types of tissue. This technique is also used to evaluate neurological diseases as multiple sclerosis and epilepsy, both associated to defects in white matter.

3.4 - High Angular Resolution Diffusion Imaging

In order to help reduce DTI - related limitations, new protocols arose such as High Angular Resolution Diffusion Imaging (HARDI) (David S Tuch et al. 2002; David S Tuch 2002). These procedures are natural extensions of the single-fibre case and consist in acquiring data with a large number of different gradient directions applied on a sphere, but with a much larger angular resolution (Le Bihan et al. 2001). The generated shape of the surface (for a single voxel) is composed with the different measured diffusion directions and can be divided into small components (tessellations) like icosahedrons. User gained the possibility of explicitly defining this spacing, and consequently defining the number of directions which corresponded to the vertices of the tessellations. This idea leads to a very simple and practical method for the identification of diffusion anisotropy without the necessity of invoking the diffusion tensor formalism and storing large files of numbers. Over the next subsections there will be discussed two types of HARDI methods: model free approaches, if we try to get a three dimensional displacement probability profile from data directly, collecting a Orientation Density Function (ODF); or if on the other hand, we try to apply a model to our data and extract a Fibre orientation Distribution (FOD), so called model based approaches.

3.4.1 - Model Free Approaches

When we first discussed the signal that one get by sensitizing water molecules with field gradients a phase distribution function was calculated. Actually, in diffusion imaging we measure the Probability Density Function (PDF) of the displacement of water molecules over time. If the model we are considering is diffusion tensor imaging that PDF will follow a Gaussian distribution which won't be the case for DKI (Maxime Descoteaux et al. 2005).

As tissue microstructure influences particles mobility, it will determine the PDF which in its turn tells information about the material microstructure (Daniel Alexander 2005b). As PDF, from now on called P for simplicity, gives us information about the distribution of water molecules, it will peak in the preferential direction of fibres, elucidating us regarding the orientation of fibres. It is possible to establish a relation between the measured signal and the Fourier Transform of P and q, or wavenumber (Price 1997):

$$A(q) = A^*(0)^{-1} A^* \int p(x) \cos{(q \cdot x)} dx \qquad\qquad 9$$

where A is the normalized measurement and q is determined by the strength, orientation, and duration of magnetic- gradient pulses in the measurement sequence. q can be related with b with the following expression:

$$b = q^2 \Delta \qquad\qquad 10$$

It is also worth mentioning that if we integrate the PDF of particle that undergoes a determined displacement R during a fixed amount of time Δ, over all possible positions, we will get the average propagator $\bar{P}$. This relation can be written as (Price 1997):

$$\bar{P}(R, \Delta) = \int \rho(r_0) P(r_0, r_0 + R, \Delta) \, dr_0 \qquad\qquad 11$$

with $\rho(r_0)$ being the molecular density and r_0 the initial position. If we use the dependece with the wavenumber we will now have:

$$E(q,\Delta) = \int \bar{P}(R,\Delta)\, e^{i2\pi q \cdot R} dR \qquad\qquad 12$$

Following this introduction about model free approaches, we will now discuss a little bit about a few of them.

3.4.1.1 - Diffusion Spectrum Imaging

Diffusion spectrum imaging (DSI) is a technique that is capable of mapping fibre architectures by imaging the 3D spectra of water molecules' displacement. First it is known that the signal that is obtained for each voxel is proportional to the average displacement of spins, according to the same sequence used in general diffusion techniques (**Figure 7**) and (equation 9).

By assuming that the duration of the gradient is negligible when compared to the mixing time (time between applied gradients) it can be postulated that the dephasing is merely a function of the relative spin displacement (R) and the gradient wave vector (q), which is the product of the gyromagnetic ratio by the gradient's intensity and duration. The signal in each voxel is therefore proportional to the density of the average relative spin displacement function (equation 12). This function is referred as diffusion spectrum and will enable the reconstruction of the diffusion spectra by taking the Fourier transform of the modulus of the complex MR signal (V J Wedeen et al. 2000).

Since the ultimate goal is to infer about fibre orientation it is a standard procedure to undertake a weighted radial summation of the diffusion spectra, projecting it in the radial direction, yielding an ODF. This function measures the quantity of diffusion in the direction of the unit vector (**Figure 13**) and provides a diffusion "intensity" in every direction.
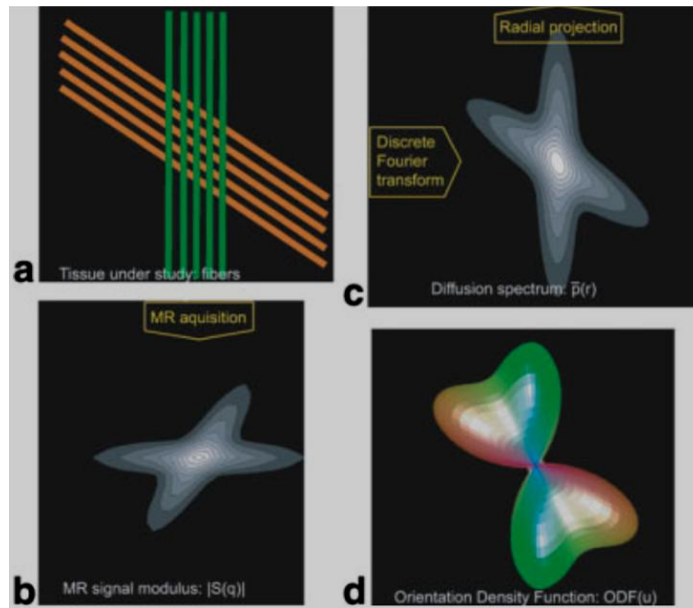
Figure 13 - Reconstruction of the diffusion ODF from DSI A: Tissue under study – crossing fibres. B: Voxel expectation of the signal – diffusion spectrum. C: Fourier Transform application to diffusion spectrum– diffusion spectra. D: Angular structure of diffusion (V J Wedeen et al. 2005)**.**

DSI samples k-space like traditional MRI techniques and q-space at the same time yielding a 6D technique, as it computes a three dimensional function over a 3D volume (Hagmann et al. 2007).

3.4.1.2 - Q-Ball Imaging

Similarly to DSI, Q-ball imaging (QBI) is a technique that relies on measures of q-space, that is, it measures the diffusion function directly (spin displacement) in a Cartesian frame of reference. Techniques based on q-space imaging (QSI) are somehow limited because by measuring the diffusion signal directly they require sampling on a three dimensional lattice. The reconstruction of the ODF from the diffusion signal requires calculating the radial projection and it may be biased since the relation between Cartesian and spherical coordinates systems may introduce artefacts.

QBI overcame this limitation by sampling the diffusion signal directly on a sphere, yielding a natural opportunity for an angular resolution, unlike what happens with the Cartesian framework. In other methods the diffusion spectra is normalized, and the ODF obtained by radial projection. This does not guarantee normalization since the ODF is a distribution on the radial projections and not on the true sphere.

The reconstruction of the ODF in a sphere is based on a spherical topographic inversion called the Funk–Radon transform (FRT), also known as the spherical Radon transform or simply the Funk transform. In QBI one can define the ODF over the sphere by integrating the solid angle. Consequently, the only requirement to estimate the diffusion probability in a certain direction is to sum the diffusion signal along the equator around that direction.
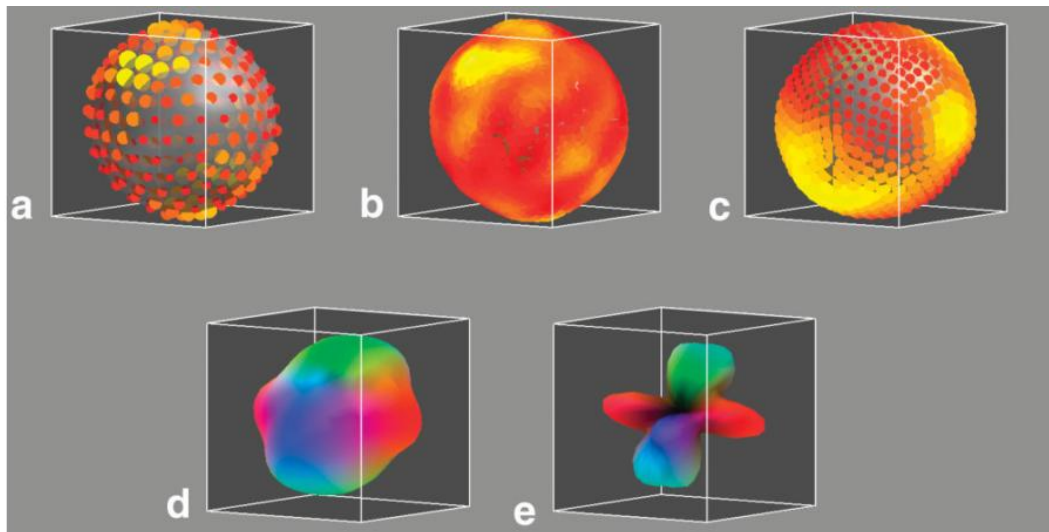
Figure 14 - Reconstruction of the diffusion ODF from QBI. A: Diffusion signal sampled on fivefold tessellated icosahedrons. Signal intensity indicated by the size and colour of the dots on the sphere. B: Sampling of diffusion signal around vertices of fivefold tessellated dodecahedron. C: Diffusion ODF calculated with FRT. D: Spherical polar plot of ODF. E: Min-max normalizes ODF (subtracted the baseline and rescaled) (David S Tuch 2004)**.**

It is also important to bear in mind that the acquisition can be targeted to specific spatial frequency bands of interest by specifying the radius of the sampling shell. Briefly, QBI is a HARDI technique that gives model-independence, linearity in the signal, an image resolution framework, and computational simplicity (David S Tuch 2004).

3.4.1.3 - Persistent Angular Structure - MRI

Analogously to other model free approaches to fit diffusion signal, Persistent Angular Structure MRI (PAS-MRI) assumes a Fourier relation between the measured signal and a function that allows to extract information about local distribution of fibre orientations. (Jansons & Daniel C Alexander 2003) In this specific case, the algorithm calculates a statistic called PAS ($\tilde{p}$) of the particle displacements density. PAS is a function of the sphere that reflect the angular structure of the particle displacement density in a three dimensional space and is defined as (Seunarine et al. 2007):

$$A(q) = r^2 \int \tilde{p}(\hat{x}) \cos{(rq \cdot x)} d\hat{x} \qquad\qquad 13$$

where r is the radius of the sphere on which $\tilde{p}$ is embedded.

3.4.2 - Model - Based Approaches

Previous HARDI techniques were based on extracting the orientation distribution function from the data rather than providing insight about the actual fibre orientations. The relationship between ODF and fibre orientation is not clear, and needs to be further investigated even though it is usually seen that the peaks in the ODF translates into a direction of a fibre population.

Therefore model based approaches appeared and first consisted in the assumption of multiple fibres per voxel as a mixture of diffusion tensors (Frank 2002). The assumption was made that the signal that came from a single voxel could be extended from a concept of single fibre. Furthermore, it was considered that there was no exchange between fibres yielding independent signals per fibres, and summing all contributions together to get the final intensity. For example, the contribution from two fibres, as seen with this approach is given by:

$$\ln\frac{S}{S_0} \approx -b\left[f_1\widehat{D}_1 + f_2\widehat{D}_2\right] + f_1 f_2 b^2 \Delta \widehat{D}^2{}_{21} \qquad\qquad 14$$

where f_1 and f_2 are volume fractions in compartments 1 and 2, respectively, so that $f_1 + f_2 = 1$ and $\Delta\widehat{D}^2{}_{21} = \widehat{D}_2 - \widehat{D}_1$.

Some specific cases of model based approaches will now be explored.

3.4.2.1 - Spherical Deconvolution

In Spherical Deconvolution (SD) it is assumed that there is no net diffusion between different fibre bundles, since the average displacement is too short, originating independent signal from different regions. Furthermore, the characteristics of all fibre populations are seen as identical in the whole brain, except when regarding to their orientation. Thus, in this context, variations in anisotropy are attributed to partial volume effects (Tournier et al. 2004)(Dell'acqua et al. 2005).

The diffusion-weighted signal attenuation that would be measured from a single fibre population is represented as a response function R, which depends on the elevation angle in spherical coordinates, regarding the z-axis. The total signal obtained (S) would then be given by the sum of all the individual response functions from a certain population, a Fibre Orientation Distribution (FOD) function, weighted by their respective volume fractions, having into account a

rotation factor such that they may be aligned along their respective orientations. The first spherical deconvolution approaches were solved in a linear manner which proved not to be the most efficient (Daniel Alexander 2005a). The Maximum Entropy Spherical Deconvolution (MESD) introduced a new non-linear algorithm to deconvolute the signal by constraining the information of fibre populations with constraints from the data. In 2007 Dell'Acqua et al, introduced a new algorithm, Richardson-Lucy (RL-SD), which identified a scalar parameter α that characterizes the fibre response that convoluted with the fibre populations yields the measured signal.
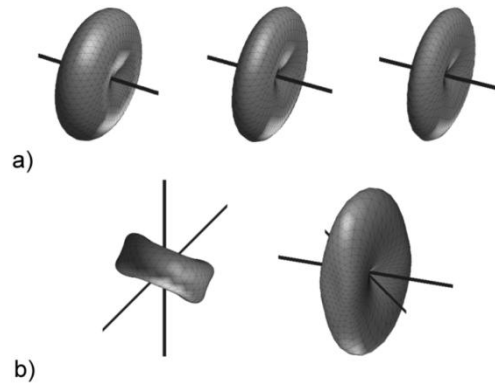
Figure 15 - a) Signal generated by a single fibre with different values of alfa; b) Signal generated by two crossing fibres (two views). Black lines indicate fibre directions (Dell'Acqua et al. 2007)**.**

The FOD models the spatial distribution of fibre orientation and any possible background and represents the weight of the fibre response along each direction. The fibre response can be seen as a sort of system impulse response function. We can consider white matter fibre tracts as being made of the same biological components, therefore any single white-matter fibre can be described with an identical fibre response function. This function is modulated by a parameter α that describes the anisotropic part of the signal, controlling the "fatness" of the signal profile generated from the a fibre. It is also important to know that the composed fibre orientation function (FOF) is weighted by a scalar, defining both the volume fraction and the isotropic component of the FOD. With increasing iteration numbers, the sharpness of the profile also increases and the standard deviation profiles grows slightly. Both these parameters work as regularization parameters in the sense that they are effective in the control of noise robustness, although at the cost of sacrificed angular resolution.
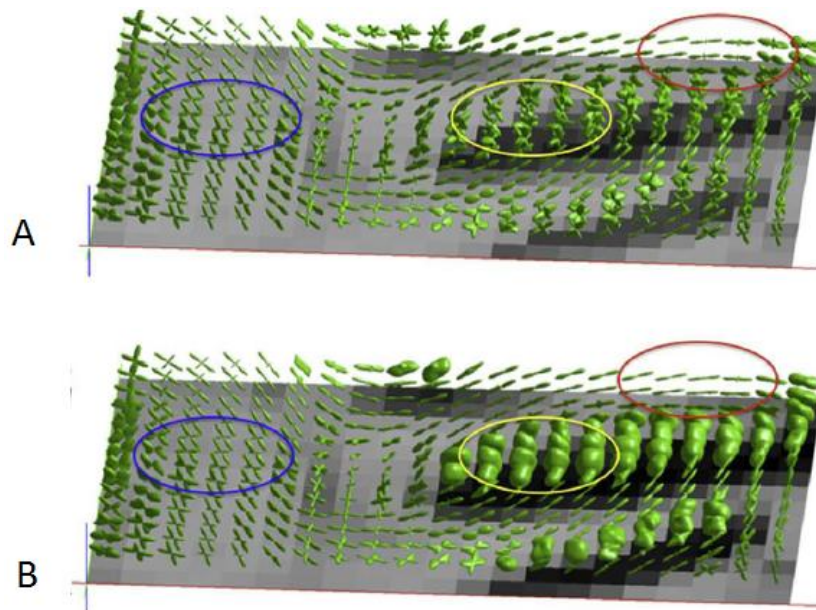
Figure 16 - Richardson Lucy algorithm with (A) non-damped and (B) damped version (Dell'acqua et al. 2010)**.**

Different levels of anisotropy can be interpreted not only as the presence of different mixture of fibre orientations but more physically also as partial volume from isotropic components. This means that in the presence of isotropic components the algorithm leads to physically meaningless spurious spikes. It can be used a threshold on FA maps to exclude GM or Cerebrospinal fluid (CSF) voxels (isotropic partial volume) but this is not viable when considering regions with low anisotropy due to highly complicated fibre orientations.

The urge for a new algorithm was great and the damped version of the RL-SD algorithm came arrived to reduce the effect of the isotropic partial volume through the use of the absolute dynamic range of the FOD amplitude. As it can be seen in **Figure 16** B, the damped version allows a much better distinction between isotropic (much rounder profiles) and anisotropic components.

3.4.2.2 - Composite hindered and restricted model of diffusion

This model based approach combines two concepts, namely water molecules behaviour in intra and extra-axonal space. As it has already been demonstrated, the intracellular space presents variable levels of anisotropy that arise from dense packing of axons (and their axonal membranes) and from the myelin sheath that surrounds them, restricting diffusion in the transverse direction (Beaulieu 2002). However, water molecules representing the extracellular component exhibit a hindered behaviour. Therefore, measuring fibre directionality in white matter also implies that the geometrical arrangement of the tissue contributes significantly to the observed diffusivity (Assaf et al. 2004).

The composite hindered and restricted model of diffusion (CHARMED) assumes that the observed signal is a combination of these two diffusion profiles. It expresses the signal decay observed in white matter in terms of Gaussian (hindered) and non-Gaussian (restricted) contributions, from extra-axonal and intra-axonal volume, respectively.
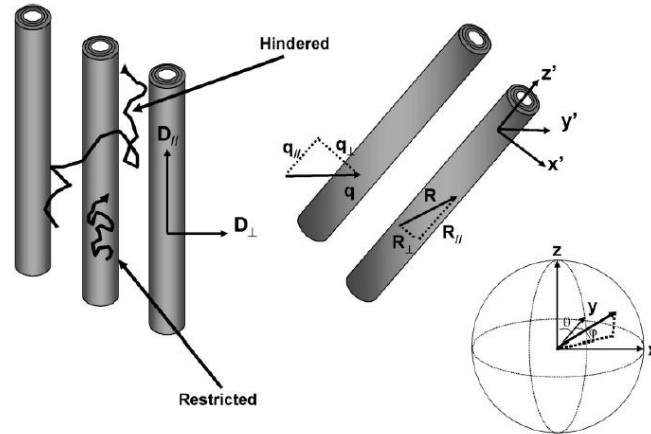
Figure 17 - CHARMED model contributions, both from hindered diffusion in extra-axonal volume and restricted diffusion in intra-axonal volume (Assaf et al. 2004)**.**

Additionally to these considerations the CHARMED model assumes that the hindered contribution can be modelled with the diffusion tensor and that the restricted part is subdivided into parallel and perpendicular, detailing a Fourier relationship with the wavenumber, similarly to QSI. Furthermore, as the condition of slow exchange is assumed, the total signal is merely the sum of both contributions (Assaf & Peter J Basser 2005).

4 - Tractography

In diffusion weighted imaging we are interested in studying tissue microstructure and infer about the underlying cytoarchitecture. One other purpose of looking into the brain by measuring the diffusion of water molecules is to be able to retrieve relevant information about white-matter anatomy and the connections between different regions. By reconstructing the fibre orientations from the diffusion profile (by any diffusion weighting technique that allows us a voxel estimation of the diffusion profile) we can generate a three-dimensional image that follows trajectory of fibres throughout the brain - tractography (S Mori et al. 1999). There are two standard conventions used differently in medical imaging softwares: neuroradiological and radiological, which differ in visualization due to the way we look towards the body. In the neuroradiological convention all the structures that are presented in the right and left side of the brain belong to those sides while in the radiological convention structures are presented on different sides.
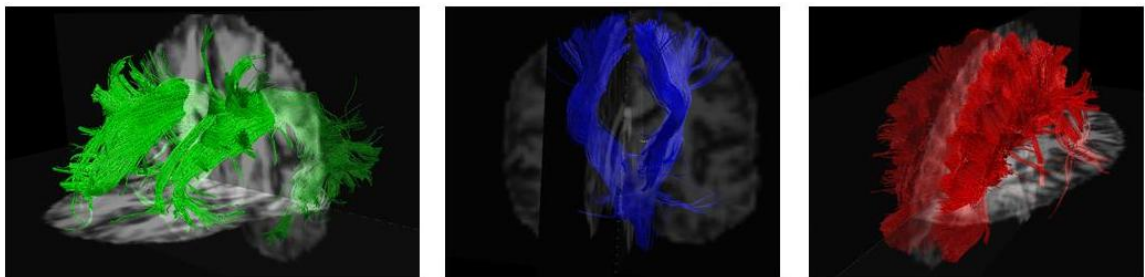
Figure 18 - Association (green), Projection (blue) and Commissural (red) fibres.

Particularly, when we are referring to human white matter and the vast range of fibres within the brain, there must be a way to identify them. There are three types of fibre tracts that are named accordingly to location and the direction in which they transmit: association, projection and commissural fibres. Association fibres connect cortical regions within the same brain hemisphere with an anterior-posterior direction, projection fibres are responsible for transmissions between the cortex and subcortical structures in a superior-inferior direction, while commissural fibres connect both hemispheres (**Figure 18**). The name for the reconstructed neuronal fibres is streamlines. In the context of tractography we can say that the reconstruction of fibre bundles yield tracks containing several streamlines (this is the standard nomenclature to distinguish between real and virtual information).

Tractography cannot distinguish between afferent and efferent connections since diffusion is symmetric. Furthermore, tractography is not commutative, which means that the reconstructed tracks from a particular point to another, might not be the same if we do it in reverse. This happens because the algorithm only cares about reaching the desired point and not about the fibre orientation at that point (**Figure 19**) (D. K. Jones 2010).
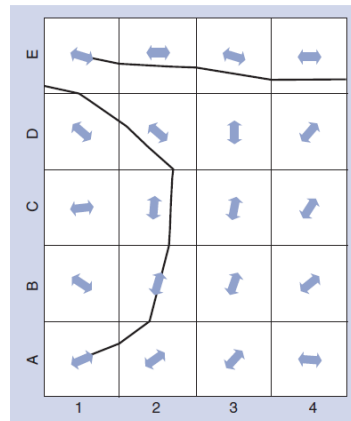
Figure 19 - Non commutative nature of tractography algorithms (D. K. Jones 2010)**.**

There are several tractography algorithms that can be used, but they can be mainly divided into: deterministic, probabilistic and global tractography algorithms. Before exploring these different types of algorithms, it is worth reminding that they share common points while generating the tracks (D. K. Jones 2008):

• the reconstruction is terminated if the front of a streamline enters a region where the FA is below the established threshold;

• the same happens if the maximum angle that is taken between voxels is higher than the predefined angle.

There is still the need to improve the tractography algorithms since the rate of false positives and false negatives that is observable disables its use as a truly reliable clinical tool.

4.1 - Algorithms - Deterministic, Probabilistic, Global

Tractography algorithms have endeavoured a constant evolution, spanning from several different techniques that have been used over the last 13 years, still making tractography the only tool for *in vivo* and non-invasive visualization of human white matter.

The birth of tractography began when the first attempts were done to map the preferred direction of water molecules diffusion. From a set of specific seed points, tracks were generated by joining the estimation of largest eigenvalue of the diffusion tensor in each voxel in a discrete way, defining the direction of the next step (S Mori et al. 1999) (Conturo et al. 1999). The reconstruction was initiated in the seed points with a specific step size and was terminated according to different thresholds, as has been described before.

These approaches consisted in extracting a vector field corresponding to the principal eigenvector of the tensor which could then be analysed in terms of curvature of fibre tracts (D. K. Jones et al. 1999). More specifically, a relation between a curve traced by the centroid in each voxel and the highest eigenvector in that same voxel would allow the determination of the curvature and possibility to determine if it was within the desired threshold, taking into account the associated uncertainty in estimation (**Figure 20**).

One limitation that was depicted in these reconstructions was the fact that they were performed in a discrete manner, which would prevent to follow a fluid, smooth and continuous trajectory (P J Basser et al. 2000). In this way, efforts were made to compute a continuous representation of fibre tracts from a discrete vector field, characterizing streamlines as curves

26

and parameterising them according to the arc length. As an analytical solution for the calculation of the tangent vector was not possible, numerical methods such as Euler integration and Runge-Kutta methods were used (Sinisa Pajevic et al. 2002) (Akram Aldroubi & P. Basser 1999). These methods could be used in an interpolation or approximation sense by either finding a function constrained to pass in every discrete point or non-linearly fitting a curve to the desired data, respectively. This parameterization allowed for an easier evaluation of indexes such as curvature and torsion to easily track the reconstruction process (P J Basser 1997).
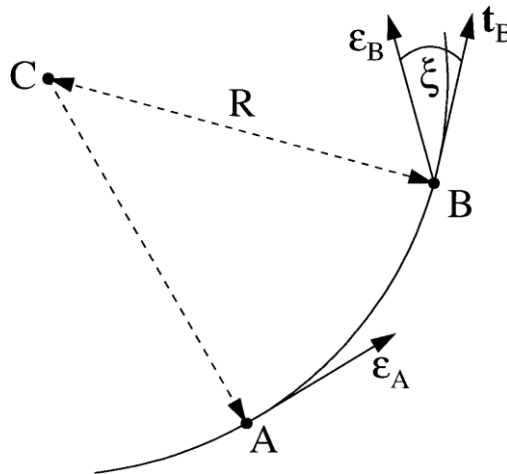
Figure 20 - Geometrical considerations for the connectivity algorithm (D. K. Jones et al. 1999)**.**

The first kind of techniques are described as deterministic algorithms where information about the neighbouring pixels is incorporated to define smooth trajectories (S Mori & P. C. M. van Zijl 2002). However, there are some limitations to deterministic tractography, like the challenge of correctly defining a ROI that includes only fibres of the fascicule of interest. One might try to apply more ROIs and Boolean logic in the reconstruction. Furthermore, it can only manage one reconstruction trajectory per seed point, generally not taking into account the branching of fasciculus.

At one stage it was clear that two main limitations remained: the fact that the reconstruction into grey matter was compromised by low anisotropy and the lack of spatial resolution which prevented the visualization of more detailed structure.

This gave birth to different kind of techniques which try to evaluate the most favourable path between predetermined regions and calculate the probability of connection given the samples of the data. Fast marching methods were the first to arise and intended to generate three–dimensional time of arrival maps. From these maps connection paths between brain regions may be identified, minimizing the energy, or in other words, finding the most coherent path between locations. This type of methods relies on the evaluation of a an interface or wave front over time, based on the diffusion tensor field (Geoffrey J M Parker et al. 2002). In each iteration, the wave evolution involves the determination of a speed function, that evaluates the position of any candidate voxels to be crossed by the its front and is linked to the information contained in the principal eigenvector. The front will then evolve faster along the direction which has stronger coherence, or highest level of orientation with the previous fibre orientation.
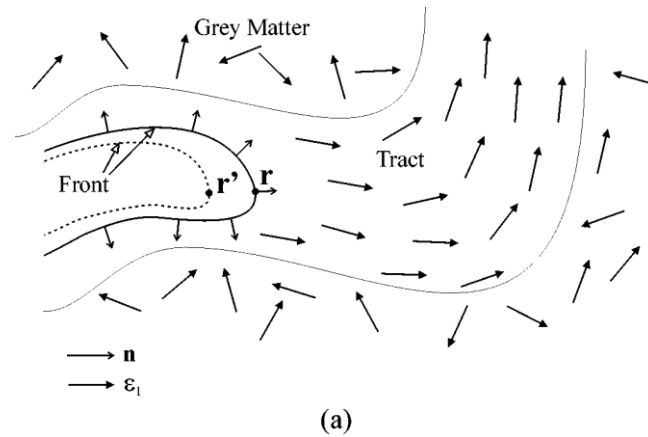
Figure 21 - **Wavefront propagation** (Geoffrey J M Parker et al. 2002).

This method allowed to overcome a limitation of deterministic tractography because it can trace branching as it makes use of a wavefront evaluation, tracking the probability of underlying neuron density. However, as it is linked to the information contained by the tensor field (by its own associated with an uncertainty) and displays several points with high connectivity, the possibility of propagating into false positives is very high (Staempfli et al. 2006). Results cannot be seen as real anatomical pathways as uncertainty is carried in each step, by the propagation of errors in each stage of the reconstruction, yielding a final indication of the percentage of streamlines that reach a voxel. Furthermore, these results strongly depend on the quality of the data.

Efforts have been done to deal with the propagation of uncertainty in probabilistic type tractography. As it has been stated before the uncertainty verified in diffusion MRI is not only present due to artefacts but also as a result of an insufficient modelling of the diffusion signal. The excess of complexity in the diffusion model that we do not take into account will cause extra uncertainty in the estimation of the parameters (T E J Behrens et al. 2003). Some approaches arose in order to compute a posterior probability density function for a set of parameters, which reflected the uncertainty and therefore allowed a better estimation of the considered model of diffusion.

It was also introduced the concept of bootstrapping methods to estimate the dispersion associated with fibre tract results (Efron 1979). The main concept of this technique is to estimate properties of parameters based on the resampling of the data which is assumed to be independently and identically distributed. The amount of resamplings that is done will allow to better characterize the distribution of such parameters. In diffusion imaging, bootstrap methods are used to randomly generate samples for every voxel in each diffusion-encoded image, which allowed to better describe uncertainty (Lazar & A. L. Alexander 2005).

Most of the developed algorithms relied on a voxel approach, which may be a limitative manner of evaluating a trajectory (King et al. 2009). Other alternative procedures, such as Random walk models, which make use of the diffusion properties of particles, also perform fibre tracking. After each step, a new starting direction is randomly assigned as the particle propagates according to its diffusivity values (Bammer et al. 2003). A particular type of these models is the Markov Chain Monte Carlo (MCMC) process, in which the next tracking step is

28

based on the distribution of the diffusion parameters of the surrounding locations (not from their spatial relation directly) and its iterative evaluation. Since there is a great deal of uncertainty on diffusion parameters, these models might be very appealing because only a small subset of voxels in the immediate locality of the current position is used to continue the fibre tracking, containing error propagation.
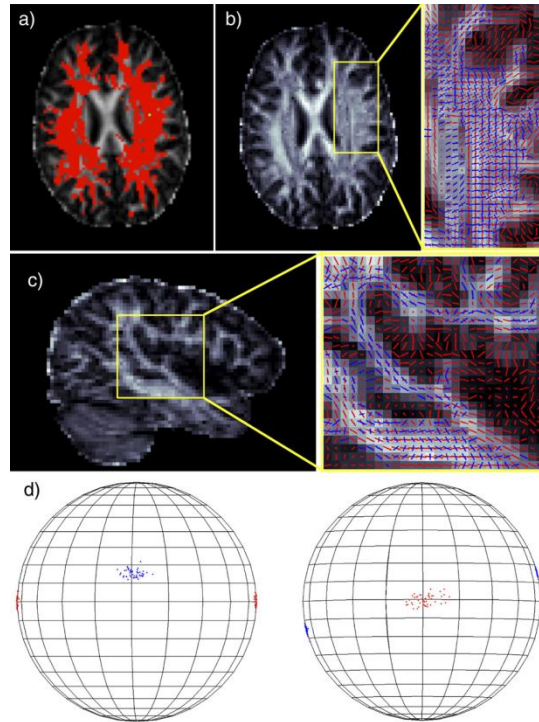
Figure 22 - a) Regions with more than one fibre population per voxel, depicted in axial (b) and sagittal (c) planes, as well as the posterior distribution samples (T E J Behrens et al. 2007)**.**

Other approaches pretended to replicate the streamline-like or deterministic like approaches repeatedly by Monte Carlo methods (Geoffrey J M Parker et al. 2003) or extended the general probabilistic approach to multiple fibre orientations (T E J Behrens et al. 2007) by generating maps of connection probability or increasing sensitivity when tracking non-dominant fibre populations, respectively. **Figure 22** is representative of the latter case, scheme based on streamline tractography, where a sample is drawn with direction of propagation of the posterior distribution on principal directions (based on the integration over all variance parameters) rather than the most likely principal direction. Similarly to this step, several samples are performed to generate a connectivity distribution. If two samples arrive at a same point in space they will choose different posterior distributions and leave the voxel along different directions, accounting for uncertainty in fibre orientation in regions where fibres cross (**Figure 22 b,c**).
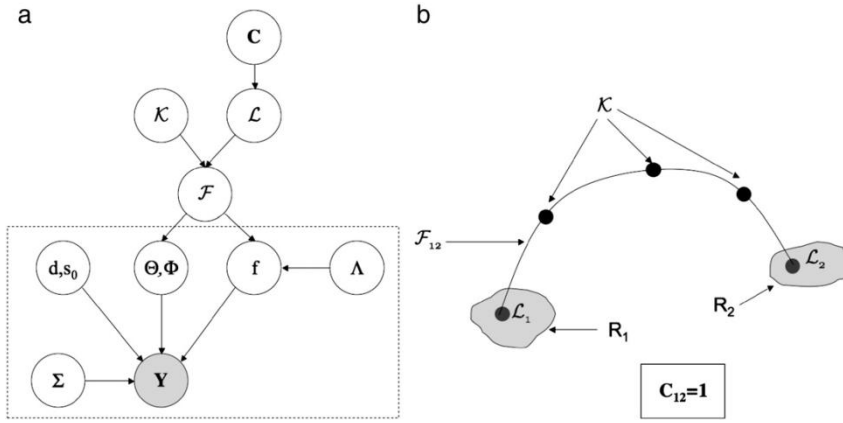
Figure 23 - a) Bayesian global tractography model and illustration of different parameters (b) (Saad Jbabdi et al. 2007)**.**

The final type of tractography algorithm that can be presented in this list is: global tractography. In this kind of approach one calculates local estimations of fibre orientations, propagating them throughout the voxels to obtain estimates of connections between brain locations. As seen by (Saad Jbabdi et al. 2007) in **Figure 23** , the data Y is generated by the parameters of the local model (inside dashed lines), which model the diffusion properties. From the observation of the data we are able to infer on the posterior distribution given the data and model (T E J Behrens et al. 2007). The connections among the brain network (F) and the anatomical priors (C) on those connections will permit to back-propagate for the rest of the network, information that is obtained by the calculated posterior distributions. It behaves like a global process, since local orientations and connections are inferred upon at the same time. (T E J Behrens & Johansen-berg 2009) More recent approaches have provided algorithms that seem to perform better comparing the some other referred techniques and in more acceptable clinical time (Aganj et al. 2011)(Reisert et al. 2011).

4.2 - Specific Cases

Other fibre tracking approaches were performed, for example diffusion tensor deflection by Lazar et al 2003. In this algorithm the next direction of fibre propagation is set from the previous integration step. The tensor operator deflects the incoming vector towards the major eigenvector direction, but limits the curvature of the deflection, which should result in smoother tract reconstructions.
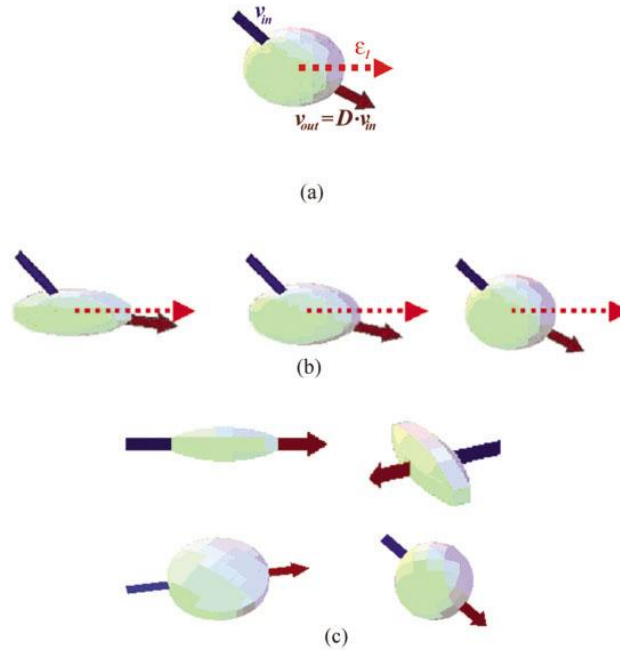
Figure 24 - Diffusion tensor Deflection. (Lazar et al. 2003)

This algorithm describes the incoming vector as a linear combination of the three eigenvectors, weighting them according to the eigenvalues and determining the next direction according to different deflection properties that correspond to different diffusion ellipsoids shapes (Lazar et al. 2003).

Analogous to level set techniques and Fast marching techniques (C Lenglet et al. 2009) there was also the description of new algorithms that classified a wavefront evolution, propagating it according to a speed profile governed by the isocontour of the diffusion tensor ellipsoid. The difference is that in this method an anisotropic distance function was adopted for front evolution, in which the discrete approximation of front normal is not required. This means that the speed by which the front propagates is given by the distance between the centre of the diffusion ellipsoid and a point on its isocontour in the front normal direction directly with no further computations (Jackowski et al. 2005).

One last approach that is worth mentioning made use of the assumption that fibres that run orthogonally to the images can more easily be tracked than fibres that run parallel to the slice layer. This assumption is based on the fact that for straight axial images tensors that represent orientations parallel to that plane, have larger differences between different slices, when we are tracking a fibre. However, with angulated DTI, which consisted in tilting the DTI to bring the mainly anteroposterior fibres as the Optic Radiation into a nearly orthogonal relation to the image, tensors will yield a more "orthogonal" reconstruction (Stieglitz et al. 2011).

4.3 - Track Indexes

After a certain point it became clear that simple by changing different algorithms or applying different thresholds the final reconstruction and underlying anatomy was different, something that is a clear limitation of tractography (Pierre Fillard et al. 2011). Fillard et al, opened a contest to evaluate tractography algorithms against a ground truth phantom that was built with the requirement of a practically feasible configuration, in particular, that should lie in-plane because they have to be squeezed in between two solid dies to ensure high density and

31

diffusion. The phantom dataset, the ground truth fibres, the evaluation methodology and the results obtained still remain publicly available[3]. The evaluation was performed on the ability of accurately reconstruct the fibres depicted in **Figure 25**.
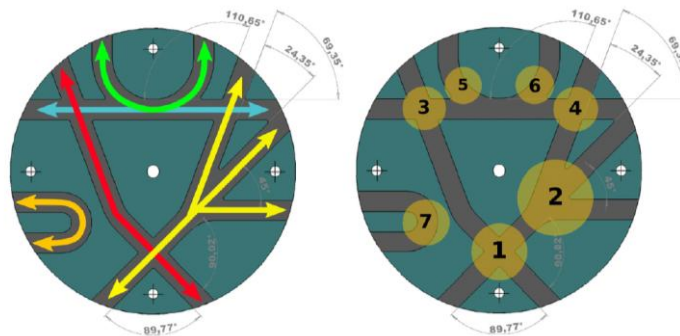
Figure 25 - Ground truth fibres (Pierre Fillard et al. 2011)**.**

Each participant had to return a dataset composed of 16 candidate fibres matching 16 ground truth fibres, where the best result would be the one which presented fibres that better fitted the ground truth ones. That evaluation was chosen to rely on the point-based Root Mean Square Error (RMSE) between the candidate fibre and the corresponding ground truth.
The method that used global tractography (Reisert et al. 2009) got the best scores and was declared the winner of the contest. However, the biggest finding concerned the inter-method variability, which is relatively high depending on the seed location (Pierre Fillard et al. 2011).

To be able to improve tractography algorithms an interest on methods that provide within tract detail arose. These methods had the purpose of enabling the possibility to incorporate along-tract detail into existing tractography analyses. In one particular study spline-based resampling strategy was followed to capture the large portion of within-tract variance that exists along the tract (Colby et al. 2012).

Other indexes arose such as Hindrance modulated Orientational Anisotropy (HMOA) and Orientation Dispersion (OD). The first one consists on the normalization to a reference amplitude of the single absolute amplitude of a FOD lobe and can, therefore, be used to detect and quantify diffusion or anisotropy changes along specific white matter orientations. In particular, by selecting as reference the highest FOD amplitude that can be realistically measured in a biological sample, an HMOA with a value of one corresponds to a signal equivalent to the reference fibre, whereas an HMOA of zero corresponds to the absence of a fibre (Dell'acqua et al. 2012). The latter allows the quantification of the angular variation of neurite orientation and the definition of a orientation dispersion index, based on a definition of a new model and parameters. In particular, these parameters are now determined not only by the neurite density, via the tortuosity model which allows exchange of water between the intra-cellular and extra-cellular compartments, but also by the orientation dispersion of neuritis (H. Zhang et al. 2012).

One of the usual criteria to stop the tractography reconstructions is the value of the fractional anisotropy which drops considerably when transiting from white matter to grey matter. In regions of transition depending on the threshold that we choose for the tractography reconstruction we can lose information or add spurious one. Recently there have also been

---

[3] http://www.lnao.fr/spip.php?rubrique79.

some techniques that try to overcome this limitation by extending white matter tracts through grey matter based on geometry (Tozer et al. 2012).

The proposed methodology determines the cortical GM region most likely to be connected to a specific WM tract by extending the tract across the WM-GM boundary defined using T1-volumetric images segmented into WM and GM. This is not a different tractography approach, rather a quantification technique that may help improve the dependence on thresholds. For example, by using this technique one could use a high threshold on FA to improve tractography reconstruction.

4.4 - Remarks

Tractography has been evolving throughout the years and we are far from knowing everything about the human brain and how this technique can help. The only certainty that we possess is that tractography is extremely useful not only to localize tracts on an individual but also to register them into an atlas, to understanding, or perhaps even predicting, dysfunction caused by (structural) disconnections in specific locations (Catani et al. 2007) or even to study structural connectivity (Dell'acqua & Catani 2012). Furthermore, it is of critical importance for surgical planning (Lacerda et al. 2012). There are still several problems that can be addressed such as finding the exact termination to connections in the boundary between grey and white matter, tracking the horizontal intra-cortical connections, detecting synapses, to name a few (Saad Jbabdi & Heidi Johansen-Berg 2011).

5 - Automatic Parcellation Techniques

In the previous chapter, emphasis was given to different approaches that one can follow to generate a three dimensional reconstruction of human white matter and still the only non-invasive and vivo visualization technique for that purpose - tractography. As it was described, three main types of tractography are possible, whether by connecting the estimations of main diffusivity in each voxel, trough the use of deterministic tractography, by generating a range of possible connections with the construction of a probabilistic map of anatomical information or analyzing the whole volume of fibres as one with the global tractography approach.

Either one of those will generate streamlines which represent fibre bundles in the form of three dimensional curves. This representations are still far from perfect and do not represent the true anatomical bundle of neural fibres. However, tractography allows us to infer about structural connectivity in a macroscopical scale and therefore is very useful for generating maps of human white matter and to help in neurosurgical planning, for example.

Tractography-based parcellation consists on determining the connections that are established between different regions by dividing the whole volume of streamlines into specific bundles of fibres. It can be performed based on regions of interest used to select or exclude tracts or by clustering techniques where similarities between streamlines are analysed (Guevara et al. 2012). The first approach has been shown to offer good results, but it is not able to detect similarities between curves and its success is highly dependent on the applied registration (Guevara et al. 2011). Clustering techniques managed to overcome this drawback but are unable to deal with the high amount of data that is generated and sometimes lose some of the more "unique" streamlines.

In this section, an overview of the most relevant methods for both approaches are described in order to elucidate the reader of what is currently available in this area. Some of the presented methods may have traces of both techniques, even though there is not still a unified method (Cloutman & Lambon Ralph 2012).

5.1 - ROI - Based Approaches
The idea behind ROI-based approaches or virtual dissection is to apply different regions of interest to our tract data and filter the specific tracts in which we are interested. Those regions can be used either to include or exclude desired tracts. Initial work was based on the definition of strategically placed ROIs drawn with reference to classical neuroanatomical works, but it didn't present itself in an automatic fashion (**Figure 26**) (Catani et al. 2002).
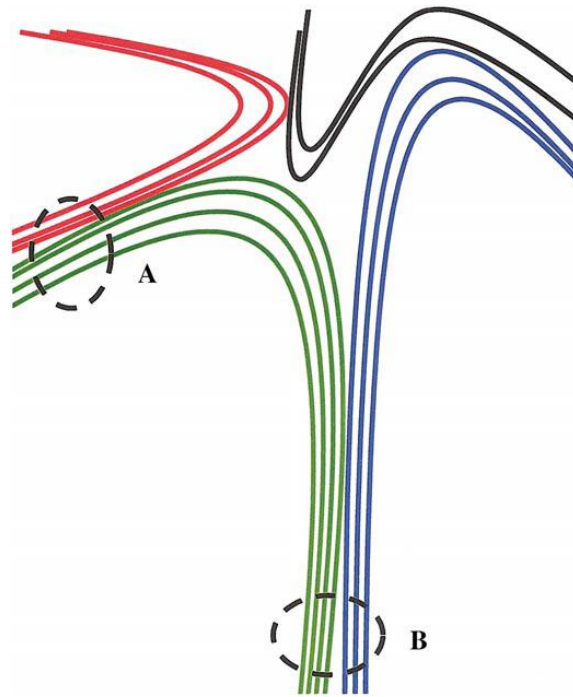
Figure 26 - Two regions of interest approach to separate fibre bundles of interest (green fasciculus in this particular case) (Catani et al. 2002)**.**

Further work comprised the elaboration of new atlases that ensured the placement of cortical regions located deep in grey matter and its projections into white matter. After tractography, these maps would then serve as anatomical labels which enabled the classification of voxels according to a specific code. Once this had been done for all the voxels in the brain a new process of connecting all the voxels with the same label was initiated, generating and parcellating desired tracts of interest (Lawes et al. 2008). Other approaches consisted in using the information of a standard fibre atlas from probabilistic tractography, which supplied information about orientation and location of major fibre tracts. Departing from a label-based segmentation with structural and diffusion images in combination with the information given by a manually dissected fibre atlas, it was possible to calculate maps of *a posteriori* probability of a new dataset. These maps demonstrated the probability of a certain voxel corresponding to a certain fibre of the manual derived atlas, given the estimative of the main fibre direction (first eigenvector) of subject's DTI computation. Furthermore that probability reflect the relation between the fibre probability in the standard space and the fibre probability given the first eigenvector of the new dataset (Hagler et al. 2009).

In Reich et al 2010, information from a fibre atlas was also used for the determination of the location of a specific voxel and its correspondent fibre, in a new dataset. However, unlike Hagler et al 2009, where the standard atlas was generated manually, it is now build having into account the amount of subjects voxels that are located in a specifically reconstructed tract (after the subject's data have been co-registered to a standard space) yielding a tract-probability map. This map can then used on a specific coregistered brain image and reflect different MRI indices along the tract of interest, weighted by the probability that each voxel belongs to the standard tract (Reich et al. 2010). Similar methods that relied on automatic labelling of streamlines using previous parcellations were also used and relied on non-linear transformations to retrieve information to a standard space. Once that step was concluded, information regarding the

36

number of streamlines connecting the Corpus Callosum and cortical regions (in this particular case) for all the participants in the study was averaged, generating the callosal population connection probability map for all cortical regions (Pannek et al. 2010). In these type of approaches the only required interaction from the user is usually regarding the choice of seeds from the anatomical registered labels in order to track the desired fibre bundle of interest (Nucifora et al. 2012).

5.2 - Clustering Approaches

As it was stated before, ROI-based approaches manage to include or exclude fibres of interest based on atlas of white matter and specific regions of interest. However, they are not able to retrieve fibre bundles based on similarity indexes with a template or amongst each other. In this way, fibre clustering methods analyze diffusion tractography datasets and separate fibres into bundles, or clusters, that present similar shape and spatial position as well as similar anatomy and function (Kubicki et al. 2006).
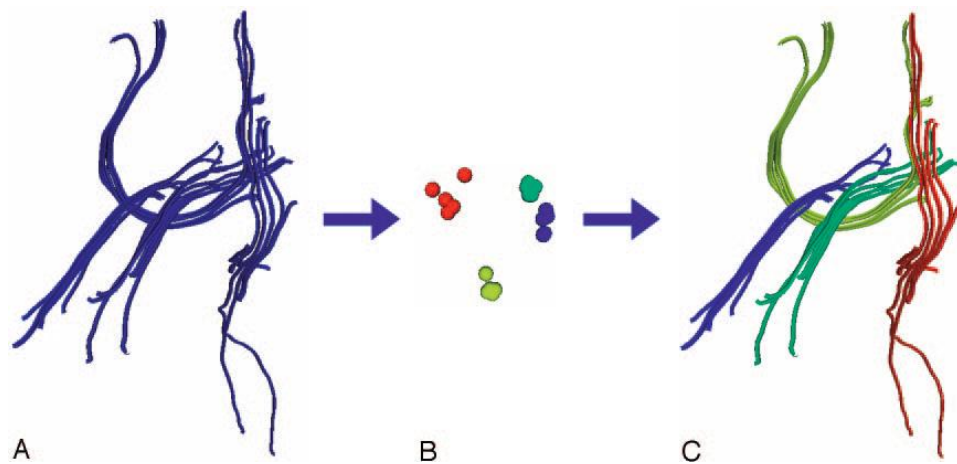
Figure 27 - A, Input fibre tracts. B, Clustering step. Each point corresponds to the similarity relationships of 1 fibre (these points come from the highest eigenvectors of the similarity matrix in a process called "spectral embedding"). C, Tracts coloured by cluster (Kubicki et al. 2006)**.**

One of the first clustering approaches consisted on using the so-called spectral clustering. In this kind of clustering each item is compared with the remaining items that constitute a determined sample and a similarity value is calculated. Similarity between items may be regarding shape, location, amongst other indices. In (Kubicki et al. 2006) the average distance between pairs of nearest points on paths was calculated to analyse the similarity between both tracts. Those similarity values are used to compute a squared matrix whose size depends on the number of tracts. After that matrix is completed, the similarity measures are converted into a "score" of similarity by inverting the distances, i.e, the lower the distance the higher the "score" or similarity between tracts. That conversion is performed by applying a Gaussian function to the above mentioned matrix, generating an affinity matrix.

Posterior to the application of this function, the most important information about shape and similarity is extracted in the form of the higher eigenvectors. This is, as the eigenvectors are only scaled by the matrix, and not rotated, they are going to be influenced for the higher eigenvalues, which present more information about similarities. Each fibre path, can

be seen as a point, so that each cluster can be clearly separate from another (**Figure 27 b**). Clusters will then be displayed in this high-dimensional space and labelled by anatomical experts so that they represent a model of white matter structures (Donnell & Westin 2007).
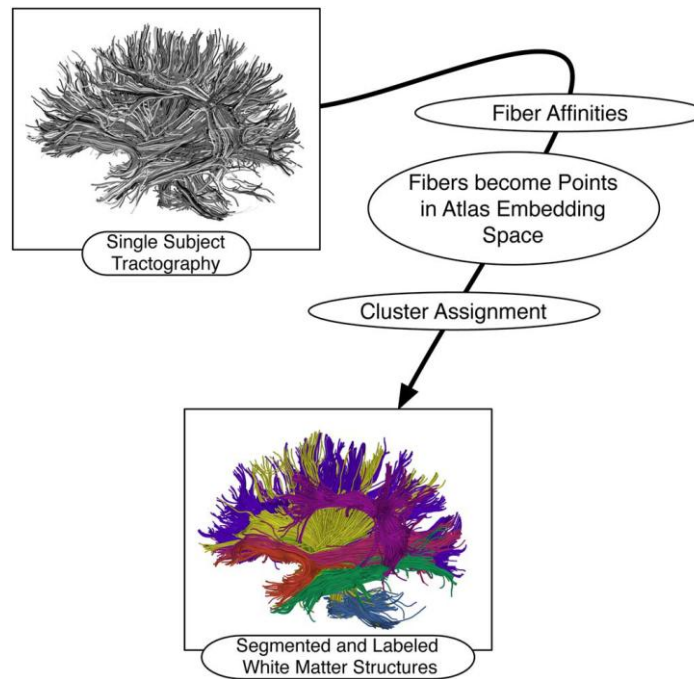
Figure 28 - Process of generating a first white-matter atlas (Donnell & Westin 2007)**.**

In order to be able to create an atlas from this first anatomical model it is necessary to register every diffusion data from new subjects to the original estimative. New affinity values will then be calculated and new fibre trajectories will be embedded in the atlas spectral space, this is, new points will be created in the space where previous clusters had been placed. The anatomical labelling for this new fibre paths will be done with the k-means algorithm where each point is clustered within a specific bundle accordingly to the minimal distance to the centroid of that bundle (M. Chen 2006).

The similarity values that were explained above are obtained differently for a variety of methods. In particular Ge et al., 2010 propose a clustering algorithm based on the symbolic sequence analysis method. In this method, an atlas was first applied to the data and each fibre was assigned a label according to the region of the atlas it traversed. A sequence alignment method based on the comparison of two symbolic label sequences (as in bioinformatics to align protein or nucleotide sequences) was then computed to generate the similarity information about the several fibres. Other techniques used a function based on the concept of morphological continuity, that claims that any two fibre trajectories belong to the same cluster if the maximum distance between points of different fibre paths is lower than a predefined value, typically in the order of 1-2 pixel spacing (F. Yeh & W. I. Tseng 2010).

There are also available techniques that are able to detect the "unique" fibres that were referred previously as a limitation of clustering techniques. In order to overcome this limitation and to deal with the high complexity of tractography datasets, Guevara et al., 2012 proposed a two-level strategy, involving intra and inter fibre clustering.

At a first level hierarchical clustering is performed so that the number of streamlines is reduced from million of tracts to a few thousand representing the whole structure of tractography. This is done having into consideration that white matter voxels are merged when they connect several tracts, leading to reconstructions that represent the underlying bundles, with less fibres. For a single subject, the whole tract volume will be split into different masks, and into different length groups. For each of the individually generated groups fibres will be clusters in a k-means fashion, generating several clusters representing underlying neuroanatomy (Guevara et al. 2011). In a second step, all the clusters obtained in the intra-subject approach will be normalized to a template and a new clustering in the same fashion is performed but with all subjects' trials yielding a much better estimative, an atlas of human white matter.

One final note that should be said about parcellation techniques is that the results strongly rely on the quality of tractography, even though, efforts are being made to ameliorate that aspect. Furthermore, combined approaches in a ROI-based and clustering way will give the opportunity to further automate and improve the parcellation process.

6 - Methods

Despite the great number of strategies available for automatic parcellation and clustering of tractography data, there isn't still an established method in which we can rely. With this project, we aim to improve automatic tractography analysis by building a software based on the use of regions of interest to perform automatic parcellation of brain regions. Following the standard pipeline of pre-processing of diffusion imaging data, including data interpolation, the first step of the project consisted in automating the usual procedure followed in manual dissections (6.3.1 - TrackVis). Secondly, to improve the flexibility of the designed tool, the generation of ROIs from different templates to native space, through the use of non-linear registrations with dedicated software (FSL) (Stephen M Smith et al. 2004) was also implemented. Automatic dissections of different brain regions were then performed according to predefined cortical and subcortical ROIs as well as other anatomical priors.

One of the advantages of an automated tool that enables this kind of analysis is the fact that eliminates user dependence as it requires minimal intervention. Furthermore, manual dissections are very time consuming and can only be conducted by extremely qualified staff with great knowledge of neuroanatomy. Extending on this, the developed tool allows not only tract data pre-cleaning, permitting specialized personal to inspect manually the output of the software, but also full automatic analysis, both for single and multi-subjects.

In this section, it will be discussed how data was obtained and processed, followed by the developmental stages of the before mentioned tool. Description of the tool will be demonstrated for one specific brain region, only as purposes of validation, since it was used more intensively (as shown in results and discussion sections). However two more studies have been conducted.

6.1 - Data Acquisition

All the data was available in the beginning of the project, which consisted in several different regions of interest drawn manually in addition to the SD-based tractography registered data. Diffusion MRI data was acquired from 30 healthy normal volunteers using a 3 T GE Signa HDx TwinSpeed system (General Electric, Milwaukee, WI). Data was acquired with the following parameters: voxel size 2.4 x 2.4 x 2.4 mm, matrix = 128 x 128, field of view = 307 x 307 mm, 60 slices, 1 average, TE = 93.4 ms, b-value = 3000 s/mm2, 60 diffusion-weighted directions and 7 nondiffusion-weighted volumes, using a spin-echo single-shot echo-planar imaging (EPI) sequence with an ASSET factor of 2. Peripheral gating was applied with an effective TR of 20/30 R-R intervals (Dell'acqua et al. 2012).

Along the project new data was acquired as so for regions of interest. Detailed explanations of the manual and automatic method are presented in the following subsections.

6.2 - Processing

6.2.1 - Quality Control

Prior to the analysis of diffusion images, quality control had to be performed, basically by opening all the datasets, checking if there were any missing or corrupted slices. It is also useful to compute estimates of different parameters, such as FA, and check if they present results with physical meaning. Despite the amount of work that is done to assure image quality, prior to the acquisition, these steps of manual inspection are still indispensable (Tournier et al. 2011). However, some attempts are being made to automate this process as well.

6.2.2 - Pre-Processing

In order to reduce motion and eddy current distortions, all images were pre-processed, recurring to FSL. ExploreDTI (Leemans & D. Jones 2009) and MRIcron were also used for purposes of visualization (Rorden & Brett 2000).

6.3 - Automating Tractography Analysis

The starting point of this thesis came from the challenge of understanding previously designed functions to run tractography-based dissections and automating that process. Therefore, the first step consisted on creating a set of basic rules which allowed one to automatically get the same results as in manual dissection. Manual dissections can be done using dedicated software applications such as TrackVis and this can be very time consuming. Therefore, the need to generate a fully automated method arises and would be an added-value to research.

6.3.1 - TrackVis

TrackVis is a program that provides 3D rendering of tractography data, offering several possibilities of visualization and manipulation of streamlines.   The pipeline for the manual dissection (**Figure 30**) is based on the following steps:
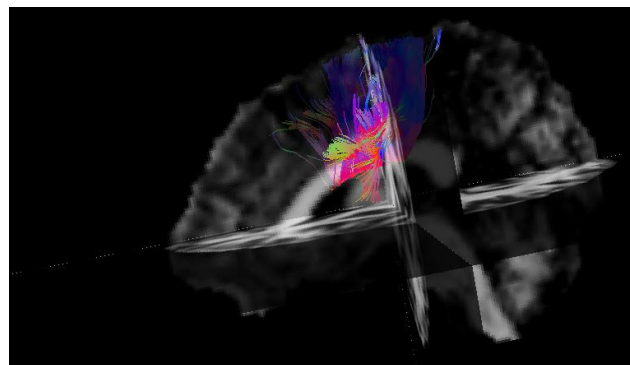
Figure 29 - Simultaneous visualization of the tracts and structural image with TrackVis.

1. We start by looking at the whole volume of streamlines and for purposes of visualization we are able to control several options on TrackVis, like the skip (percentage of streamlines visualized), streamline length threshold (in mm), amongst others;
2. After visualizing the whole volume, one wishes to filter out only the streamlines that cross the region to parcellate. <u>For purposes of demonstration, in this description the Corpus Callosum is chosen as the region to parcellate.</u> This can be done by loading a ROI

with the shape of Corpus Callosum and toggling it to the volume of streamlines, yielding only the desired ones;

3. Following this step, begins the actual parcellation of the Corpus Callosum. One of the ROIs with which we want to parcellate the Corpus Callosum is loaded and the same procedure is followed – toggle that region to the tracks and generate only the desired streamlines.

4. Amongst the generated streamlines there will be spurious ones that need to be cleansed. These streamlines are tagged spurious according to direct visualization of its trajectory and neuroanatomical knowledge. In order to cleanse the streamlines we load regions of interest, toggle them to the volume of streamlines and use them as NOT filters. In this way all the spurious streamlines will be excluded.

5. After excluding all possible streamlines with the available regions of interest (NOT ROIs) it is possible to save the streamlines filtered both in a .trk file (track file) or in a .nii (density map). Those can be later used for statistical analysis, with specific software like FSL. There is also the possibility of saving the scene you are working in, which provides an opportunity to continue the dissection at other time.
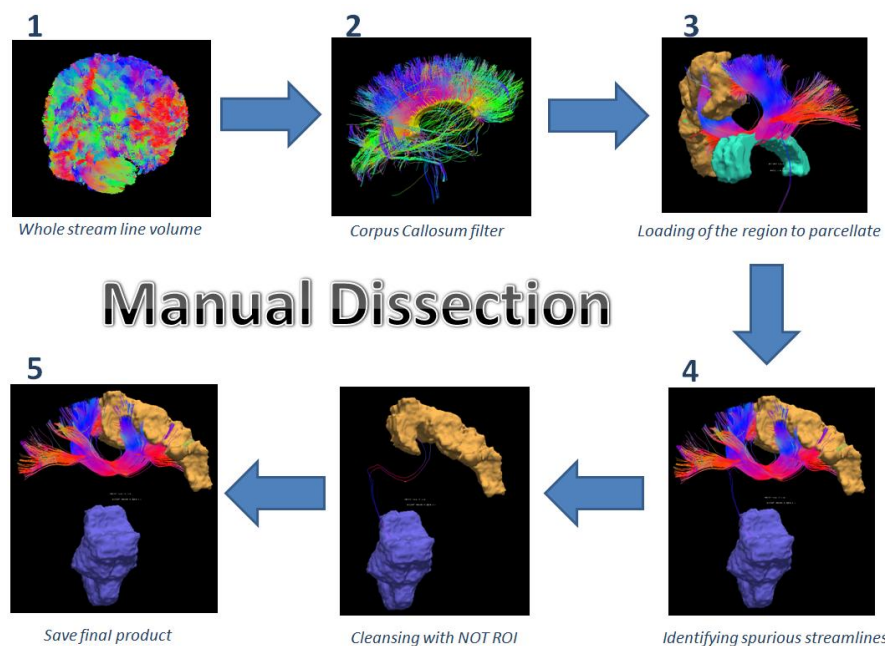
Figure 30 - Manual dissection pipeline with TrackVis.

6.4 - Software for Automated Tractography

As it has been explained before it is of critical matter that an automated tool is developed to perform the procedure explained in **Figure 30**. The basic method from which we can depart into smarter ways of performing parcellation is now explained thoroughly. It is important to notice that this project has been evolving gradually and the tool is explained according to different developmental stages.

The main function that was created is ttad_full.m, which can automatically parcellate the chosen region with different ROIs in subject space. This function is subdivided into three other

functions – NBL_Initializing.m, NBL_filtermain.m and NBL_Saving.m – responsible for initializing relevant variables, performing the filtering and saving the outputs, respectively.

Function NBL_initializing.m is responsible for loading the tract, through the use of the function NBL_readtrk.m, and convert data to a matrix. The reason why this is performed is because the .trk file is in mm and we need to the map it into pixels in order to run the analysis. Conversion is performed by NBL_tractsFOV2MTX.m and yields a structure containing information about the track, its 3D coordinates and other parameters. At this stage, under NBL_initializing.m, there was one function responsible for reading a textfile that retrieved information about: the shifting that occurs when converting the track; the save mode (detailed under the function NBL_Saving.m); and the number of ANDROIs, SHORTROIs and NOTROIs, as well as the threshold associated to each ROI - NBL_ROISfilt.m. However, as explained later in the text, this function evolved into a function which loads all inputs required for the automated tool as well as other parameters, all kept into a configuration text file.

When relevant information is retrieved it shall be passed to NBL_filtermain.m where the filtering will take place. There are three basic types of filtering that can be done - NBL_filterTract_full.m, NBL_filterTract_short.m and NBL_NOTROIfilter.m – but all evaluate the coordinates of the streamlines inside specified ROIs. The first one evaluates which streamlines simultaneously cross the initial volume (basic .trk file) and the specified ANDROI, storing those streamlines. NBL_filterTract_short.m is a small modification of NBL_filterTract_full.m because it only evaluates the ten first and last points of the streamlines, rather than all the points. NBL_NOTROIfilter.m works in a similar way to NBL_filterTract_full.m but instead of storing the streamlines it excludes them, and keeps only those which do not cross the NOTROI.

Something that is important to say is that if we wish to perform the two first filters more than once we must do it sequentially for different AND/SHORTROIs. That is not the case for the NBL_NOTROIfilter.m, because one may choose all the NOTROIs and join them in a bigger NOTROI, by the use of the function NBL_Concatenate.m. The reason why it can be done with the two first filters is that it is not the same selecting streamlines that cross two regions simultaneously, than selecting streamlines which cross a region first and then another (**Figure 19**) (D. K. Jones 2010). For the NBL_NOTROIfilter.m that is not an issue because we wish to exclude every spurious streamlines.

There should also be stated that filters are activated depending on the number of ANDROIs, SHORTROIs and NOTROIs specified in the text file. This means that, for example, if there are no SHORTROIs in the text file, the NBL_filterTract_short.m will not take place.
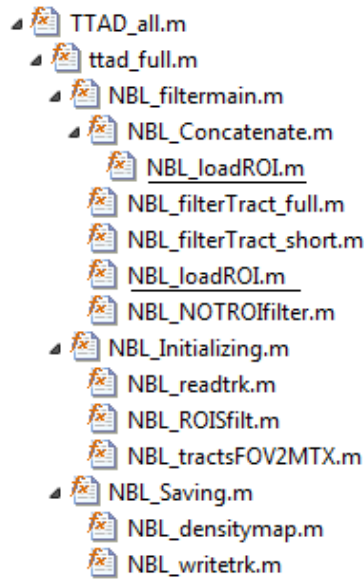
TTAD_all.m
  ttad_full.m
    NBL_filtermain.m
      NBL_Concatenate.m
        NBL_loadROI.m
      NBL_filterTract_full.m
      NBL_filterTract_short.m
      NBL_loadROI.m
      NBL_NOTROIfilter.m
    NBL_Initializing.m
      NBL_readtrk.m
      NBL_ROISfilt.m
      NBL_tractsFOV2MTX.m
    NBL_Saving.m
      NBL_densitymap.m
      NBL_writetrk.m

Figure 31 - Initial code structure

In **Figure 31** we can see the initial structure of the automated tool and the underlying code. One of the functions is underlined because it is the same function which is called from different places. NBL_loadROI.m, as it states, is responsible for loading the ROIs (which are all written in the textfile) specified for the filter functions. This brings us to the last step of the automated method which is NBL_Saving.m. The variable save mode retrieved from the textfile plays an essential role to define if NBL_densitymap.m, NBL_writetrk.m or both are called. NBL_densitymap.m originates a kind of visitation map, which maps the density of streamlines per voxel. NBL_writetrk.m simply writes the final filtered track.

These first steps establishes the framework for the method to be applied but require a way to switch between subjects. For that purpose, it was created the function TTAD_all.m, which evaluates how many subjects comprehend the study and runs the method (function ttad_full.m) for every subject.

6.5 - Additional Rules and Filtering

After the first step of the project had been concluded, there was the need to implement further rules and filtering that could lead to a more robust analysis. The first one was to develop a way to include further anatomical priors such as planes that helped in excluding spurious streamlines. A function called generate_plane was created in order to allow the user to define different planes in one of the different planes of interest (sagittal, coronal or axial). The generated ROI would then be used as a NOTROI in the process of the streamline filtering. **Figure 32** elucidates the dissection of the Optic Radiation, which connects the thalamus and the occipital lobe. Since the Optic Radiation, departs from the Lateral Geniculate Nucleus (LGN), in the most posterior part of the thalamus and connects the occipital lobe, no streamlines should be propagating to frontal areas. Therefore, in this case, the coronal plane is working as an anatomical prior in the sense that would exclude all the streamlines that travelled anteriorly in the brain. This prior is placed, having into consideration the variability of the Optic Radiation.
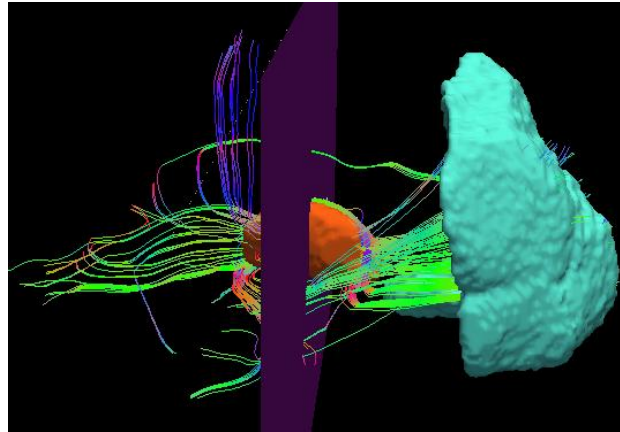
Figure 32 - Visualization of a plane as an anatomical prior

Additionally to the possibility of generating these anatomical priors, a new type of filtering was implemented through the function NBL_filterTract_cut.m. This type of filtering allows one to evaluate the streamlines between two regions of interest selecting only the points located between them. It checks all points on the streamlines saving the information about those which are located inside the two regions of interest. After that, according to the order of the points in the streamline, this filter selects only the points that belong to the path between the two ROIs saving only that path.

6.6 - Registration with Different Regions of Interest

As it was said before, the idea was to enhance the automatic tool by making it flexible in the sense that it could also be used to generate ROIs from different templates to native space. This became the second step of the project, which implementation brought us to the current organization of the software depicted in **Figure 33**.
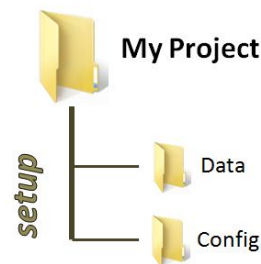
Figure 33 - Initial setup for the software to work.

Before explaining the actual generation process of the regions of interest it is worth mentioning the structure necessary for the code to work. Initially, the user is required to setup the folder where the analysis is going to be run (My Project). Inside that folder, there are two more folders, named Data and Config, which are responsible for storing data and configuration rules regarding the automatic analysis, respectively.

6.6.1 - Data Folder

This folder contains different subfolders necessary for the preparation of the software (**Figure 34**). Tractography_Data contains the diffusion data that has been processed and will be used to automatically parcellate different brain regions (one folder with diffusion maps per

subject). Additionally to the data to be parcellated, it was introduced the possibility of generating ROIs from different template spaces to native space in order to use them in the automatic dissection. Therefore, folders with different regions of interest and corresponding template can be stored inside Data folder, with no limit on the number of folders (ROI_...). These folders contain a subfolder called Regions, which holds all the different regions that the user want to transform to native space, and a standalone file corresponding to the template brain for that particular space.
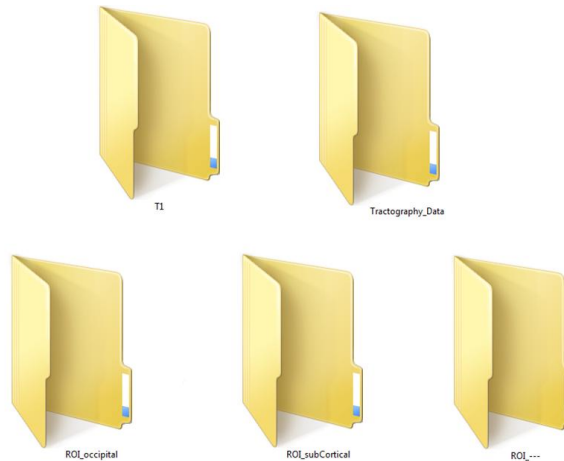
Figure 34 - Data folder structure

The last folder that can be seen inside Data is the one related to the structural images of all the subjects, that are assumed to be correctly oriented. However, as an utility for the software a function called orient.m has been created to allow the user the possibility of reorienting the considered images. These images will be important in the process of registering the original regions of interest to native space, as it will be explained in the Registration Process sub-section.

6.6.2 - Config Folder

As it can be seen from **Figure 33**, the Config folder is the other important folder to setup the initial structure for the software to be run. Besides having configuration files necessary for the registration process, it includes the text file where additional rules that will be read by Config_Struct.m are defined. This function has evolved from NBL_ROISfilt.m and it is responsible for loading the text file located in the Config folder and saving variables that will be used by the software in latest stages. An example of the configuration text file is displayed below.

```
#main_root=/media/Acer/CNS/MyProject
#technique=sd
#coord_shift=1 1 1
#target_space=MNI_1mm_template


%letters in target space must be in the template placed in ROIs
folder

Batch1 CC_frontal_L
T corpus_callosum
C on

A CC.nii.gz %50 ROI_Original
A frontal_L.nii.gz %50 ROI_cc_maps
N coronal_not_slice_167.nii.gz %50 ROI_rules

$savemode=2

density_masking_reg1 Right_white.nii.gz %50 ROI_Original

_

Batch2 CC_frontal_R
T corpus_callosum
```

Figure 35 - Structure of the text file that holds all configuration parameters for the code to work properly.

Besides defining the root directory (into MyProject) it is also needed to detail which technique has been used to generate data - important in the process of interpolation - as well as the target space where the automatic dissections results should be saved. These variables will be further explained in the relevant steps of the project. Coord_shift is a variable that takes into account the shift that we get when we use the NBL_tractsFOV2MTX.m function to convert tractography data from mm to pixel space.

The configuration text file also specifies different filtering batches, according to the tract volume (T), which regions to be used (different ROI and ROI folder) and how to use them (and - A, not - N). It determines whether to save the density map (savemode 0), the track file (savemode 1) or both (savemode 2). Finally, it optionally allows the saving of a filtered density map with a pre-chosen region of interest and whether or not to use the NBL_filterTract_cut.m, by choosing on or off.

6.6.3 - Registration Process

After the initial setup described by placing all the necessary contents in both folders mentioned above, the actual process of generating the regions of interest into native space begins. The first step is the creation of a Track_analysis folder, where we will find a determined number of folders with the name of each subject, containing all the generated ROIs and data to be parcellated, in native space. In **Figure 36** we can visualize the outputs created in the registration process for subject BRC001, for purposes of demonstration, as Track_analysis is completed with other subjects' folder with the same structure.
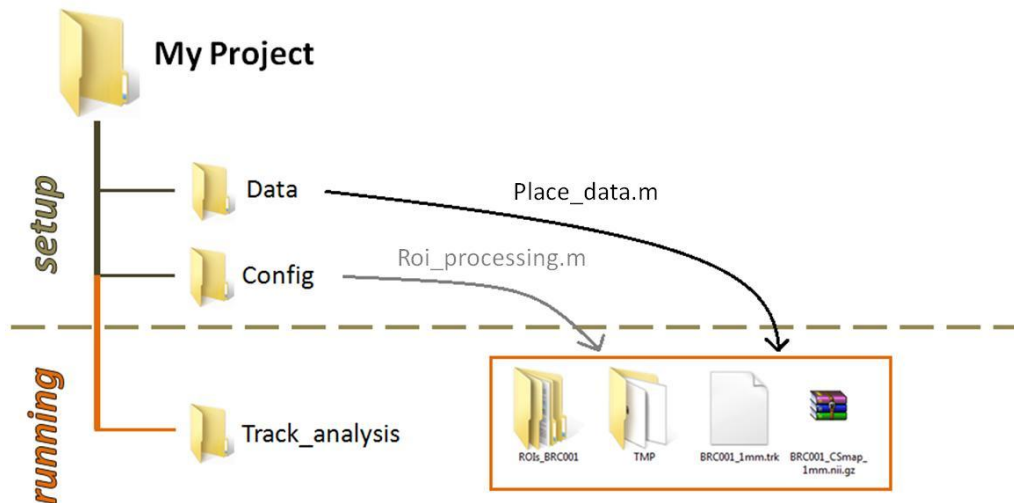
Figure 36 - Creating the folder Track_analysis where the final results will be saved.

The first function to be called is Place_data.m that is responsible for copying the diffusion maps as well as the track file to the folder created for a specific subject. The first evaluation that is done on the data is if it already has 1 mm resolution, in which case data is copied directly from the initial folder to the newly created one. However, the resolution that we are able to get for diffusion MR images isn't still that high, being data generally acquired with 2-2.4 mm isotropic voxels. To be able to get the desired resolution, two functions were created: interpolate_data and interpolate_data_DTI. Both these functions are identical, and only differ in the diffusion data they deal with (which is specified in the configuration file), as the first one expects Spherical Deconvolution data and the second one, Diffusion Tensor Imaging data. The way this function works, is to generate a header with the desired resolution (in our case, 1 mm voxels) to which the original diffusion map is registered. After we get this transformation, we use it to generate the 1 mm diffusion map and the 1 mm track file. To generate the track file, specific commands are used from the dedicated software TrackVis. In order to get all the data for the generation of the regions of interest, a brain extraction is performed on the subject's anatomical image so that it can later be used in the registration process. This step is once again performed recurring to FSL.

At this stage, all diffusion data is already at 1 mm and we proceed to the generation of the regions of interest by calling the function Roi_processing. This process will be the way to obtain a transformation that can be applied to the regions of interest in standard space and generate them into native space. Built to allow great flexibility and easiness of usage, the software first evaluates if the transformation from MNI to native space for each subject has already been performed. If that is the case, it makes use of that transformation (that is stored in the folder TMP, one of the final results in Track_analysis) and follows to the generation of the region of interest by applying that same transformation. If the registration process hasn't been run before, there are a few steps that have to be followed which are indicated below.
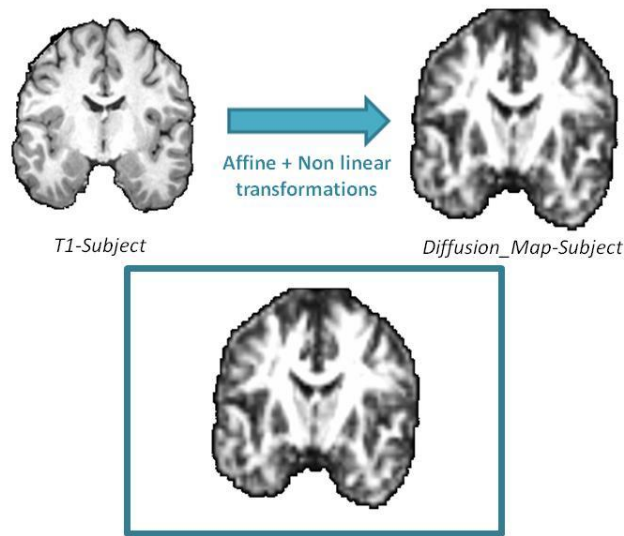
Figure 37 - First registration step, transforming the anatomical image of the subject to his diffusion map.

The first step is the registration of the anatomical image of the subject to his diffusion map through a set of registrations. Several attempts were made to identify the best registration possible, such as: the only use of rigid-body transformations as the volume and shape of the brain are the same; affine transformations, which included shearing and global scaling as well as rigid-body transformations; and finally non-linear transformations through the application of warping fields. The registration that proved to be the most efficient was the one where a first affine transformation was performed which generated a matrix that served as initial point for the non-linear registration. Both these steps were performed with FSL, through the use of FLIRT and FNIRT for the affine and non-linear registrations, respectively.

The second step of the registration process is similar to first one in and is the one that allow us to get the transformation field from MNI to native space as shown in **Figure 38**. The MNI anatomical image is going to be registered to the output image of the first registration step, the anatomical image of the subject transformed into diffusion space. The reason why this was done, is because the registration of the anatomical template image matches better into diffusion subject space if it is registered indirectly, through the use of the first intermediate step (**Figure 37**). These results were compared with the direct registration of the anatomical template to the diffusion subject space, which proved not to be the best procedure. This second step is show in the figure below.

2 - Registration of T1-MNI_template into T1-Subject registered into Diffusion space

T1-MNI_Template

Affine + Non linear transformations

T1-Subject_registered to Diffusion space
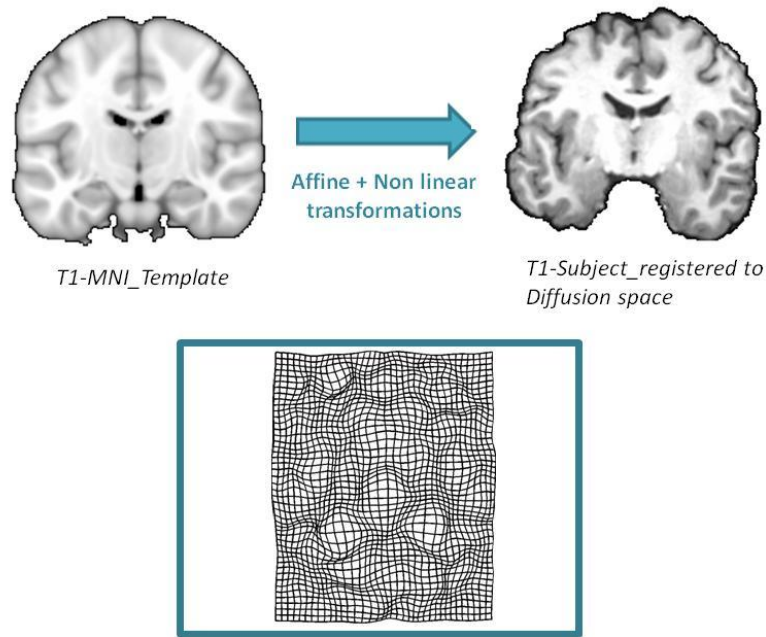
Figure 38 - Second step of the registration process, which registers the anatomical template to the output of the first registration step.

6.6.4 - Map Generation

After all the regions of interest have been created inside specific folders according to the name in the original placement of the data, the automatic dissection process can begin. As it is described in the operation of the software, there is the possibility of generating both track files and density maps. With the purpose of obtaining an atlas of the different structures that can be studied, these maps must be converted back to MNI space.

To this purpose two more functions were created: create_maps and average_MNI_maps. The first function is responsible for inverting the transformation obtained in the second registration step, in order to convert the final density maps of the subject into MNI space. It evaluates beforehand if the transformation has already been calculated and only proceeds if it is still absent. The second function takes care of binarizing all the MNI maps of each subject and average them according to a specific structure, for example the Optic Radiation (**Figure 39**).

Individual Density Map

Create_maps

Conversion of all individual maps to MNI space

Average_MNI_maps

Average of all maps (MNI space), after binarization

Final Density Map

Figure 39 - Processing of generating final density maps of the structure of interest

6.7 - Performed Studies

In order to test and use the software above mentioned, three different studies were performed with different levels of complexity. For all of them manual dissections were carried out to some extent so that results could be compared with the ones obtained by the automated method. As it was stated before, a list of predetermined ROIs had already been drawn manually by specially dedicated professionals. It includes cortical and sub-cortical regions that are specified in **Table 1** and **Table 2** respectively. However, the delineation of specific ROIs required f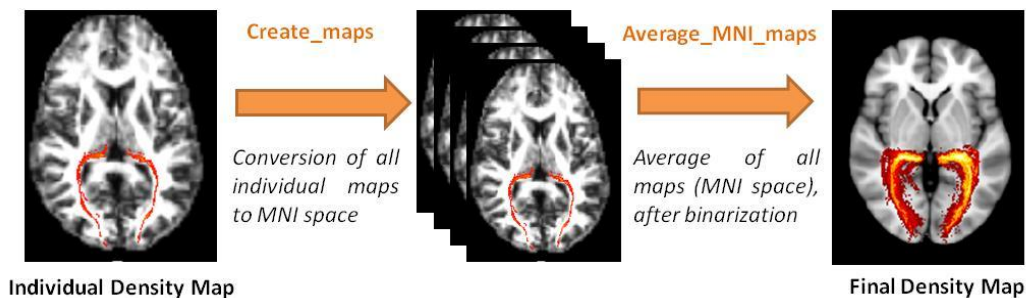or each analysis were drawn in this study as the need for them was found. It is worth mentioning that the data that was available comprised 20 spherical deconvolution datasets and only 19 datasets from diffusion tensor imaging. Therefore, when comparing between DTI and SD only 19 subjects were used to generate atlas in both techniques.

Table 1 - Cortical regions used in this study

Cortical Regions	
Angular Gyrus	Middle Temporal Gyrus, temporooccipital part
Central Opercular Cortex	Occipital Fusiform Gyrus
Cingulate Gyrus, anterior division	Occipital Pole
Cingulate Gyrus, posterior division	Paracingulate Gyrus
Cuneal Cortex	Parahippocampal Gyrus, anterior division
Frontal Medial Cortex	Parahippocampal Gyrus, posterior division
Frontal Operculum Cortex	Parietal Operculum Cortex
Frontal Orbital Cortex	Planum Polare
Frontal Pole	Planum Temporale
Heschl's Gyrus (includes H1 and H2)	Postcentral Gyrus
Inferior Frontal Gyrus, pars opercularis	Precentral Gyrus
Inferior Frontal Gyrus, pars triangularis	Precuneous Cortex
Inferior Temporal Gyrus, anterior division	Subcallosal Cortex
Inferior Temporal Gyrus, posterior division	Superior Frontal Gyrus
Inferior Temporal Gyrus, temporooccipital part	Superior Parietal Lobule
Insular Cortex	Superior Temporal Gyrus, anterior division
Intracalcarine Cortex	Superior Temporal Gyrus, posterior division
Juxtapositional Lobule Cortex (formerly Supplementary Motor Cortex)	Supracalcarine Cortex
Lateral Occipital Cortex, inferior division	Supramarginal Gyrus, anterior division
Lateral Occipital Cortex, superior division	Supramarginal Gyrus, posterior division
Lingual Gyrus	Temporal Fusiform Cortex, anterior division
Middle Frontal Gyrus	Temporal Fusiform Cortex, posterior division
Middle Temporal Gyrus, anterior division	Temporal Occipital Fusiform Cortex
Middle Temporal Gyrus, posterior division	Temporal Pole

Table 2 - Sub cortical and general regions used in this study

Sub-cortical Regions	General
Accumbens	Left ventricle
Amygdala	Right ventricle
Brain Stem	White matter left
Caudate	White matter right
Corpus Callosum	
Hippocampus	
Pallidum	
Putamne	
Thalamus	

Studies specifications are now approached as well as the different files used for the parcellation.

6.7.1 - Arcuate Fasciculus

The parcellation of the Arcuate Fasciculus consisted in the first test of the automated tool. At this stage the procedure to be followed consisted in delineating regions of interest accordingly to the two-method ROI described by Catani (Catani et al. 2002).
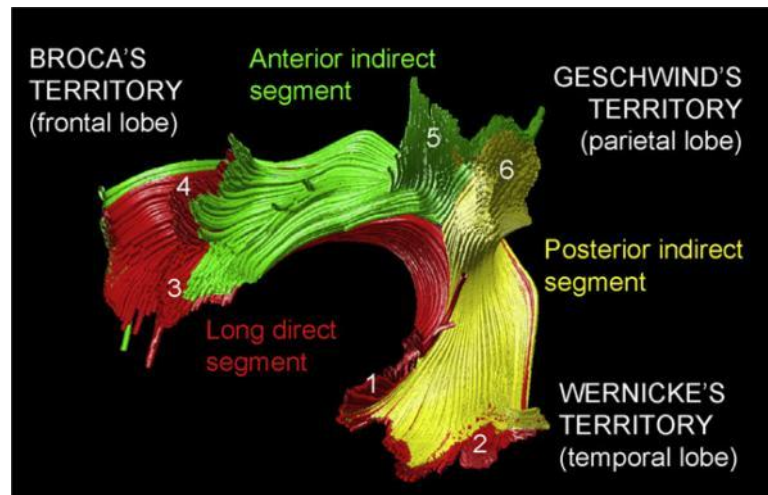
Figure 40 - Division of Arcuate Fasciculus in three segments in DTI (Catani & M. Mesulam 2008a)**.**

The regions of interest were drawn in order to isolate the long segment of the Arcuate Fasciculus. A coronal and an axial ROI were drawn as seen in **Figure 41**. These regions were then used to automatically parcellate the volume of tracts for all DTI datasets with use of no other rules and NOTROIs.
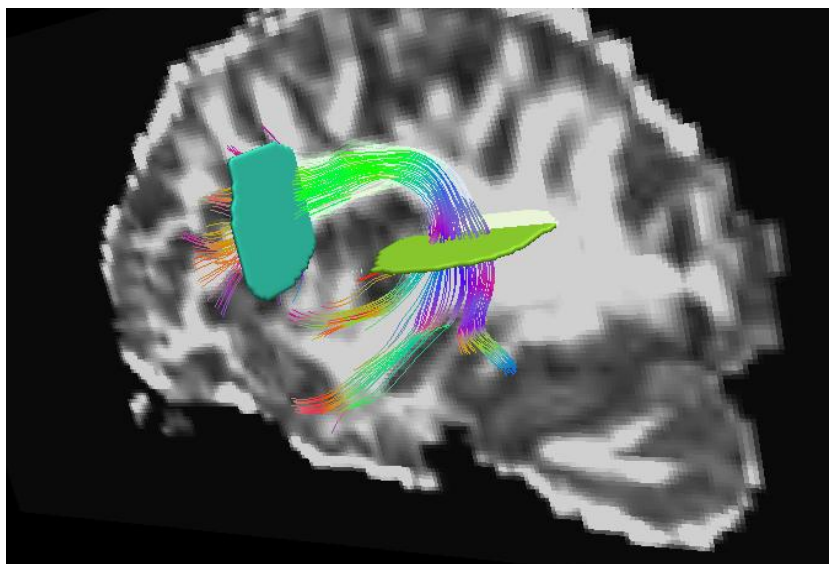
Figure 41 - Delineation of the two regions of interest.

6.7.2 - Corpus Callosum

The Corpus Callosum consisted in an evolution considering the study of Arcuate Fasciculus in the sense that this analysis already involved the use of NOTROIs. In this study, the purpose was to use the automated tool to parcellate the Corpus Callosum based on its structural connectivity and not only based on geometric considerations (Witelson 1989). Two approaches were followed: the parcellation of the Corpus Callosum based on all individual cortical regions considered and into "lobes", i.e, the individual regions were combined as to form big regions which could then be seen as individual lobes. For both cases, the analysis was run for the left and right side.

Figure 42 - Lobar division of the dorsolateral (A) and medial (B) surface of the left cerebral hemisphere (Catani & Thiebaut de Schotten 2012)**.**

The cortical regions were grouped as followed based on the subdivision presented by Catani & Thiebaut de Schotten, 2012:

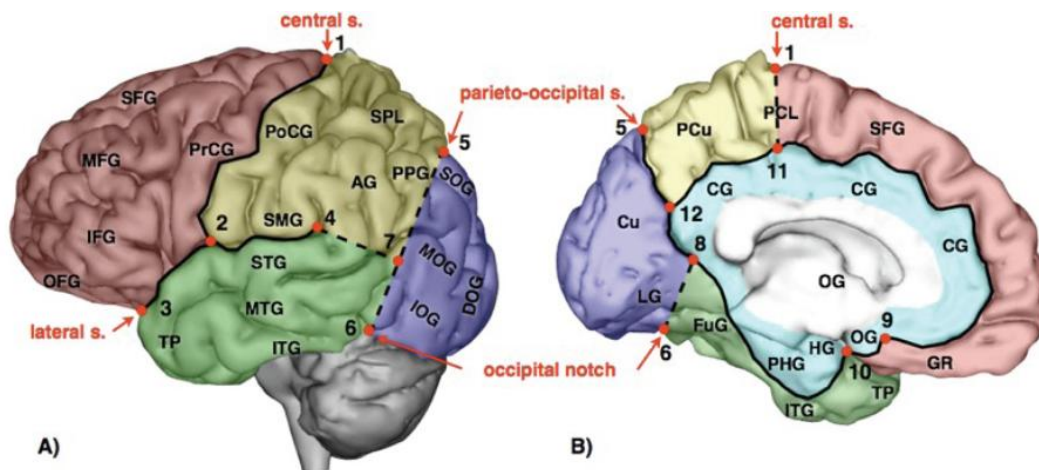- **Frontal region**: Frontal Pole, Insular Cortex, Superior Frontal Gyrus, Middle Frontal Gyrus, Inferior Frontal Gyrus Pars Triangularis, Inferior Frontal Gyrus Pars Opercularis, Frontal Medial Cortex, Juxtapositional Lobule Cortex, Subcallosal Cortex, Paracingulate Gyrus, Cingulate Gyrus Anterior Division, Frontal Orbital Cortex, Frontal Operculum Cortex;
- **Pre Central region**: Pre Central Gyrus;
- **Pos Central region:** Pos Central Gyrus;
- **Temporal region**: Temporal Pole, Superior Temporal Gyrus Anterior Division, Superior Temporal Gyrus Posterior Division, Middle temporal Gyrus Anterior Division, Middle temporal Gyrus Posterior Division, Middle temporal Gyrus Temporoocipital Part, Inferior Temporal Gyrus Anterior Division, Inferior Temporal Gyrus Posterior Division, Inferior Temporal Gyrus Temporoocipital Part, Parahippocampal Gyrus Anterior Division, Parahippocampal Gyrus Posterior Division, Temporal Fusiform Cortex Anterior Division, Temporal Fusiform Cortex Posterior Division, Temporal Occipital Fusiform Cortex, Planum Polare, Heschls gyrus, Planum temporal;
- **Parietal region**: Superior Parietal Lobule, Supramarginal Gyrus Anterior Division, Supramarginal Gyrus Posterior Division, Angular Gyrus, Cingulate Gyrus Posterior Division, Precuneous Cortex, Parietal Operculum Cortex;
- **Occipital region**: Lateral Occipital Cortex Superior Division, Lateral Occipital Cortex Inferior Division, Intracalcarine Cortex, Cuneal cortex, Lingual gyrus, Occipital Fusiform Gyrus, Supracalcarine Cortex, Occipital pole.

As it can be seen by **Figure 12**, the anatomy is more reliably presented with HARDI techniques, in particular with SD. Therefore in this second study only Spherical Deconvolution datasets were used. Regarding the NOTROIs used: for the parcellation with the temporal region, a region of interest to avoid fibres that belong to the Fornix (**Figure 43 d**) was used as well as the brain stem region (Catani & Thiebaut de Schotten 2008); in the parcellation with the frontal region a coronal plane placed several voxels anteriorly to the splenium (accounting for inter-subject variability - **Figure 43 a**) was used to avoid spurious streamlines projecting to the posterior region of the brain and also two coronal circular ROIs to avoid contribution of the Inferior Frontal Occipital Fasciculus (IFOF); in the same way, to avoid propagation for the anterior region of the brain a coronal plane was used in the parcellation with the occipital region and with parietal region (even though they were placed in different slices - **Figure 43 b** and **c** respectively); there were not used any NOTROIs for the Pre-central and Pos-central region.
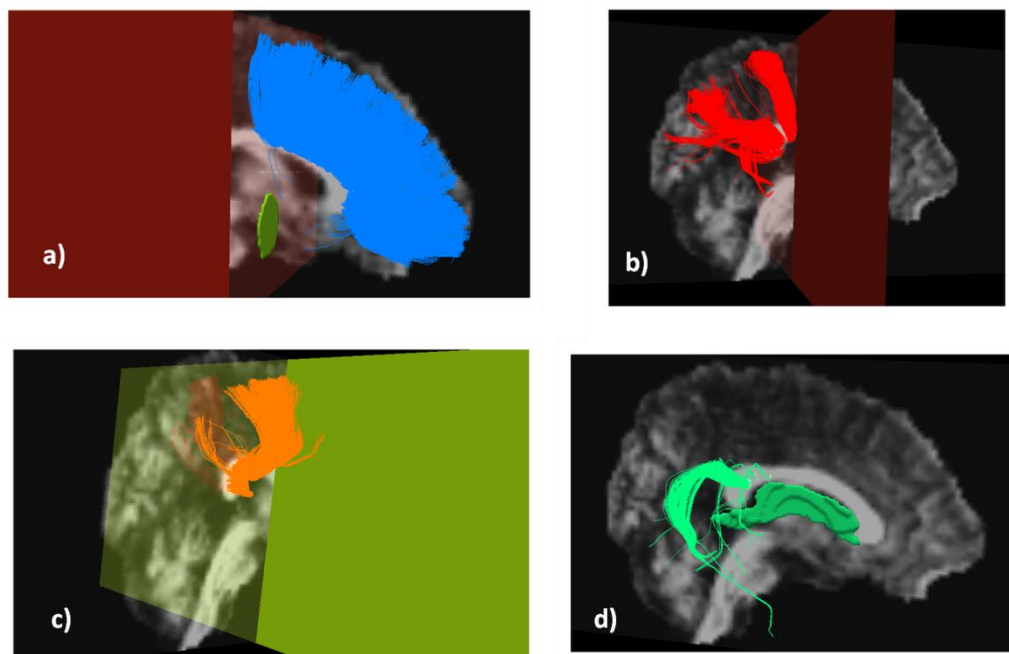
Figure 43 - Regions of interest used to exclude spurious streamlines for the a) Frontal region, b) Occipital region, c) Parietal region and d) Temporal Region.

This second study consists on a pre-cleaning strategy where the final results can still be improved by some minor manual adjustments. Maps for all different big regions and individuals were generated.

6.7.3 - Optic Radiation

This study was the one that involved more steps and can therefore be considered the most elaborated. It comprised the creation of density maps of the Optic Radiation for DTI and SD, as well as the comparison between both atlases. The regions of interest that were used were the thalamus and the Occipital pole, as it corresponds mainly to Visual Area 1, where the Optic Radiation projects. The use of NOTROIs was also present, through the use of a coronal plane (to avoid streamlines propagating to do the anterior portion of the brain), a sagittal plane (to avoid any commissural fibres of being present) and the brain stem. Additionally to these rules, the NBL_filterTract_cut.m function was also used.
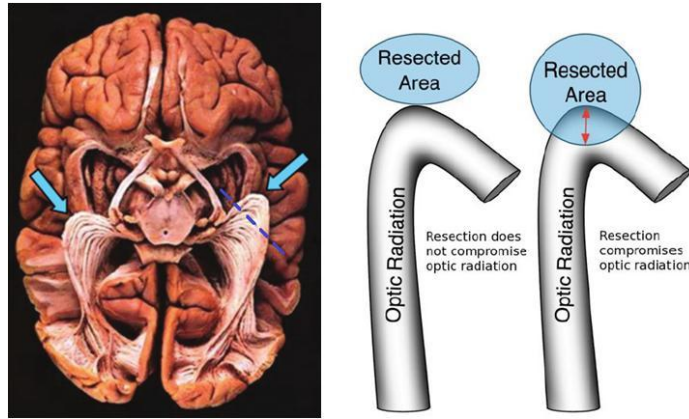
Figure 44 - Delineation of Optic Radiation is essential for neurosurgical planning (Daga et al. 2011)**.**

This study was very important because it was able to present a new atlas of the Optic Radiation which is more accurate when compared with other studies (check Results and Discussion) and has given place to one oral communication in the International School of Clinical Neuroanatomy, Sicily, May, 2012 and to a Poster in the Workshop of Biomedical Engineering Lisbon, April, 2012. A modified and updated version of these communications has also been accepted for an oral communication in the European Society for Magnetic Resonance in Medicine and Biology, which took place in Lisbon, October 2012. The abstracts regarding this work are present in the appendixes section.

7 - Results

The outcome of the studies described in the last chapter is now summarized and major conclusions are reserved for the next chapter.

7.1 - Arcuate Fasciculus

The approach to automatically parcellate the Arcuate Fasciculus was the same followed by (Catani & M. Mesulam 2008a) and the regions of interest were drawn once so they could be used in the automatic software, as seen in **Figure 41**. The width and height of the regions were chosen so they could take into account inter-subject variability. As it can be seen by **Figure 40** the Arcuate Fasciculus can be subdivided into three segments, but In this study we focused only on the parcellation of the long segment.
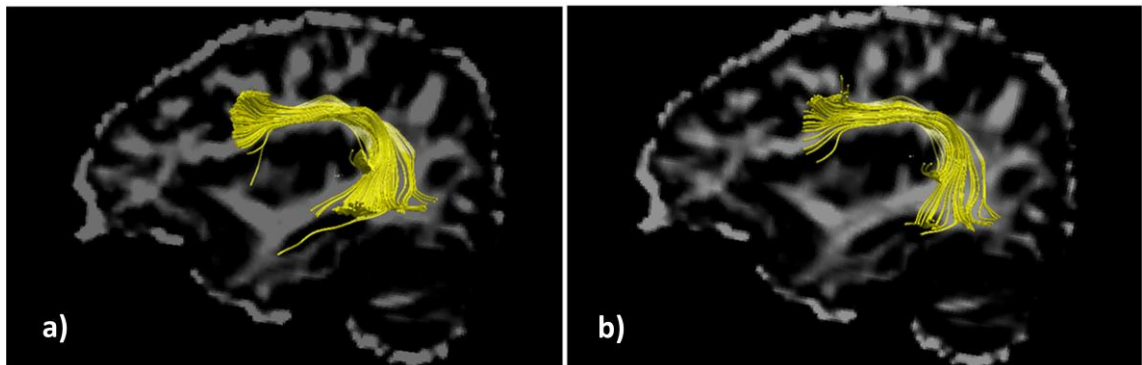
Figure 45 -Automatic a) and Manual b) dissection of the Arcuate Fasciculus for one individual subject.

In **Figure 45** it is possible to identify some spurious streamlines which derived from the fact that only simple filtering of the desired tracts was performed. This process was followed for 19 subjects, and then an atlas was created by the process detailed in **Figure 39**. The results for the automatic and manual atlas are presented for the three main views: sagittal, coronal and axial.
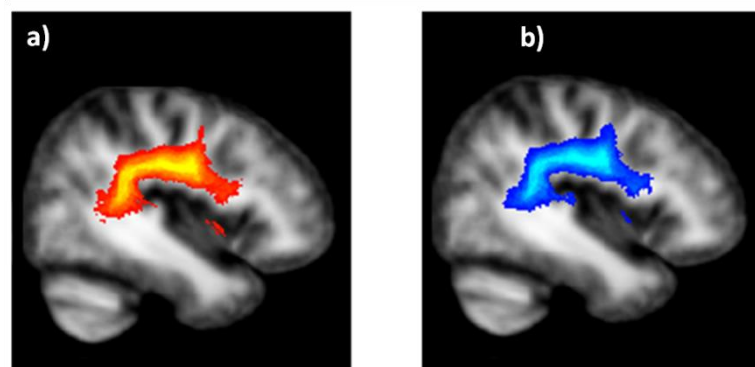
Figure 46 - Automatic a) and Manual b) atlas of the Arcuate Fasciculus (DTI), sagittal view (left side for visualization purposes).
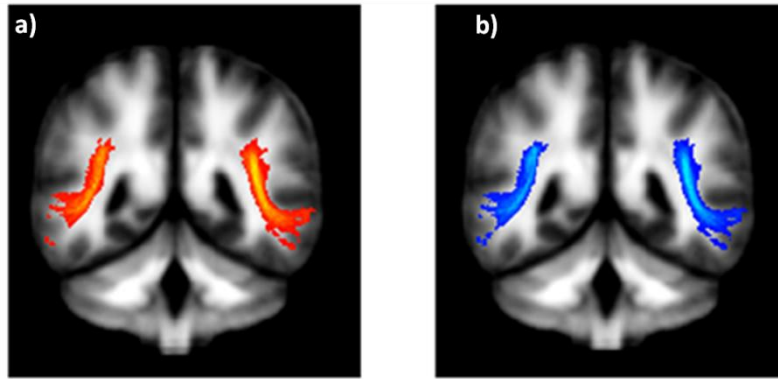
Figure 47 - Automatic a) and Manual b) atlas of the Arcuate Fasciculus (DTI), coronal view.
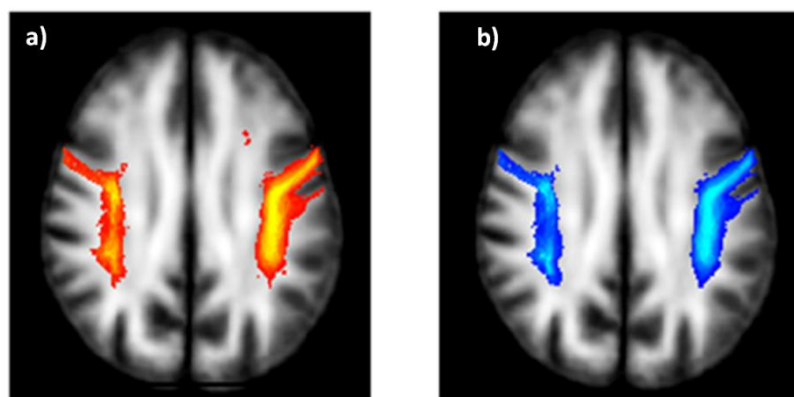
Figure 48 - Automatic a) and Manual b) atlas of the Arcuate Fasciculus (DTI), axial view.

7.2 - Corpus Callosum

The analysis of the Corpus Callosum comprised an progress regarding the Arcuate Fasciculus since the use of NOTROIs was also applied (**Figure 43**). The colour code for the images is: red for the Frontal region, yellow for Pre-central region, green for Pos-central region, green for Pos-central region, blue for Temporal region, pink for Parietal region and grey/purple (it was difficult to visualize streamlines in grey with TrackVis) for Occipital region.

Once again the procedure of atlas generation detailed in **Figure 39** was followed. However, two different approaches were taken: firstly, the individual maps for each region were converted to MNI space, combined into big regions and then averaged to create an atlas; secondly, individual maps were combined in native space as big regions and then the regions were converted to MNI.
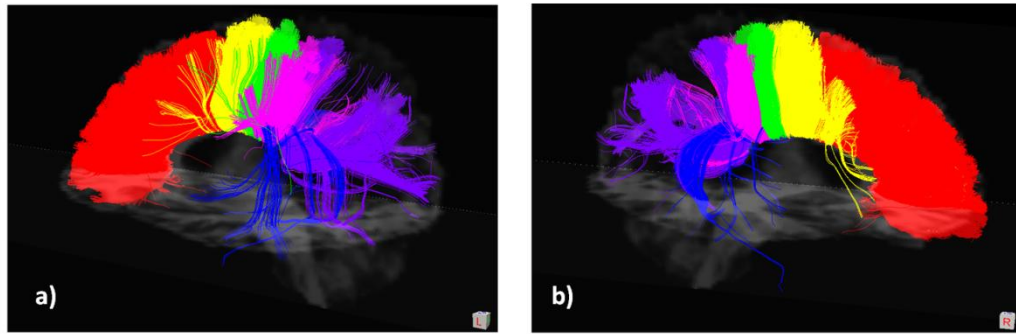
Figure 49 - Parcellation of the Corpus Callosum according different "lobes" (one subject) as seen from the left a) and right side of the brain b), respectively.

The second approach proved to be the best, as information wasn't lost when converting individual maps and then combining them into regions, because they were already forming a big region. Below are the maps for the big regions showing the projection of callosal fibres in cortical regions from different views (**Figure 50**) and a geometric division based on different connecting lobes (**Figure 51**).
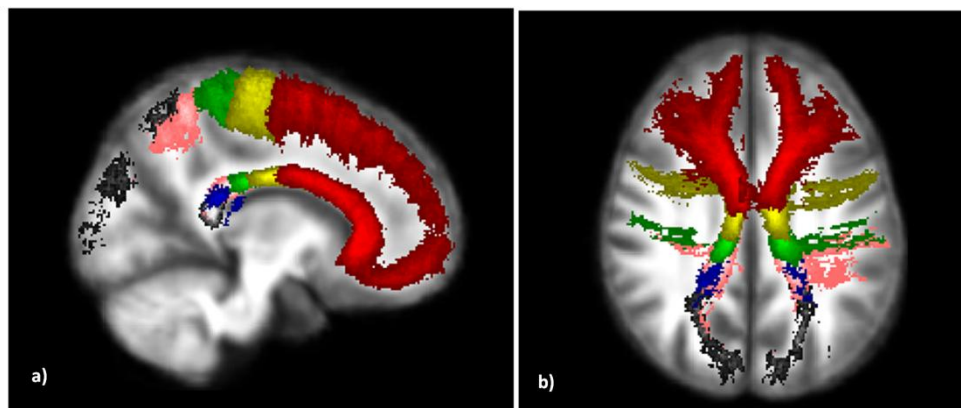
Figure 50 - Projection of Callosal fibres into cortical regions from a) sagittal view and b) axial view.
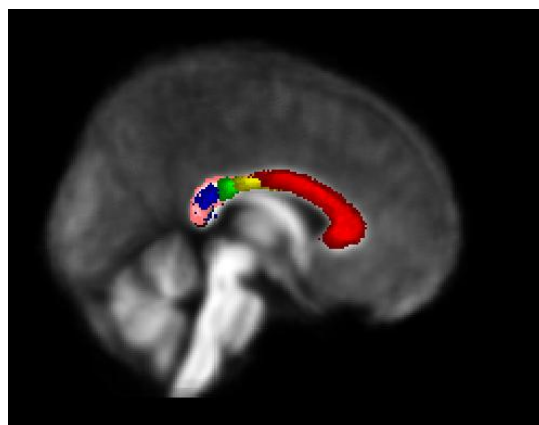
Figure 51 - Structural division of the Corpus Callosum into six different lobes.

It is important to remember that this analysis was performed on 20 subjects and with spherical deconvolution data. Recalling what has been said before, with HARDI techniques it is clear that the lateral projections of the Corpus Callosum are better visualized, in this case situation shown for the pre-central (**Figure 52 a**) and pos-central (**Figure 52 b**) region.
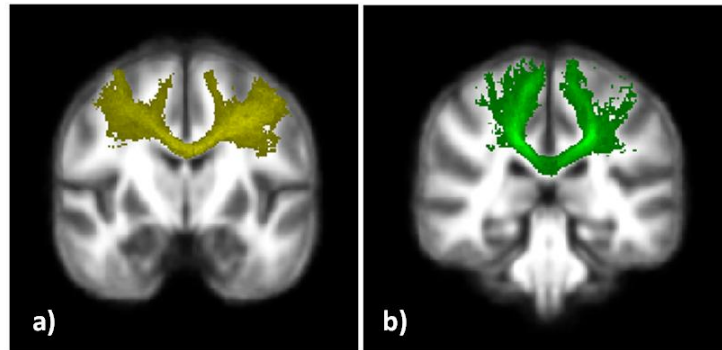
Figure 52 - Density maps of Callosal projections into a) Pre-central region and b) Pos-central region

7.3 - Optic Radiation

The third and more complete analysis was run on the Optic Radiation. Besides the use of ROIs for including and excluding streamlines, a different filter (NBL_filterTract_cut.m) was also used to produce better results. Similarly to previous studies presented in this thesis a comparison between manual and automatic dissection is shown for an individual (**Figure 53**) followed by the atlas that was generated (**Figure 54**).
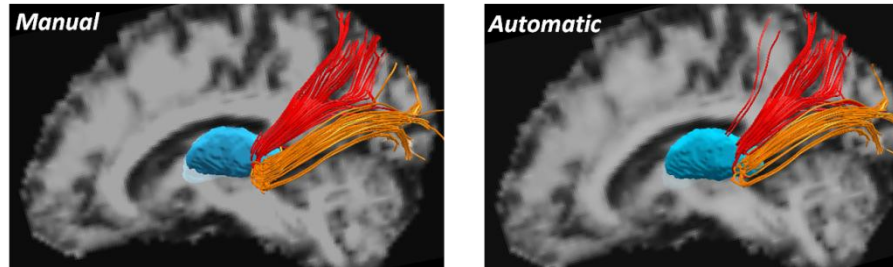
Figure 53 - Comparison between manual and automatic dissection of the Optic Radiation for an individual subject.
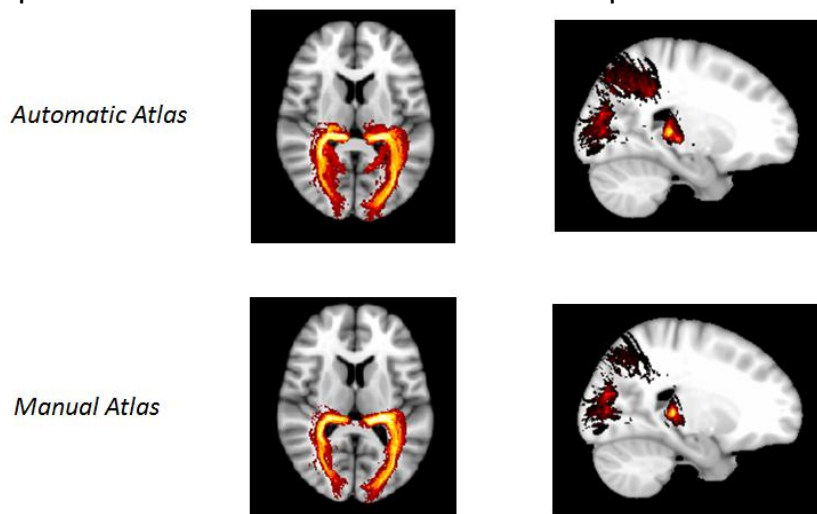
Figure 54 - Atlas of the Optic Radiation, presented in the form of Maximum Projection Intensity (MIP).

The obtained atlas of the Optic Radiation in the MIP form was compared to the splenium of the Corpus Callosum in order to evaluate how well crossing fibres could be resolved (**Figure 55**). Furthermore, comparison between an existing DTI atlas (Catani & Thiebaut de Schotten 2008) and the SD-based atlas obtained by the automatic process was performed (**Figure 56**).
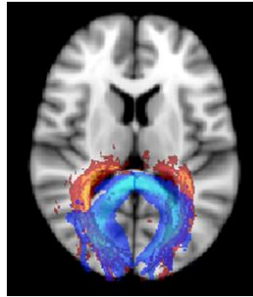
Figure 55 - MIP of the Optic Radiation (red-yellow) and the splenium (light-blue).
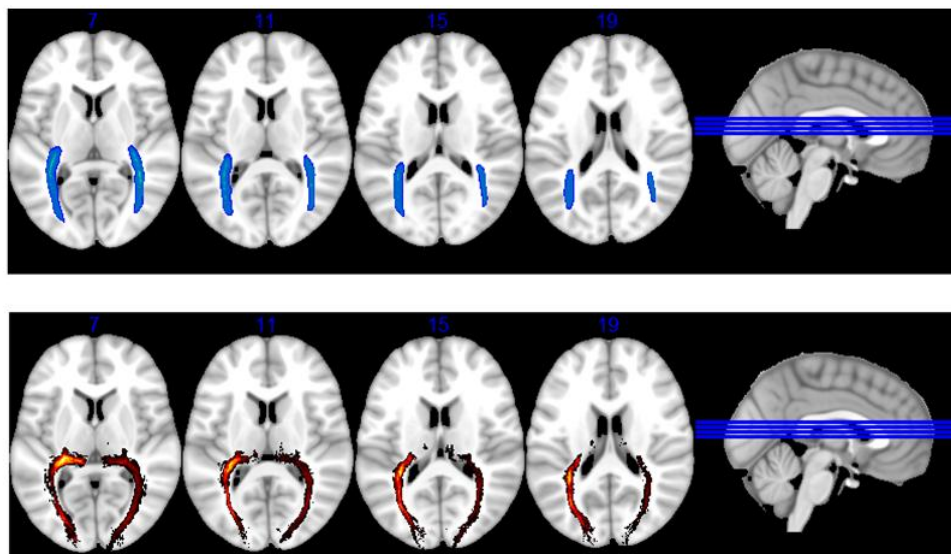
Figure 56 - Comparison between the automatic atlas of the Optic Radiation with SD (red-yellow colour) and DTI (light-blue).

8 - Discussion

This last section comprises a more detailed description of the obtained results, putting them into context and highlighting their importance in light of other scientific and neuroanatomical work.

As a proof of concept to the developed automated tool, an initial study was performed to dissect the Arcuate Fasciculus (**Figure 45**). The Arcuate Fasciculus is an association tract that is involved in language and visuospatial processing, connecting frontal, parietal and temporal regions (Catani & M. Mesulam 2008a). Its virtual dissection was first performed by Catani et al (2002) and allowed the identification of three segments in DTI (as depicted by **Figure 40**), revealing an unknown complex anatomy. In fact, since it was first described by dissection studies the Arcuate Fasciculus was named as superior longitudinal fasciculus (SLF) interchangeably (Catani & Thiebaut de Schotten 2012). However, it was found that the Arcuate Fasciculus run alongside the superior longitudinal system and only arcuate's anterior segment can be named as superior longitudinal fasciculus III. The results obtained in **Figure 46, Figure 47** and **Figure 48** are well matched with the anatomy and previous studies, validating the developed tool (Catani & Thiebaut de Schotten 2008). It is important to recall that this study was based on DTI tractography and more advanced techniques are required to elucidate the highly complex underlying anatomy. In Thiebaut de Schotten et al. 2012 the comparison between monkey studies and SD-based tractography in humans led to the delineation of three branches of the superior longitudinal fasciculus, when classical dissection work has only identified the most ventral component (SLF III) (**Figure 57 b)**)(Catani & Thiebaut de Schotten 2012). Further studies are necessary to evaluate the anatomical differences found between DTI and SD and to make a definitive statement about the anatomy of this system. In this manner, an automated tool like the one described in this thesis will be of great importance allowing to test new and more advanced data in a much more flexible and straightforward way.
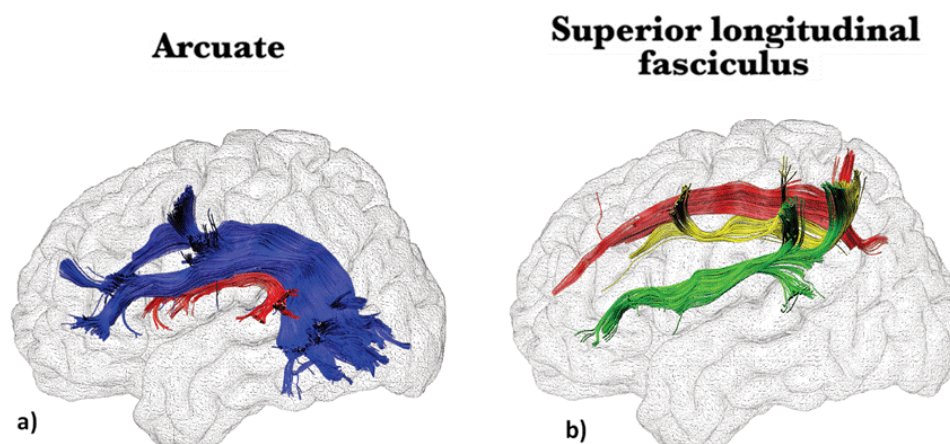
Figure 57 - a) Arcuate Fasciculus, where differences with monkey studies is depicted in blue and similarities in red. b) Superior Longitudinal Fasciculus, with the SLF I, SLF II and SLF III depicted in red, yellow and green, respectively; adapted from (Thiebaut de Schotten et al. 2012)**.**

The second main part of this thesis consisted on the automatic parcellation of the Corpus Callosum. The Corpus Callosum is the largest commissural pathway in the human brain and is responsible for exchanging information between both hemispheres. It is very important to

know how it connects different regions of the brain specifically when there is a disconnection syndrome, this is, when the connectivity between different important centres of information in the brain is lost (Catani & M. Mesulam 2008b). It is important not only to understand the normal brain but also to help understand mechanisms of recovery in pathological cases (Glickstein & Berlucchi 2008). Something that was also unknown was the fact that not only lesions in the midline of the Corpus Callosum could create disconnections but also along the white matter tracts that project into cortical regions (Doron & Gazzaniga 2008).

The geometric subdivision of the Corpus Callosum that is more widely accepted is that it is divided into seven distinct areas: rostrum, genu, truncus (subdivided into rostral body, anterior and posterior midbody), isthmus and splenium.
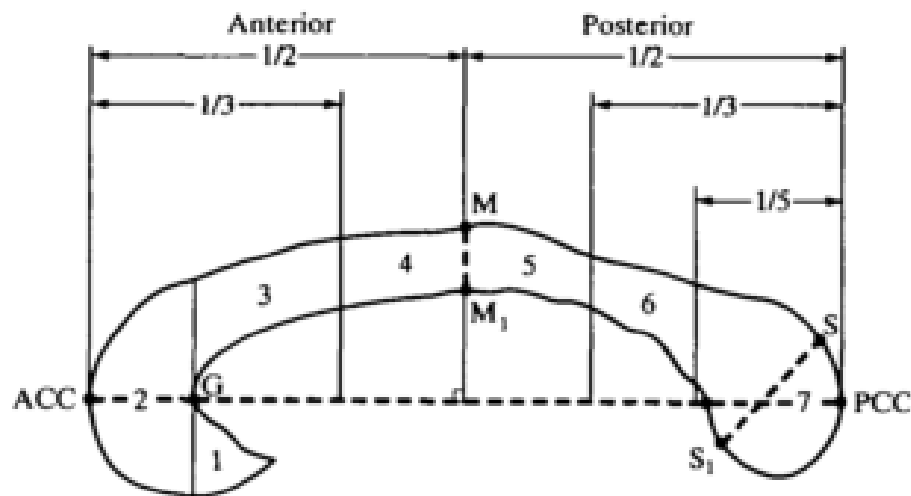
Figure 58 - Geometric sub-division of the Corpus Callosum: 1- Rostrum; 2-Genu; 3-Rostral body; 4-Anterior midbody; 5-Posterior midbody; 6-Isthmus; and 7-Splenium. ACC and PCC represent the most anterior and posterior point of the Corpus Callosum, respectively (Witelson 1989)**.**

This subdivision was mainly achieved by comparing animal work (mainly monkey studies), degeneration studies (Pandya et al. 1971) and post-mortem dissections (Witelson 1989). However, as the findings in animal studies were used to translate information about different parcels of the Corpus Callosum, there might have been an underestimation of the motor area (larger in humans) which result in an inaccurate geometrical subdivision (Catani & Thiebaut de Schotten 2012). The composition of the Corpus Callosum has also been described histologically, as a consistent pattern throughout its own length with variable density of fibres. Thinner fibres are mostly present in the rostrum, genu and mid splenium, while large diameter fibres tend to be more dense in rostral body and anterior midbody as well in the posterior portion of the splenium (Aboitiz et al. 1992). The rest of the Corpus Callosum, namely posterior mid-body and isthmus are represented by the higher density of larger fibres.

These results suggested that the posterior parts of the Corpus Callosum are responsible for faster conducting in contrast to more anterior areas (Yuksel 2011). Tractography studies were also performed and introduced the possibility of studying white matter anatomy non-invasively (S Mori et al. 1999)(Conturo et al. 1999) (D. K. Jones et al. 1999). First approaches were based on the seed placement in the mid-sagittal portion of the Corpus Callosum, retrieving

the streamlines that crossed ROIs placed in specific regions (Huang et al. 2005) and streamlines that presented similar characteristics (Kubicki et al. 2006). Probability algorithms were then introduced to study the callosal connections with several cortical regions (Sherbondy et al. 2008) resulting in an extensive map of the callosal connections as depicted in **Figure 59**.
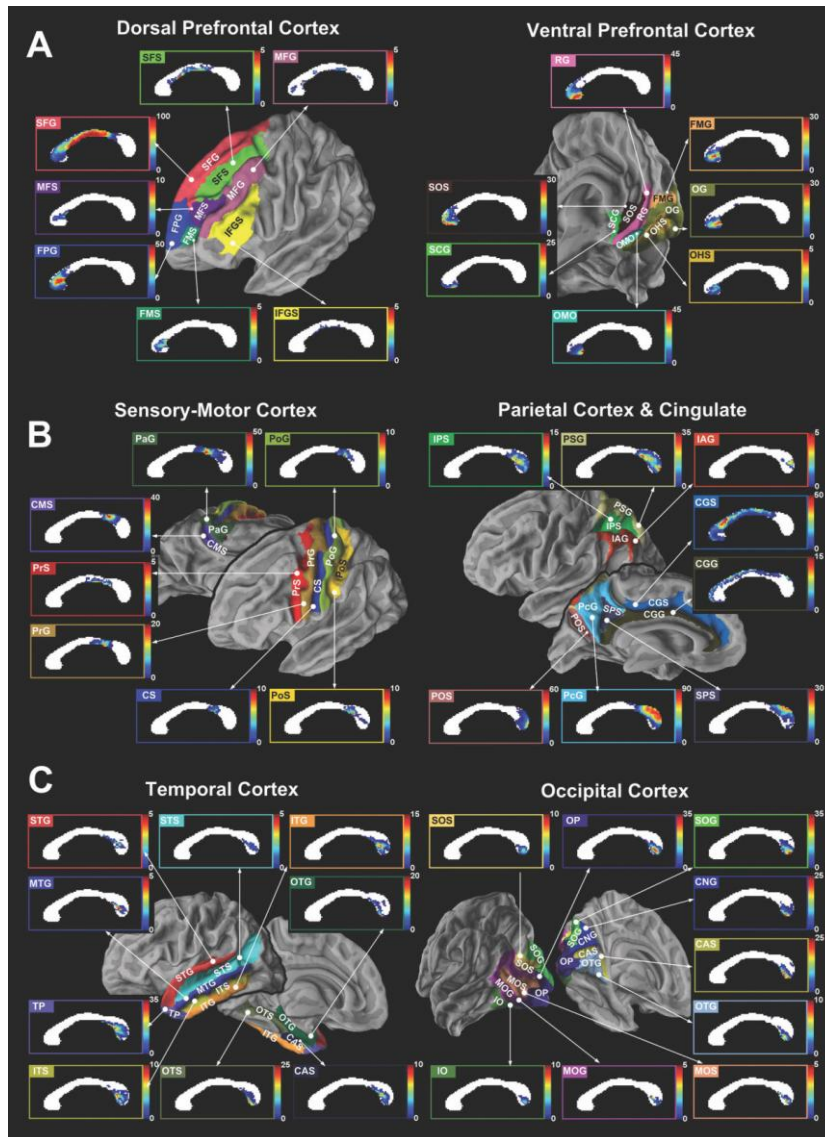
Figure 59 - Probabilistic callosal connection maps of the cortex (Park et al. 2008)**.**

Despite presenting more detailed resolution of callosal connections than the previously shown results, probabilistic approaches present problems as in areas susceptible to artefacts, they retrieve a measure of reproducibility of the data rather than anatomical certainty (Chao et al. 2009).

Furthermore, most of the presented approaches are based merely on the geometry of the Corpus Callosum, not taking into account its projections into different functional areas of cortical grey matter (Pannek et al. 2010). In fact, several tractography studies have also shown that geometric subdivisions of the Corpus Callosum do not always correspond to functional subdivisions delineated (Lebel et al. 2010).

To overcome the limitation of probabilistic based tractography, a global approach was followed in this thesis, were the Corpus Callosum was automatically parcellated according to the subdivision made in (6.7.2 - Corpus Callosum). Even though the current subdivision of the Corpus Callosum is made of seven different regions, we included the pre-motor region in the frontal area. The parcellation was achieved successfully for all subjects, which is representatively pictured in **Figure 49**. As we were only interested in functional areas rather than individual connection maps, only the projections of the Corpus Callosum into different "lobes" are presented **Figure 50**. It was also possible to visualize the benefit of HARDI techniques by the advent of visualizing lateral projections of the Corpus Callosum (**Figure 52**). The fact that anatomical priors in the form of planes were used as well as regions of interest to exclude spurious streamlines, all in an automatic fashion, gave an added value to the developed tool. The anatomy of the Corpus Callosum was therefore validated according to existing studies but needs further improvements. Those may come from the delineation of better regions of interest, validated according to functional studies and also from the use of clustering techniques, since this was a purely ROI-based approach.
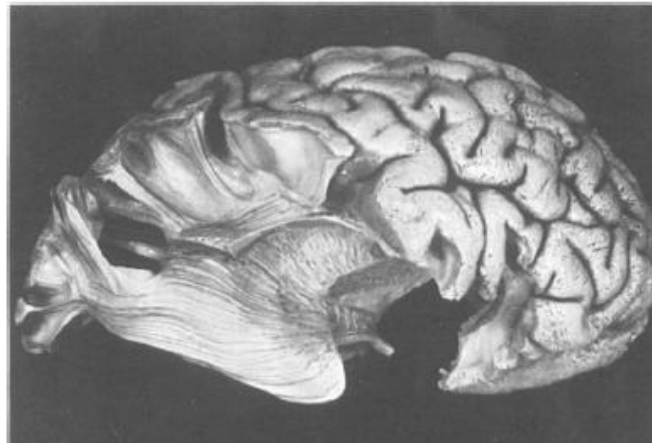
Figure 60 - Optic Radiation prepared with the Klinger method. (Ebeling & Reulen 1988)

The last application of the developed tool was to automatically parcellate and delineate the Optic Radiation. The Optic Radiation is part of the visual system and is responsible for carrying visual stimulus into the occipital lobe. Major works have been performed to depict the anatomical structure of this tract. First approaches based on Klinger's technique (Ebeling & Reulen 1988) and histological mapping allowed to reveal its characteristics (Bürgel et al. 1999) (Bürgel et al. 2006). It departs from the thalamus and can be subdivided into three bundles: an anterior bundle that departs from the LGN and projects deeply into the temporal lobe, passing anteriorly to the inferior horn. This bundle, denominated Meyer's Loop, describes a highly angulated turn from the temporal lobe to terminate in the lower lip of the calcarine fissure; similarly to the Meyer's Loop, a central bundle departs laterally from the LGN and crosses temporal and parietal regions along the lateral wall of the ventricle projecting into the occipital pole; and a dorsal bundle that departs from the pulvinar (thalamus) in a posterior direction and irradiates the upper lip of the calcarine (Tamraz et al. 2006)(Sherbondy et al. 2009)(Hofer et al. 2010).

It has been long documented there are always risks associated with medical procedures and from poorly surgical planning might arise new conditions. Particularly, in temporal lobectomy, a resection is made in order to avoid propagation of epileptic seizures. (**Figure 44**) However, if there is not an accurate surgical planning visual field deficits may be present after surgery (Falconer & Wilson 1958)(Krolak-Salmon et al. 2000).

The advent of tractography has once again allowed new insights on discovering the anatomy of white matter, in this case for the Optic Radiation. Probabilistic approaches were followed (Ciccarelli et al. 2003)(Clatworthy et al. 2010) as well as deterministic (T. Taoka et al. 2008) but the planning was not still accurate as the reconstruction of the Optic Radiation is affected by other tracts and the algorithms have limitations (Catani et al. 2003)(Miki et al. 2007) . In Powell et al., 2005 a patient had a tumour, that was removed after planning of the Optic Radiation. However, as it can be seen in **Figure 61** the resection affected the Optic Radiation as it was not well estimated, and the patient developed a quadranatopia (deficit of one quadrant of the visual field).
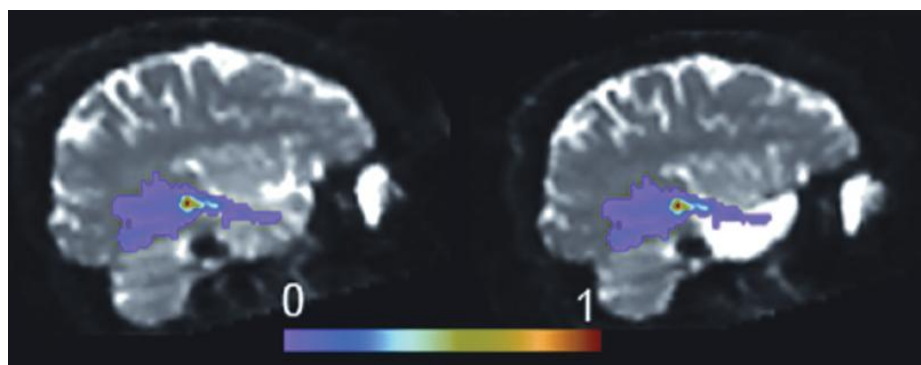
Figure 61 - **Resection of a tumour results into visual field deficit** (Powell et al. 2005)**.**

The Optic Radiation is therefore one of the most difficult tracts to reconstruct due to its high angulated fibres and due to the fact that techniques like DTI can't resolve such situations (Mandelstam 2012). Therefore, a further improvement in the developed automatic tool that has been described in this thesis was achieved by using different kinds of filters and spherical deconvolution data to get a better estimation of the Optic Radiation.

As it can be seen by **Figure 56** there are clear limitations in the DTI based atlas (Catani & Thiebaut de Schotten 2008) because of the fact that it does not begin in the LGN or by its lack of projection inside the visual areas. Furthermore, it is not able to resolve the highly angulated fibres of the Meyer's Loop and its projections inside the temporal lobe as the spherical deconvolution atlas. Crossing with splenium was also partially resolved as it can be seen in **Figure 55**. This atlas arose from the average of 20 subjects, having had automatic dissections for each one of them (**Figure 53**). In our approach we chose only to depict the Meyer's Loop and the pulvinar connections, which were obtained successfully. For comparison and validation purposes the manual atlas was also generated. One can see from that there are some false positives even though the results are very similar (**Figure 54**) As limitations of this approach we can point out the fact that some false negatives were observed regarding the ending point of the Optic Radiation in the calcarine fissure.

9 - Conclusion

This work has proven how useful Diffusion weighted imaging is for non-invasively determining physiological information and inferring about tissue microstructure. By quantifying the random thermal movement of water molecules and understanding that the human body is filled with barriers, underlying anisotropic behaviour of diffusion allows the reconstruction of average diffusivities in each voxel. There are several techniques that address this topic such as DTI, which has some limitations. In regions with highly angulated fibres, or complex configurations such as kissing or bending it has insufficient resolution. To overcome these issues, new protocols arose such as High Angular Resolution Diffusion Imaging (HARDI) arose. These procedures are natural extensions of the single-fibre case and consist in acquiring data with a large number of different gradient directions applied on a sphere, but with a much larger angular resolution.

The reconstruction of the main directions of diffusivity in each voxel leads to a three dimensional trajectory of white matter pathways - Tractography. There are different algorithms that either generate tracks by joining the estimation of largest eigenvalue of the diffusion tensor in each voxel in a discrete way (determinsitic), propagate the probability of strongest connection by resampling data several times (probabilistic) or even behave like a one stage process, since local orientations and connections are inferred upon at the same time (global). Tractography has two main purposes: better mapping of human white matter anatomy and neurosurgical planning. The use of parcellation techniques is therefore very useful to achieve those purposes. There are two different kind of approaches that can be performed based on regions of interest used to select/exclude tracts or by clustering techniques where similarities between streamlines are analysed.

It is very important to map human neuroanatomy in healthy subjects in order to know which fibres to track and to deal with abnormalities in patient's structural organization. This thesis intended to develop an automated tool that relied on ROI-based parcellation for automating that process. The outcome was very successful yielding the application of the software to three major tracts in the human brain: Arcuate Fasciculus, Corpus Callosum and Optic Radiation.

The parcellation of the Arcuate Fasciculus presented itself as a good initial test for the software, displaying the long segment as it has previously been described in the literature. The two-ROI method was recreated automatically with same results for DTI data and confirmed that further studies are necessary to make a definitive statement about the anatomy of this system, namely the evaluation of the differences found between DTI and SD.

A structural division of the Corpus Callosum, major inter-hemispheric white matter tract was obtained as seen in Figure 51, according to previous anatomic work. Contrarily to other studies, the parcellation was obtained according to the structural connectivity of the Corpus Callosum into major areas instead of geometric based assumptions, additionally to the implementation of anatomical constraints and NOTROIs. The reason why such approach was followed is due to the fact that several tractography studies have shown mismatch between geometric subdivisions of the Corpus Callosum and functional subdivisions. Furthermore, the

benefit of using HARDI techniques, namely Spherical Deconvolution data, became clear by the advent of visualizing lateral projections of the Corpus Callosum (**Figure 52**).

Finally, the developed tool was used with all its functionalities for a thorough analysis of the Optic radiation. Moreover, a comparison between DTI and SD was undergone which revealed a clear limitation of DTI based tractography. The reconstruction with SD showed that the Optic Radiation accurately departs from the LGN and arrives into the calcarine fissure, while projecting deeply into the temporal lobe (Figure 54), which is not visible with DTI (Figure 56). Its correct delineation is of major importance in a clinical environment and this work has led the way for that to be accomplished.

A new tool for automatic parcellation of brain connectivity, feasible in a clinically setting and flexible by the use of regions of interest from different standard spaces, was created and has shown potential to become a new to improve neurosurgical planning. However, this tool has still space for improvements. Besides using better data, the next step would follow by combining this approach with clustering techniques, making use of tract specific indexes to improve estimatives. It will also be useful to have a way to depict cases that don't follow the standard anatomy (Saloi & Alonso 2012). A final word is reserved for the ongoing and unstopping evolution of data analysis techniques and algorithm development that will certainly be of great use, but need to be carefully managed because one can easily get lost in the era where information is worldly wide available.

10 - Publications and Communications

10.1 - List of publications

• **<u>L. Lacerda</u>**, F,Dell'Acqua, "Spherical Deconvolution Tractography: Towards an Atlas of Optic Radiation for Clinical Applications/Neurosurgery", 4th "Workshop on Biomedical Engineering" (Lisbon, Portugal, Mar 2012) (Attachment I)

• **<u>L. Lacerda</u>**, F,Dell'Acqua, "Spherical Deconvolution Tractography: Towards an Atlas of Optic Radiation for Clinical Applications/Neurosurgery", "International School of Clinical Neuroanatomy - Occipital Lobes (Ragusa, Italy, Jun 2012) (Attachment II)

• **<u>L. Lacerda</u>**, H. A. Ferreira, F,Dell'Acqua. "Automated Method for Parcellation of Structural Brain Connectivity: application to Epilepsy and to the accurate delineation of the optic radiation", accepted for Oral presentation at the "European Society for Magnetic Resonance in Medicine and Biology" (Lisbon, Portugal, Apr 2012) (Attachment III)

10.2 - List of communications

10.2.1 - Oral communications

• Oral presentation "Towards an Atlas of the Optic Radiation for Clinical Applications and Neurosurgical Planning" at the 2nd International School of Clinical Neuroanatomy - Occipital Lobes (Ragusa, Italy, May 2012)

• Oral presentation "Automated Method for Parcellation of Structural Brain Connectivity: application to Epilepsy and to the accurate delineation of the optic radiation", 29th "European Society for Magnetic Resonance in Medicine and Biology" (Lisboa, Portugal, Oct 2012)

10.2.2 - Posters in Conferences

• Poster presentation "Spherical Deconvolution Tractography: Towards an Atlas of Optic Radiation for Clinical Applications/Neurosurgery", 4th "Workshop on Biomedical Engineering" (Lisbon, Portugal, Apr 2012)

11 - Appendixes

11.1 - Appendix I - WBME abstract

Spherical Deconvolution Tractography: Towards an Atlas of Optic Radiation for Clinical Applications/Neurosurgery

Luis, LACERDA [1,2]; Flavio, DELL' ACQUA [1]

[1] NATBRAINLAB, Center for Neuroimaging Sciences, Institute of Psychiatry - King's College - United Kingdom
[2] Institute of Biomedical Engineering and Biophysics - IBEB - Faculty of Sciences - University of Lisbon, Portugal

All medical procedures related with the visual system require a very detailed planning in order to avoid implications. Temporal lobectomy (TL) is a particular surgery that is performed in subjects with Epilepsy and may result in visual field deficits (VFD) if the resection affects the optic radiation (OR) (Figure 1- Optic Radiation Exposed. [1]   Figure 2 - Comparison of Optic Radiation atlas between DTI (blue) [8] and SD (red).). [1],[2]. Even though intra-operative approaches have already been taken based on existing information, the inter-subject variability is very high and therefore a reliable atlas of the OR is still demanded for the optimization of neuronavigation and surgical planning. [3],[4]

Most of the automated tractography tools currently available rely on the accurate disposition of seeds for the reconstruction of different fiber bundles of interest. Diffusion Tensor Imaging (DTI) has been used successfully to achieve the parcellation of brain regions, however it cannot fully reflect the index of anisotropic diffusion in regions of crossing, kissing or highly angulated fibers.[5] New methods such as Spherical Deconvolution (SD) are able to overcome some of these limitations.[6] In this work we present an atlas of the optic radiation that is being built through the use of a fully automatic developed tool.

Data was acquired using a 3T GE system following an acquisition and analysis protocol fully optimized for Spherical Deconvolution tractography as described in [7]. The developed automatic tool was able to perform semi-automatic dissections of the OR on a preliminary group of 8 subjects according to predefined cortical and subcortical regions, requiring minimal user intervention. It comprises the generation of regions into native space of each subject via non-linear registration, and the further computation of density maps back to template space. We compared the attained atlases of the optic radiation with the literature [8] and it was possible to visualize a new and more accurate white matter atlas (**Error! Reference source not found.**). This can be further demonstrated by the fact that with SD, the optic radiation is less affected by crossing with splenium and projects deeper into visual region, whilst allowing a much deeper reconstruction inside the temporal lobe. Moreover, it is less affected by crossing with other tracts and by partial volume effects.

Results will be presented on a larger group of sample and potential applications to neurosurgery will be discussed and a comparison with previous white matter atlases will be displayed.

References

[1] Mandelstam, S. a. (2012). Challenges of the Anatomy and Diffusion Tensor Tractography of the Meyer Loop. AJNR. American journal of neuroradiology,1-7.

[2] Daga, P., Winston, G., Modat, M., White, M., Mancini, L., Cardoso, M., Symms, M., et al. (2011). Accurate Localisation of Optic Radiation during Neurosurgery in an Interventional MRI Suite. IEEE transactions on medical imaging, (c), 1-10.

[3] Hofer, S., Karaus, A., & Frahm, J. (2010). Reconstruction and dissection of the entire human visual pathway using diffusion tensor MRI. Frontiers in neuroanatomy, 4(April), 15.

[4] Nucifora, P. G. P., Wu, X., Melhem, E. R., Gur, R. E., Gur, R. C., & Verma, R. (2012). Automated Diffusion Tensor Tractography: Implementation and Comparison to User-driven Tractography. Academic radiology, 19(5), 622-629. Elsevier Ltd.

[5] Tuch, D. S., Reese, T. G., Wiegell, M. R., Makris, N., Belliveau, J. W., & Wedeen, V. J. (2002). High Angular Resolution Diffusion Imaging Reveals Intravoxel White Matter Fiber Hetreogeneity. Radiology, 582, 577-582.

[6] Dell'acqua, F., Scifo, P., Rizzo, G., Catani, M., Simmons, A., Scotti, G., & Fazio, F. (2010). A modified damped Richardson-Lucy algorithm to reduce isotropic background effects in spherical deconvolution. NeuroImage, 49(2), 1446-58. Elsevier Inc.

[7] Dell'acqua, F., Simmons, A., Williams, Steven C.R., Catani, M. (2012). Can Spherical Deconvolution Provide More Information Than Fiber Orientations? Hindrance Modulated Orientational Anisotropy, a True-Tract Specific Index to Characterize White Matter Diffusion. Human Brain Mapping, In Press

[8] Catani, M., & Thiebaut de Schotten, M. (2008). A diffusion tensor imaging tractography atlas for virtual in vivo dissections. Cortex; a journal devoted to the study of the nervous system and behavior, 44(8), 1105-32.

Optic radiation exposed; Comparison of optic radiation atlas between DTI (red) [8] and SD (blue). In light blue we find the left thalamic region.

11.2 - Appendix II - ISOCN abstract

Spherical Deconvolution Tractography: Towards an Atlas of Optic Radiation for Clinical Applications/Neurosurgery

Luis, LACERDA [1,2]; Flavio, DELL' ACQUA [1]

[1] NATBRAINLAB, Center for Neuroimaging Sciences, Institute of Psychiatry - King's College - United Kingdom
[2] Institute of Biomedical Engineering and Biophysics - IBEB - Faculty of Sciences - University of Lisbon, Portugal

Temporal lobectomy (TL) is a particular surgery performed in subjects with Epilepsy that may result in visual field deficits (VFD) if resection affects the Optic Radiation (OR) (Figure 1) [1-2]. Even though intraoperative approaches have already been explored based on existing atlases, the inter-subject variability is still very high. Therefore, a reliable tool enabling automatic personalised dissections of the OR is needed. Additionally, an updated atlas is utterly important for optimisation of neuronavigation and surgical planning. [3-4] In this work we developed an automatic tool and used it to obtain preliminary results towards a new atlas of the OR.

Diffusion Tensor Imaging (DTI) has been used successfully to achieve the parcellation of brain regions, yet failing to fully reflect anisotropic diffusion in regions of crossing, kissing or highly bending fibers.[5] New methods such as Spherical Deconvolution (SD) are able to overcome some of these limitations.[6] In this study, data was acquired using a 3T GE system following an acquisition and analysis protocol fully optimised for SD tractography ([7]). The developed automatic tool was able to perform automatic dissections of the OR on a group of 20 subjects according to predefined cortical and subcortical regions, requiring minimal user intervention. Average of all maps yielded the creation of an atlas which allowed us to more accurately visualise OR (Figure 2) when compared with previous studies [8]. More specifically, OR reconstruction is less affected by crossing with other tracts (particularly splenium) and projects deeper into visual region, as well as allowing a much deeper reconstruction inside the temporal lobe (Meyer's Loop). Furthermore, compared to previous DTI atlases, we identified a discrepancy regarding the starting point of OR, which begins in Lateral Geniculate Nucleus in SD but more anteriorly in DTI, suggesting a limitation of DTI-based tractography in this region.

Advantages and limitations of this approach will be discussed at the meeting.

References

[1] Mandelstam, S. a. (2012). Challenges of the Anatomy and Diffusion Tensor Tractography of the Meyer Loop. AJNR. American journal of neuroradiology,1-7.

[2] Daga, P., Winston, G., Modat, M., White, M., Mancini, L., Cardoso, M., Symms, M., et al. (2011). Accurate Localisation of Optic Radiation during Neurosurgery in an Interventional MRI Suite. IEEE transactions on medical imaging, (c), 1-10.

[3] Hofer, S., Karaus, A., & Frahm, J. (2010). Reconstruction and dissection of the entire human visual pathway using diffusion tensor MRI. Frontiers in neuroanatomy, 4(April), 15.
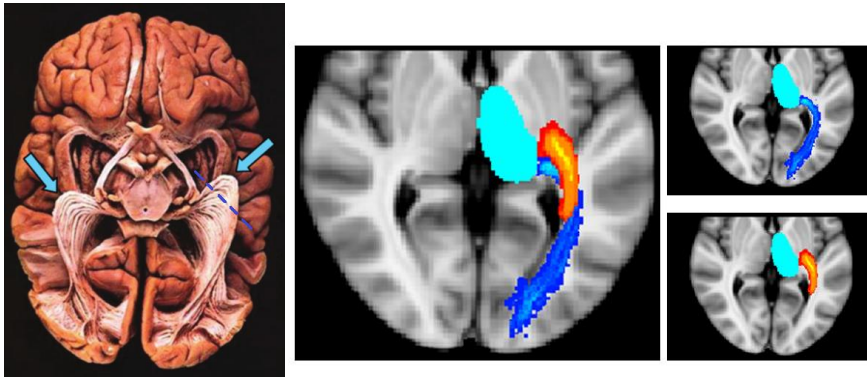
[4] Nucifora, P. G. P., Wu, X., Melhem, E. R., Gur, R. E., Gur, R. C., & Verma, R. (2012). Automated Diffusion Tensor Tractography: Implementation and Comparison to User-driven Tractography. Academic radiology, 19(5), 622-629. Elsevier Ltd.

[5] Tuch, D. S., Reese, T. G., Wiegell, M. R., Makris, N., Belliveau, J. W., & Wedeen, V. J. (2002). High Angular Resolution Diffusion Imaging Reveals Intravoxel White Matter Fiber Hetreogeneity. Radiology, 582, 577-582.

[6] Dell'acqua, F., Scifo, P., Rizzo, G., Catani, M., Simmons, A., Scotti, G., & Fazio, F. (2010). A modified damped Richardson-Lucy algorithm to reduce isotropic background effects in spherical deconvolution. NeuroImage, 49(2), 1446-58. Elsevier Inc.

[7] Dell'acqua, F., Simmons, A., Williams, Steven C.R., Catani, M. (2012). Can Spherical Deconvolution Provide More Information Than Fiber Orientations? Hindrance Modulated Orientational Anisotropy, a True-Tract Specific Index to Characterize White Matter Diffusion. Human Brain Mapping, In Press

[8] Catani, M., & Thiebaut de Schotten, M. (2008). A diffusion tensor imaging tractography atlas for virtual in vivo dissections. Cortex; a journal devoted to the study of the nervous system and behavior, 44(8), 1105-32.
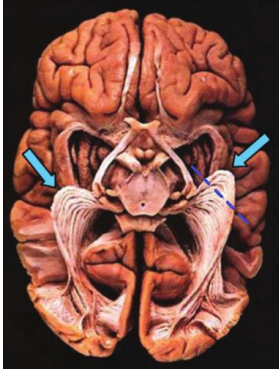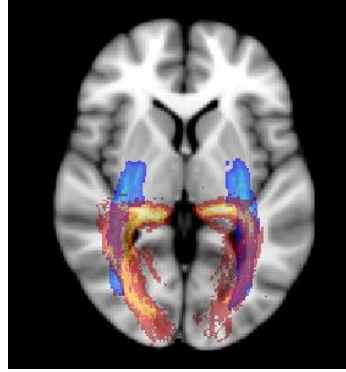
Figure 1- Optic Radiation Exposed. [1]

Figure 2 - Comparison of Optic Radiation atlas between DTI (blue) [8] and SD (red).

11.3 - Appendix III - ESMRMB abstract

Automated Method for Parcellation of Structural Brain Connectivity: application to Epilepsy and to the accurate delineation of the optic radiation

LACERDA, Luis[1,2]; FERREIRA, Hugo[2], Flavio, DELL' ACQUA [1]

[1] NATBRAINLAB, Center for Neuroimaging Sciences, Institute of Psychiatry - King's College - United Kingdom
[2] Institute of Biomedical Engineering and Biophysics - IBEB - Faculty of Sciences - University of Lisbon, Portugal

Purpose/Introduction - Temporal lobectomy (TL) is a particular surgery performed in subjects with Epilepsy (Figure 1) that may result in visual field deficits (VFD) if Optic Radiation is affected (OR). [1-3] Even though intraoperative approaches have already been explored based on existing atlases, the inter-subject variability is still very high. Moreover, Diffusion Tensor Imaging (DTI) cannot fully reflect the index of anisotropic diffusion in regions of crossing, kissing or highly angulated fibers.[4] New methods such as Spherical Deconvolution (SD) were able to overcome some of these limitations [5].However, there is still missing a reliable tool that enables automatic personalised dissections of brain regions instead of very time consuming and user dependent manual techniques. In this work we developed an automatic tool for the parcellation of brain regions and used it to build a new atlas of the OR, contributing for the improvement of neuronavigation and surgical planning.

Subjects and Methods – 20 subjects with no prior neurologic or psychiatric disease were scanned using a 3T GE system following an acquisition/analysis protocol fully optimised for SD tractography ([6]) with 60 directions and b-value of 3000 s.mm-2. The developed automatic tool was able to perform dissections according to predefined cortical and subcortical regions, requiring minimal user intervention. Once the individual maps of the Optic Radiation were generated, conversion to MNI-space followed through non-linear registrations.

Results - Averaging all maps yielded the creation of an atlas that allowed a more accurately visualisation than previous studies [7]. More specifically, OR reconstruction is less affected by crossing with other tracts and projects deeper into visual region, as well as having a much deeper reconstruction inside the temporal lobe (Meyer's Loop). Furthermore, we identified a discrepancy regarding the starting point of OR, which begins in Lateral Geniculate Nucleus (LGN) in SD but more anteriorly in DTI, suggesting a limitation of DTI-based tractography in this region (Figure 2). To further validate the developed tool, manual dissections for all subjects were performed and evaluated against automatic results, as seen schematically for one subject in Figure 3. When comparing both SD atlases (Figure 4) we notice that there are still some false positives, arising from the limitations of tractography.

Discussion/Conclusion - This study introduces a novel automatic method for parcellation of different brain regions. It was applied successfully to dissect the OR and generate a new atlas, essential to neuronavigation and neurosurgery planning. The use of more information, such as tract-specific indexes, can improve the presented method.

References

[1] Mandelstam, S.(2012). AJNR.1-7.
[2] Daga, P et al. (2011) IEEE transsactions on medical imaging, 1-10.
[3] Hofer, S et al (2010).Frontiers in neuroanatomy, 1-7.
[4] Tuch, D. S et al (2002). Radiology, 577-582.
[5] Dell'acqua, F et al (2010). NeuroImage, 1446-58.
[6] Dell'acqua, F et al (2012) Human Brain Mapping, In Press
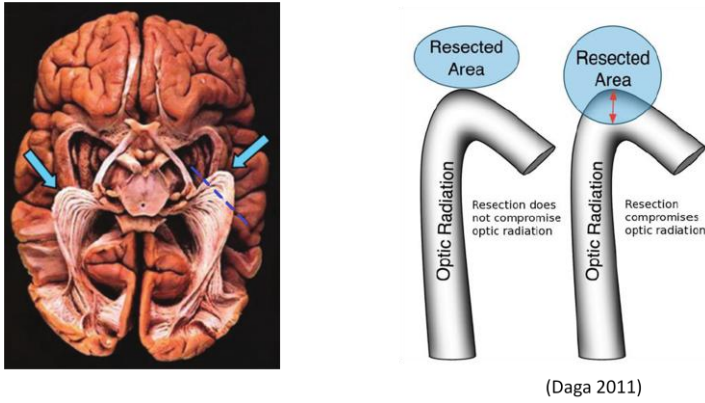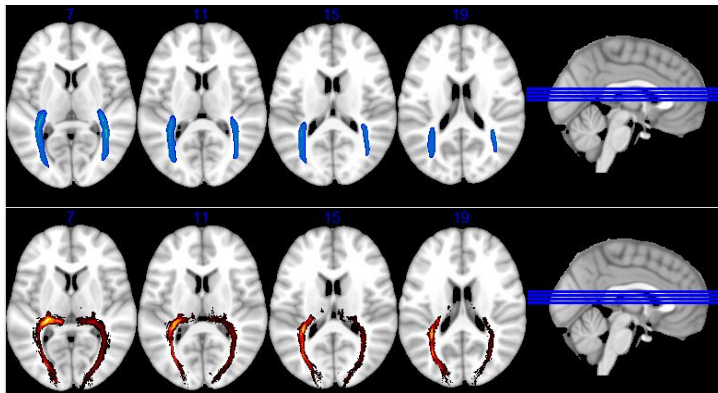[7] Catani, M et al (2008). Cortex, 1105-32.

fig1

(Daga 2011)

fig2

fig3

Manual   Automatic
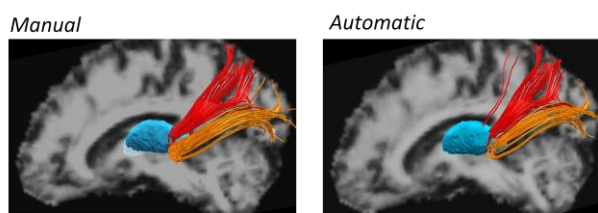

fig4

Manual Atlas   Automatic Atlas

78

12 - Bibliography

Aboitiz, F. et al., 1992. Fiber composition of the human corpus callosum. *Brain research*, 598(1-2), pp.143–53. Available at: http://www.ncbi.nlm.nih.gov/pubmed/1486478.

Aganj, I. et al., 2011. A Hough transform global probabilistic approach to multiple-subject diffusion MRI tractography. *Med Image Anal*, 15(4), pp.414–425.

Aldroubi, Akram & Basser, P., 1999. Reconstruction of vector and tensor fields from sampled discrete data. *Contemporary Mathematics*, pp.1–15.

Alexander, D, 2006. An Introduction to Computational Diffusion MRI: the Diffusion Tensor and Beyond.

Alexander, Daniel, 2005a. *Maximum Entropy Spherical Deconvolution for Diffusion MRI*, London.

Alexander, Daniel, 2005b. Multiple-fiber reconstruction algorithms for diffusion MRI. *Ann N Y Acad Sci*, 1064, pp.113–133.

Assaf, Y. et al., 2004. New modeling and experimental framework to characterize hindered and restricted water diffusion in brain white matter. *Magnetic resonance in medicine : official journal of the Society of Magnetic Resonance in Medicine / Society of Magnetic Resonance in Medicine*, 52(5), pp.965–78. Available at: http://www.ncbi.nlm.nih.gov/pubmed/15508168 [Accessed July 12, 2012].

Assaf, Y. & Basser, Peter J, 2005. Composite hindered and restricted model of diffusion (CHARMED) MR imaging of the human brain. *Neuroimage*, 27(1), pp.48–58.

Bammer, R., Acar, B. & Moseley, M.E., 2003. In vivo MR tractography using diffusion imaging. *Eur J Radiol*, 45(3), pp.223–234.

Basser, P J et al., 2000. In vivo fiber tractography using DT-MRI data. *Magn Reson Med*, 44(4), pp.625–632.

Basser, P J, 1995. Inferring microstructural features and the physiological state of tissues from diffusion-weighted images. *NMR Biomed*, 8(7-8), pp.333–344.

Basser, P J, 1997. New histological and physiological stains derived from diffusion-tensor MR images. *Annals of the New York Academy of Sciences*, 820, pp.123–38. Available at: http://www.ncbi.nlm.nih.gov/pubmed/9237452.

Basser, P J & Jones, D.K., 2002. Diffusion-tensor MRI: theory, experimental design and data analysis - a technical review. *NMR Biomed*, 15(7-8), pp.456–467.

Basser, P J, Mattiello, J. & LeBihan, D., 1994. MR diffusion tensor spectroscopy and imaging. *Biophys J*, 66(1), pp.259–267.

Beaulieu, C., 2002. The basis of anisotropic water diffusion in the nervous system - a technical review. *NMR Biomed*, 15(7-8), pp.435–455.

Beaulieu, C. & Allen, P.S., 1994. Determinants of Anisotropic Water Diffusion in Nerves. *Magn Reson Imaging*, 31, pp.394–400.

Behrens, T E J et al., 2003. Characterization and propagation of uncertainty in diffusion-weighted MR imaging. *Magn Reson Med*, 50(5), pp.1077–1088.

Behrens, T E J et al., 2007. Probabilistic diffusion tractography with multiple fibre orientations: What can we gain? *NeuroImage*, 34(1), pp.144–55. Available at: http://www.ncbi.nlm.nih.gov/pubmed/17070705 [Accessed July 15, 2012].

Behrens, T E J & Johansen-berg, H., 2009. *Diffusion MRI - From Quantitative Measurement to in vivo Neuroanatomy* First., Oxford: Elsevier.

Berman, J., 2005. Diffusion MRI.

Le Bihan, D. et al., 2001. Diffusion tensor imaging: concepts and applications. *J Magn Reson Imaging*, 13(4), pp.534–546.

Le Bihan, D., 1995. Molecular diffusion, tissue microdynamics and microstructure. *NMR in biomedicine*, 8(7-8), pp.375–86. Available at: http://www.ncbi.nlm.nih.gov/pubmed/8739274.

Le Bihan, D., Grenier, P. & Lallemand, D., 1986. MR Imaging of Intravoxel Incoherent Motions: Application to Diffusion and Perfusion in Neurological Disorders. *Radiology*, 161, pp.401–407.

Bürgel, U. et al., 1999. Mapping of histologically identified long fiber tracts in human cerebral hemispheres to the MRI volume of a reference brain: position and spatial variability of the optic radiation. *NeuroImage*, 10(5), pp.489–99. Available at: http://www.ncbi.nlm.nih.gov/pubmed/10547327.

Bürgel, U. et al., 2006. White matter fiber tracts of the human brain: three-dimensional mapping at microscopic resolution, topography and intersubject variability. *Neuroimage*, 29(4), pp.1092–1105.

Carroll, T.J. et al., 2010. Advanced Imaging Techniques, Including Fast Imaging. In *Clinical Magnetic Resonance Imaging*. pp. 1–69.

Catani, M. et al., 2003. Occipito-temporal connections in the human brain. *Brain*, 126(Pt 9), pp.2093–2107.

Catani, M. et al., 2007. Symmetries in human brain language pathways correlate with verbal recall. *Proc Natl Acad Sci U S A*, 104(43), pp.17163–17168.

Catani, M. et al., 2002. Virtual in vivo interactive dissection of white matter fasciculi in the human brain. *Neuroimage*, 17(1), pp.77–94.

Catani, M. & Mesulam, M., 2008a. The arcuate fasciculus and the disconnection theme in language and aphasia: history and current state. *Cortex; a journal devoted to the study of the nervous system and behavior*, 44(8), pp.953–61. Available at:

http://www.pubmedcentral.nih.gov/articlerender.fcgi?artid=2740371&tool=pmcentrez&rendertype=abstract [Accessed July 16, 2012].

Catani, M. & Mesulam, M., 2008b. What is a disconnection syndrome? *Cortex; a journal devoted to the study of the nervous system and behavior*, 44(8), pp.911–3. Available at: http://www.ncbi.nlm.nih.gov/pubmed/18603236 [Accessed July 16, 2012].

Catani, M. & Thiebaut de Schotten, M., 2008. A diffusion tensor imaging tractography atlas for virtual in vivo dissections. *Cortex*, 44(8), pp.1105–1132.

Catani, M. & Thiebaut de Schotten, M., 2012. *Atlas of Human Brain Connections* First., New York: Oxford University Press.

Chao, Y.-P. et al., 2009. Probabilistic topography of human corpus callosum using cytoarchitectural parcellation and high angular resolution diffusion imaging tractography. *Human brain mapping*, 30(10), pp.3172–87. Available at: http://www.ncbi.nlm.nih.gov/pubmed/19241418 [Accessed August 8, 2012].

Chen, M., 2006. *Clustering of Fiber Tracts on DT-MRI Data Set*. University of Leipzig.

Ciccarelli, O. et al., 2003. Diffusion tractography based group mapping of major white-matter pathways in the human brain. *Neuroimage*, 19(4), pp.1545–1555.

Clatworthy, P.L. et al., 2010. Probabilistic tractography of the optic radiations--an automated method and anatomical validation. *NeuroImage*, 49(3), pp.2001–12. Available at: http://www.ncbi.nlm.nih.gov/pubmed/19900564 [Accessed October 9, 2012].

Cloutman, L.L. & Lambon Ralph, M. a., 2012. Connectivity-based structural and functional parcellation of the human cortex using diffusion imaging and tractography. *Frontiers in Neuroanatomy*, 6(August), pp.1–18. Available at: http://www.frontiersin.org/Neuroanatomy/10.3389/fnana.2012.00034/abstract [Accessed September 5, 2012].

Colby, J.B. et al., 2012. Along-tract statistics allow for enhanced tractography analysis. *NeuroImage*, 59(4), pp.3227–42. Available at: http://www.ncbi.nlm.nih.gov/pubmed/22094644 [Accessed July 18, 2012].

Conturo, T.E., Lori, N.F. & Cull, T.S., 1999. Tracking neuronal fiber pathways in the living human brain. *Sciences-New York*, 96(August), pp.10422–10427.

Crook, N. & Robinson, L., 2009. A review of the safety implications of magnetic resonance imaging at field strengths of 3Tesla and above. *Radiography*, 15(4), pp.351–356. Available at: http://linkinghub.elsevier.com/retrieve/pii/S1078817409000625 [Accessed July 13, 2012].

Daga, P. et al., 2011. Accurate Localisation of Optic Radiation during Neurosurgery in an Interventional MRI Suite. *IEEE*, pp.1–10.

Dell'Acqua, F. et al., 2007. A model-based deconvolution approach to solve fiber crossing in diffusion-weighted MR imaging. *IEEE transactions on bio-medical engineering*, 54(3), pp.462–72. Available at: http://www.ncbi.nlm.nih.gov/pubmed/17355058.

Dell'acqua, F. et al., 2005. A Deconvolution Approach Based on Multi-Tensor Model to Solve Fiber Crossing in Diffusion-MRI. *Conf Proc IEEE Eng Med Biol Soc*, 2, pp.1415–1418.

Dell'acqua, F. et al., 2010. A modified damped Richardson-Lucy algorithm to reduce isotropic background effects in spherical deconvolution. *Neuroimage*, 49(2), pp.1446–1458.

Dell'acqua, F. et al., 2012. Can spherical deconvolution provide more information than fiber orientations? Hindrance modulated orientational anisotropy, a true-tract specific index to characterize white matter diffusion. *Hum Brain Mapp*.

Dell'acqua, F. & Catani, M., 2012. Structural human brain networks: hot topics in diffusion tractography. *Curr Opin Neurol*, 25(4), pp.375–383.

Descoteaux, Maxime et al., 2005. *Apparent Diffusion Coefficients from High Angular Resolution Diffusion Images : Estimation and Applications*,

Donnell, L.J.O. & Westin, C., 2007. Automatic Tractography Segmentation Using a High-Dimensional White Matter Atlas. *IEEE Trans Med Imaging*, 26(11), pp.1562–1575.

Doron, K.W. & Gazzaniga, M.S., 2008. Neuroimaging techniques offer new perspectives on callosal transfer and interhemispheric communication. *Cortex; a journal devoted to the study of the nervous system and behavior*, 44(8), pp.1023–9. Available at: http://www.ncbi.nlm.nih.gov/pubmed/18672233 [Accessed September 8, 2012].

Ebeling, U. & Reulen, H., 1988. Neurosurgical Topography of the Optic Radiation in the Temporal Lobe. *Acta Neurochir (Wien)*, 92, pp.29–36.

Efron, B., 1979. Bootstrap Methods : Another Look at the Jackknife. *The Annals of Statistic*, 7(1), pp.1–26.

Falconer, M.A. & Wilson, J.L., 1958. Visual Field Changes Following Anterior Temporal Lobectomy: Their Significance in Relation to "Meyer's Loop" of the Optic Radiation. *Brain*, 81(March), pp.1–14.

Fillard, Pierre et al., 2011. Quantitative evaluation of 10 tractography algorithms on a realistic diffusion MR phantom. *Neuroimage*, 56(1), pp.220–234.

Frank, L.R., 2002. Characterization of anisotropy in high angular resolution diffusion-weighted MRI. *Magn Reson Med*, 47(6), pp.1083–1099.

Ge, B. et al., 2010. Automatic clustering of white matter fibers based on symbolic sequence analysis. *Proc. of SPIE*, 7623, pp.1–8. Available at: http://link.aip.org/link/PSISDG/v7623/i1/p762327/s1&Agg=doi [Accessed August 20, 2012].

Glickstein, M. & Berlucchi, G., 2008. Classical disconnection studies of the corpus callosum. *Cortex; a journal devoted to the study of the nervous system and behavior*, 44(8), pp.914–27. Available at: http://www.ncbi.nlm.nih.gov/pubmed/18603234 [Accessed August 13, 2012].

Guevara, P. et al., 2012. Automatic fiber bundle segmentation in massive tractography datasets using a multi-subject bundle atlas. *NeuroImage*, 61(4), pp.1083–99. Available at: http://www.ncbi.nlm.nih.gov/pubmed/22414992 [Accessed July 21, 2012].

Guevara, P. et al., 2011. Robust clustering of massive tractography datasets. *Neuroimage*, 54(3), pp.1975–1993.

Habib, J., Auer, D.P. & Morgan, P.S., 2010. A quantitative analysis of the benefits of cardiac gating in practical diffusion tensor imaging of the brain. *Magn Reson Med*, 63(4), pp.1098–1103.

Hagler, D.J. et al., 2009. Automated white-matter tractography using a probabilistic diffusion tensor atlas: Application to temporal lobe epilepsy. *Hum Brain Mapp*, 30(5), pp.1535–1547.

Hagmann, P. et al., 2007. Mapping human whole-brain structural networks with diffusion MRI. *PloS one*, 2(7), p.e597. Available at: http://www.pubmedcentral.nih.gov/articlerender.fcgi?artid=1895920&tool=pmcentrez&rendertype=abstract [Accessed July 30, 2012].

Hendrix, A., 2004. Magnets , Flows , and Artifacts. , p.162.

Hofer, S., Karaus, A. & Frahm, J., 2010. Reconstruction and dissection of the entire human visual pathway using diffusion tensor MRI. *Front Neuroanat*, 4, p.15.

Huang, H. et al., 2005. DTI tractography based parcellation of white matter: application to the mid-sagittal morphology of corpus callosum. *Neuroimage*, 26(1), pp.195–205.

Jackowski, M. et al., 2005. White matter tractography by anisotropic wavefront evolution and diffusion tensor imaging. *Med Image Anal*, 9(5), pp.427–440.

Jansons, K.M. & Alexander, Daniel C, 2003. Persistent angular structure: new insights from diffusion magnetic resonance imaging data. *Inverse Problems*, 19(5), pp.1031–1046. Available at: http://stacks.iop.org/0266-5611/19/i=5/a=303?key=crossref.1939aed841d7b17cbc040a1563e475d3.

Jbabdi, Saad et al., 2007. A Bayesian framework for global tractography. *NeuroImage*, 37(1), pp.116–29. Available at: http://www.ncbi.nlm.nih.gov/pubmed/17543543 [Accessed July 24, 2012].

Jbabdi, Saad & Johansen-Berg, Heidi, 2011. Tractography: where do we go from here? *Brain Connect*, 1(3), pp.169–183.

Jensen, J.H. et al., 2005. Diffusional Kurtosis Imaging : The Quantification of Non- Gaussian Water Diffusion by Means of Magnetic Resonance Imaging. *Magnetic Resonance in Medicine*, 53, pp.1432–1440.

Jensen, J.H. & Helpern, J.A., 2010. MRI quantification of non-Gaussian water diffusion by kurtosis analysis. *NMR in biomedicine*, (August 2009).

Jones, D.K., 2010. Challenges and limitations of quantifying brain connectivity in vivo with diffusion MRI. *Imaging Med*, 2(3), pp.341–355.

Jones, D.K. et al., 1999. Non-invasive assessment of axonal fiber connectivity in the human brain via diffusion tensor MRI. *Magn Reson Med*, 42(1), pp.37–41.

Jones, D.K., 2008. Studying connections in the living human brain with diffusion MRI. *Cortex*, 44(8), pp.936–952.

King, M.D., Gadian, D.G. & Clark, C. a, 2009. A random effects modelling approach to the crossing-fibre problem in tractography. *NeuroImage*, 44(3), pp.753–68. Available at: http://www.ncbi.nlm.nih.gov/pubmed/19007890 [Accessed August 12, 2012].

Krolak-Salmon, P. et al., 2000. Anatomy of optic nerve radiations as assessed by static perimetry and MRI after tailored temporal lobectomy. *The British journal of ophthalmology*, 84(8), pp.884–9. Available at: http://www.pubmedcentral.nih.gov/articlerender.fcgi?artid=1723582&tool=pmcentrez&rendertype=abstract.

Kubicki, M., Shenton, M.E. & O'Donnell, L.J., 2006. A Method for Clustering White Matter Fiber Tracts. *AJNR Am J Neuroradiol*, 27(May), pp.1032–1036.

Lacerda, L., Ferreira, H.A. & Dell'acqua, F., 2012. Automated Method for Parcellation of Structural Brain Connectivity: application to Epilepsy and to the accurate delineation of the optic radiation. In *ESMRMB*. pp. 1–4.

Larkman, D.J. & Nunes, Rita G, 2007. Parallel magnetic resonance imaging. *Physics in medicine and biology*, 52(7), pp.R15–55. Available at: http://www.ncbi.nlm.nih.gov/pubmed/17374908 [Accessed July 13, 2012].

Lawes, I.N.C. et al., 2008. Atlas-based segmentation of white matter tracts of the human brain using diffusion tensor tractography and comparison with classical dissection. *Neuroimage*, 39(1), pp.62–79.

Lazar, M. et al., 2003. White matter tractography using diffusion tensor deflection. *Hum Brain Mapp*, 18(4), pp.306–321.

Lazar, M. & Alexander, A.L., 2005. Bootstrap white matter tractography (BOOT-TRAC). *Neuroimage*, 24(2), pp.524–532.

Lebel, C., Caverhill-Godkewitsch, S. & Beaulieu, C., 2010. Age-related regional variations of the corpus callosum identified by diffusion tensor tractography. *Neuroimage*, 52(1), pp.20–31.

Leemans, A. & Jones, D., 2009. ExploreDTI : a graphical toolbox for processing , analyzing , and visualizing diffusion MR data. *Proceedings of the ISMRM*, 17(2), p.3537.

Lenglet, C et al., 2009. Mathematical methods for diffusion MRI processing. *Neuroimage*, 45(1 Suppl), pp.S111–22.

Mandelstam, S.A., 2012. Challenges of the Anatomy and Diffusion Tensor Tractography of the Meyer Loop. *AJNR Am J Neuroradiol*, 10, pp.1–7.

Mattiello, J., Basser, Peter J & LeBihan, D., 1994. Analytical Expressions for the b Matrix in NMR Diffusion Imaging and Spectroscopy. *Journal of magnetic resonance imaging : JMRI*, A(108), pp.131–141.

Miki, Y. et al., 2007. Diffusion Tensor Fiber Tractography of the Optic Radiation : Analysis with 6- , 12- , 40- , and 81- Directional Motion-Probing Gradients, a Preliminary Study. *AJNR Am J Neuroradiol*, 28, pp.92–96.

Minati, L. & We, W.P., 2007. Physical Foundations , Models , and Methods of Diffusion Magnetic Resonance Imaging of the Brain : A Review. *Concepts in Magnetic Resonance*, 30 A(5), pp.278–307.

Mori, S et al., 1999. Three-dimensional tracking of axonal projections in the brain by magnetic resonance imaging. *Annals of neurology*, 45(2), pp.265–9. Available at: http://www.ncbi.nlm.nih.gov/pubmed/9989633.

Mori, S & Barker, P.B., 1999. Diffusion magnetic resonance imaging: its principle and applications. *The Anatomical record*, 257(3), pp.102–9.

Mori, S & van Zijl, P.C.M., 2002. Fiber tracking: principles and strategies - a technical review. *NMR Biomed*, 15(7-8), pp.468–480.

NessAiver, M., 2008. http://simplyphysics.com/flying_objects.html. *Simply Physics*.

Nucifora, P.G.P. et al., 2012. Automated Diffusion Tensor Tractography: Implementation and Comparison to User-driven Tractography. *Acad Radiol*, 19, pp.622–629.

Nunes, Rita G, Jezzard, P. & Clare, Stuart, 2005. Investigations on the efficiency of cardiac-gated methods for the acquisition of diffusion-weighted images. *Journal of magnetic resonance (San Diego, Calif. : 1997)*, 177(1), pp.102–10. Available at: http://www.ncbi.nlm.nih.gov/pubmed/16112886 [Accessed July 15, 2012].

Pajevic, Sinisa, Aldroubi, Akram & Basser, Peter J, 2002. A continuous tensor field approximation of discrete DT-MRI data for extracting microstructural and architectural features of tissue. *J Magn Reson*, 154(1), pp.85–100.

Pandya, D.N., Karol, E.A. & Heilbronn, D., 1971. The topographical distribution of interhemispheric projections in the corpus callosum of the rhesus monkey. *Brain research*, 32, pp.31–43.

Pannek, K. et al., 2010. An automated strategy for the delineation and parcellation of commissural pathways suitable for clinical populations utilising high angular resolution diffusion imaging tractography. *NeuroImage*, 50(3), pp.1044–53. Available at: http://www.ncbi.nlm.nih.gov/pubmed/20079446 [Accessed September 8, 2012].

Park, H.-J. et al., 2008. Corpus callosal connection mapping using cortical gray matter parcellation and DT-MRI. *Hum Brain Mapp*, 29(5), pp.503–516.

Parker, Geoffrey J M, Haroon, H.A. & Wheeler-Kingshott, Claudia A M, 2003. A framework for a streamline-based probabilistic index of connectivity (PICo) using a structural interpretation of MRI diffusion measurements. *J Magn Reson Imaging*, 18(2), pp.242–254.

Parker, Geoffrey J M, Wheeler-kingshott, C.A.M. & Barker, Gareth J, 2002. Estimating Distributed Anatomical Connectivity Using Fast Marching Methods and Diffusion Tensor Imaging. *IEEE Trans Med Imaging*, 21(5), pp.505–512.

Philibert, J., 2005. One and a Half Century of Diffusion : Fick , Einstein , before and beyond. *Diffusion Fundamentals*, 2, pp.1–10.

Pottumarthi, V., 2006. *Magnetic Resonance Imaging - Methods and Biologic Applications* P. V. Prasad, ed., Totowa, NJ: Humana Press. Available at: http://www.springerlink.com/openurl.asp?genre=book&id=doi:10.1385/1597450103.

Powell, H.W.R. et al., 2005. MR tractography predicts visual field defects following temporal lobe resection. *Neurology*, 65(4), pp.596–599.

Price, W.S., 1997. Basic Theory. In *Pulsed-Field Gradient Nuclear Magnetic Resonance as a Tool for Studying Translational Diffusion.* pp. 299–336. Available at: http://doi.wiley.com/10.1002/chin.199750339.

R. Hashemi, W.G Bradley, et al, 2010. *MRI - The Basics* Third., Philadelphia: Wolters Kluwer.

Reese, T G et al., 2003. Reduction of eddy-current-induced distortion in diffusion MRI using a twice-refocused spin echo. *Magnetic resonance in medicine : official journal of the Society of Magnetic Resonance in Medicine / Society of Magnetic Resonance in Medicine*, 49(1), pp.177–82. Available at: http://www.ncbi.nlm.nih.gov/pubmed/12509835 [Accessed July 15, 2012].

Reich, D.S. et al., 2010. Automated vs. conventional tractography in multiple sclerosis: variability and correlation with disability. *Neuroimage*, 49(4), pp.3047–3056.

Reisert, M. et al., 2011. Global fiber reconstruction becomes practical. *NeuroImage*, 54(2), pp.955–62. Available at: http://www.ncbi.nlm.nih.gov/pubmed/20854913 [Accessed September 8, 2012].

Reisert, M., Mader, I. & Kiselev, V., 2009. Tracking a Physical Phantom by Global Fibre Reconstruction. *Lecture Notes in Computer Science*, pp.1–4.

Rorden, C. & Brett, M., 2000. Stereotaxic display of brain lesions. *Behavioural neurology*, 12(4), pp.191–200. Available at: http://www.ncbi.nlm.nih.gov/pubmed/11568431.

Saloi, R. & Alonso, A.S., 2012. Automatic Procedure for Measuring Brain Tumor Volumetric Change. In *European Society for Magnetic Resonance In Medicine and Biology*. p. 1.

Seunarine, K.K. et al., 2007. Exploiting peak anisotropy for tracking through complex structures. *IEEE 11th International Conference on Computer Vision*, 2, pp.1–8. Available at: http://ieeexplore.ieee.org/lpdocs/epic03/wrapper.htm?arnumber=4409168.

Sherbondy, A.J. et al., 2008. ConTrack : Finding the most likely pathways between brain regions using diffusion tractography. *Journal of Vision*, 8(15), pp.1–16.

Sherbondy, A.J., Dougherty, R.F. & Wandell, B.A., 2009. Identifying the human optic radiation using diffusion imaging and fiber tractography. *J Vis*, 8(10), pp.1–19.

Simmons, Andrew & Hakansson, K., 2011. Magnetic Resonance Safety. In M. Modo & J. W. M. Bulte, eds. *Magnetic Resonance Neuroimaging*. Totowa, NJ: Humana Press, pp. 17–29. Available at: http://www.springerlink.com/index/10.1007/978-1-61737-992-5 [Accessed July 18, 2012].

Smith, Stephen M et al., 2004. *Advances in Functional and Structural MR Image Analysis and Implementation as FSL*,

Staempfli, P. et al., 2006. Resolving fiber crossing using advanced fast marching tractography based on diffusion tensor imaging. *Neuroimage*, 30(1), pp.110–120.

Stejskal, E.O. & Tanner, J.E., 1965. Spin Diffusion Measurements: Spin Echoes in the Presence of a Time-Dependent Field Gradient. *The Journal of Chemical Physics*, 42(1), pp.288–292. Available at: http://link.aip.org/link/JCPSA6/v42/i1/p288/s1&Agg=doi [Accessed July 15, 2012].

Stieglitz, L.H. et al., 2011. Optic radiation fiber tracking using anteriorly angulated diffusion tensor imaging: a tested algorithm for quick application. *Neurosurgery*, 68(5), pp.1239–1251.

Tamraz, J.C., Comair, Y.G. & Edition, S., 2006. *Atlas of Regional Anatomy of the Brain Using MRI*, Germany: Springer.

Taoka, T. et al., 2008. Diffusion tensor tractography of the Meyer loop in cases of temporal lobe resection for temporal lobe epilepsy: correlation between postsurgical visual field defect and anterior limit of Meyer loop on tractography. *AJNR Am J Neuroradiol*, 29(7), pp.1329–1334.

Thiebaut de Schotten, M. et al., 2012. Monkey to human comparative anatomy of the frontal lobe association tracts. *Cortex*, 48(1), pp.82–96.

Tournier, J. et al., 2004. Direct estimation of the fiber orientation density function from diffusion-weighted MRI data using spherical deconvolution. *Children*, 23, pp.1176–1185.

Tournier, J., Mori, Susumu & Leemans, A., 2011. Diffusion tensor imaging and beyond. *Magn Reson Med*, 65(6), pp.1532–1556.

Tozer, D.J. et al., 2012. Linking white matter tracts to associated cortical grey matter: a tract extension methodology. *NeuroImage*, 59(4), pp.3094–102. Available at: http://www.ncbi.nlm.nih.gov/pubmed/22100664 [Accessed July 24, 2012].

Tuch, David S, 2002. *Diffusion MRI of Complex Tissue Structure*. Massachusetts Institute of Technology.

Tuch, David S et al., 2002. High Angular Resolution Diffusion Imaging Reveals Intravoxel White Matter Fiber Hetreogeneity. *Radiology*, 582, pp.577–582.

Tuch, David S, 2004. Q-ball imaging. *Magn Reson Med*, 52(6), pp.1358–1372.

Turner, R., Lebihan, D. & Pekar, J.J., 1990. Echo-Planar Imaging of Intravoxel Incoherent Motion. *Radiology*, 177, pp.407–414.

Wedeen, V J et al., 2005. Mapping complex tissue architecture with diffusion spectrum magnetic resonance imaging. *Magnetic resonance in medicine : official journal of the Society of Magnetic Resonance in Medicine / Society of Magnetic Resonance in Medicine*, 54(6), pp.1377–86. Available at: http://www.ncbi.nlm.nih.gov/pubmed/16247738 [Accessed July 15, 2012].

Wedeen, V J et al., 2000. Mapping fiber orientation spectra in cerebral white matter with Fourier-transform diffusion MRI. *Proceedings of the ISMRM*, 8, p.82.

Witelson, S., 1989. Hand And Sex Differences In The Isthmus And Genu Of The Human Corpus Callosum. , 112, pp.799–835.

Yeh, F. & Tseng, W.I., 2010. Automatic Tractography Segmentation by Morphological Continuity Clustering. *Proceedings of the ISMRM*, p.1.

Yuksel, B.F., 2011. *Manual and Automated Methods of Dissection for Callosal Fibres*. King's College London.

Zhang, H. et al., 2012. NODDI: Practical in vivo neurite orientation dispersion and density imaging of the human brain. *Neuroimage*, 61, pp.1000–1016.